WA School of Mines: Minerals, Energy and Chemical Engineering

Stabilities and Phase Diagrams of Fast Pyrolysis Bio-oils

Mingyang Li

This thesis is presented for the Degree of

Doctor of Philosophy

of

Curtin University

May 2020

To the best of my knowledge and belief, this thesis contains no material previously published by any other person except where due acknowledgement has been made.

This thesis contains no material which has been accepted for the award of any other degree or diploma in any university.

Signature:.....

Date: 08/05/2020

To my beloved family
and friends

Abstract

The world's total energy consumption has been increasing rapidly since the beginning of the twentieth century while the reserves of fossil fuels (e.g. petroleum, coal and natural gas) decline gradually. Substantial research & development across the world have been devoted to the utilization of renewable energy to at least partially replace fossil fuels. For biomass utilization, fast pyrolysis is one of the promising options for produce bio-oil at 450-600 °C in the absence of oxygen. Bio-oil can find many applications including heat supply, power generation and production of value-added chemicals etc. However, bio-oil has some undesired features (i.e., unstable, high acidity and high viscosity) that hinder its commercialization. Particularly, phase instability that occurs during storage and transportation is a major concern because it can cause severe consequences such as pumping problems, blockages and combustion issues. Therefore, this PhD study aims at carrying out a systematic investigation into the stabilities and phase diagrams of fast pyrolysis bio-oils. The ternary phase diagram is a useful, straightforward, and important tool to understand, predict and control the phase behaviour of bio-oil.

This PhD thesis reports the ternary phase of pyrolytic lignin, mixed solvent and water systems. The detailed objectives of this project include (1) to study the solubility of pyrolytic lignin (PL) in representative mixed solvents that are prepared from model compounds based on the key components in the water-soluble fraction of bio-oil; (2) to develop ternary phase diagrams of PL/MS/water; (3) to reveal the effect of ageing on the phase diagrams of PL/MS/water; (4) to assess the effect of minor components on the ternary phase diagrams of PL/MS/water; (5) to evaluate the effect of temperature on the ternary phase diagrams of PL/MS/water. All the mentioned objectives have been successfully achieved.

Firstly, this study reports the solubilities of PL in various solvents (hereafter referred as "single/mixed model solvents") prepared from model compounds representing key components in the water-soluble fraction of bio-oil and the corresponding ternary phase diagrams for systems among PL, single/mixed_model_solvent, and water. Acetic acid, hydroxyacetone, furfural, phenol and methanol are selected as model compounds to form mixed model solvents. Each model compound represents a specific chemical family (i.e., acids, aldehydes, furans, phenols and alcohols). As PL is not

soluble in phenol, or only slightly soluble in furfural alone; therefore, this study starts with investigating the PL solubilities in other three single model solvents. The PL solubilities in acetic acid, hydroxyacetone and methanol are ~214, ~239 and ~615 g per 100 g of solvent, respectively. The PL solubilities in two-component model solvents decrease as furfural and phenol are included in mixed model solvents. For example, the PL solubilities in acetic acid/furfural (1:1), hydroxyacetone/furfural (1:1) and methanol/furfural (1:1) drop to ~87, ~91 and ~170 g per 100 g of model solvent, respectively. Although both furfural and phenol can reduce the PL solubilities in a corresponding mixed model solvent, furfural and phenol should not be excluded in the formulation of mixed model solvents. This is because phenolics and furfurals are major chemical families in fast pyrolysis bio-oil; therefore, in order to develop a universal tool for the prediction of bio-oil phase stability, phenol and furfural must be taken into consideration for developing representative mixed model solvent.

Secondly, previous reports on bio-oil composition produced from different biomass feedstock and reaction conditions (reactor system, heating rate, etc.) were reviewed. Based on the principle "Like dissolves like" (a solvent is more likely to dissolve a solute with a similar solubility parameter) and as well as the bio-oil compositions, a mixed solvent (MS) has been developed to represent the water-soluble fraction of bio-oil. Five model compounds were selected to represent the five major chemical groups in bio-oil. The MS with the solubility parameter being 11.99 $cal^{1/2}$ $cm^{-3/2}$ has been developed with the composition of 33.3 wt % acetic acid, 33.3 wt % hydroxyacetone, 13.3 wt % phenol, 13.3 wt % furfural, 6.8 wt % methanol. Then several phase diagrams of PL and its fractions/MS/water were constructed, and the solubilities of PL in various MS/water mixtures were also studied. In addition, the presence of free sugar (i.e., levoglucosan, present in bio-oil as solute) also influences the ternary phase diagram of the PL/MS/system, but only at a low water content (i.e., < 20 wt %). The results suggest that such ternary diagrams may be potentially an important tool for predicting the phase separation of bio-oil, as a result of changes in the bio-oil chemistry in various processes (e.g., cold-water precipitation and ageing).

Thirdly, this study reports the phase behaviours and phase diagrams of PL samples derived from both fresh and aged bio-oils, a mixed solvent (MS), and water. The maximal values of PL (average molecular weight ranging from 1360-550 Da) solubilities are between ~89 and ~221 g per 100 g of MS/water. Because the presence

of sugars also affects the phase behaviours of bio-oils. In this study, the data on the compositions of bio-oil samples (with a total sugar content range of 54.2−64.5 mg g^{-1} bio-oil) are processed and then replotted in the phase diagrams on a sugar-free basis to verify the correctness of the phase diagrams. The results show that it such phase diagrams can be used to predict phase stability of a given bio-oil sample.

Fourthly, this paper studies the effect of bio-oil minor components on the phase diagrams of pyrolytic lignin (PL), mixed solvent (MS), water that represents a simulated bio-oil system. Decane, pentadecane, 1,4-benzoquinone, cyclohexanecarboxylic acid (representing extractives)/KCl (representing inorganics)/methyl acetate, furfuryl acetate, phenylacetate, methyl α-D-glucopyranoside (representing esters) were added into the PL/MS/water systems at different concentrations based on the compositions of extractives/ash/ether in fresh bio-oils reported by other researchers. The results show that the addition of selected extractive model compounds can distinctively affect phase conversion curves. For example, the added 0.1 wt % decane and pentadecane have negative effects on the phase behaviours of PL/MS/water when the water content in the PL/MS/water ternary system is > ~27 and ~21 wt % respectively. Furfural acetate and phenylacetate have similar effects on the phase behaviours of PL/MS/water systems as extractive model compounds. However, methyl acetate has positive effects on the phase stability of PL/MS/water systems. The existing of 7.5 and 15 wt % methyl acetate increase the maximal PL concentrations to ~67 and ~69 wt %, in contrast to ~66 wt % without methyl acetate is added.

Fifthly, the effect of temperature on the phase behaviour of the PL sample in various MS/water systems are studied, and the ternary phase diagrams of the PL/MS/water systems at different temperatures are developed. The results clearly show that an increase in temperature largely increases the solubility of PL in the MS/water system. The maximal PL concentration in the PL/MS/water system increases from ~62 wt % at 0 °C (equivalent to a PL solubility of ~161 g PL per 100 g of MS/water mixture) to ~70 wt % (equivalent to a PL solubility of ~229 g PL per 100 g of MS/water mixture) at 40 °C. This is because the dissolution of PL is an endothermic process, and increasing the temperature will shift the dissolution equilibrium towards the PL solution side. The presence of sugar also influences the PL solubility in the MS/water system, but only up to a critical water content (i.e., ~11–18 wt % at 5–7 wt % sugar

concentration and 0–40 °C) depending on the temperature and sugar concentration. The results suggest that a set of ternary phase diagrams of PL/MS/water systems at different temperatures and sugar concentrations are essential to predicting the phase stability of bio-oil during storage and transportation.

Acknowledgement

I gratefully acknowledge ARC Discovery Projects to support my PhD research project partially, and the CIPRS Scholarship received from Curtin University.

I would like to express my gratitude to my supervisor, Professor Hongwei Wu, for offering me this priceless opportunity of pursuing my PhD study under his supervision. Prof Wu has devised the original idea and the research program for this project that has opened a completely new research avenue. He has been a great mentor, and I benefited a lot from what he taught me during my PhD period. I would like to thank Dr Yun Yu, and Dr Mingming Zhang, who are my associate supervisors, for their patient guidance and help in this project. Without my supervisors, my PhD would not be possible.

I would like to acknowledge our group members including Sui Boon Liaw, Matthew Witham, Yu Long, Chao Feng, Bing Song, Xujun Chen, Yee Wen Chua, Rashedul Khondakar, Changya Deng, Jinxiu Cao, Yanshan Yin, Qiqing Shen, Fanhui Guo and Zhiliang Wu for their assistance in various aspects. In addition, I would also like to thank all Chemical Engineering Department lab technical staffs, Andrew Chan, Melina Miralles, Xiao Hua, Roshanak Doroushi, Araya Abera, and Jason Wright, for their assistance and technical support in the lab.

List of Publications from My PhD Study

Papers published in refereed journals:

- **Mingyang Li**, Mingming Zhang, Yun Yu, and Hongwei Wu. "Ternary System of Pyrolytic Lignin, Mixed Solvent, and Water: Phase Diagram and Implications." *Energy & Fuels*, **2018**, *32*, 465−474
- **Mingyang Li**, Mingming Zhang, Yun Yu, Hongwei Wu. "Effect of Temperature on the Ternary Phase Diagrams of Pyrolytic Lignin, Mixed Solvent and Water" *Fuel*, accepted. DOI: j.fuel.2019.116458
- **Mingyang Li**, Yun Yu, Hongwei Wu. "Effect of Single/Mixed Model Solvents on the Phase Diagrams of Pyrolytic Lignin, Model Solvent and Water." *Energy &Fuels*, acceptance pending, ef-2020-023156

Manuscripts in preparation for submission to refereed journals:

- **Mingyang Li**, Changya Deng, Yee Wen Chua, Sui Boon Liaw, Mingming Zhang, Yun Yu and Hongwei Wu. "Effect of Ageing on the Phase Diagrams of Pyrolytic Lignin, Mixed Solvent and Water" In preparation
- **Mingyang Li**, Mingming Zhang, Yun Yu, Hongwei Wu. "Effect of Bio-Oil Minor Components on the Phase Diagrams of Pyrolytic Lignin, Mixed Solvent and Water" In preparation

Related paper and award:

- Mingming Zhang, **Mingyang Li**, Hongwei Wu "Ageing of bio-oil and its fractions in presence of surfactants" *Fuel*, **2019**, *252*, 403-407.
- **Mingyang Li**, Best Student Presentation Award @ Pyroliq 2019.

Table of content

List of Tables

List of Figures

Figure 8-4 Solubilities of PL in various MS/water mixtures with the presence of sugar at different temperature. Point A_1-C_1 and A_2-C_2 in panel (a), (b) and (c) correspond to point A_1-C_1 and A_2-C_2 in Figure 3a, 3b and 3c respectively. Panel (a): at 0 °C the maximal solubilities of PL with 5 % and 7 % levoglucosan being added are achieved at point B_1 or B_2, corresponding to water contents of ~19 and ~23 % respectively; the 5 % and 7 % levoglucosan has no effect beyond point C_1 and C_2, corresponding to water contents of ~30 or ~35 % respectively. Panel (b): at 25 °C the maximal solubilities of PL with 5 % and 7 % levoglucosan being added are achieved at point B_1 and B_2, corresponding to water contents of ~24 or ~29 % respectively; the 5 % or 7 % levoglucosan has no effect beyond point C_1 and C_2, corresponding to water contents of ~31 or ~36 % respectively. Panel (c): at 40 °C the maximal solubilities of PL with 5 % and 7 % levoglucosan being added are achieved at point B_1 and B_2, corresponding to water contents of ~26 and ~30 % respectively; the 5 % or 7 % levoglucosan has no effect beyond point C_1 and C_2, corresponding to water contents of ~33 or ~38 % respectively. [Legend: PL, pyrolytic lignin; MS, mixed solvent.] 127

Chapter 1 Introduction

1.1 Background and Motive

The energy consumption has been increasing dramatically as a result of a rapid increase in the world's population, while the finite fossil fuel reserves are continuously decreasing.[1] Biomass is regarded as a renewable energy source to at least partially replace the non-renewable fossil fuels.[2] Biomass mainly consists of carbohydrates (i.e., cellulose, hemicellulose, lignin) and some other minor components such as extractives and inorganic matter.[3] Biomass fast pyrolysis is a thermochemical method to convert biomass into gases, solids, and liquids (bio-oil) under the inert conditions at 450 – 600 °C.[4, 5] The compositions of bio-oil are very complicated and include over three hundred different organic compounds.[4, 5] Bio-oil consists of five major organic compound families: anhydro sugars, organic acids, alcohols, phenols and furans, plus some other minor components.[6] Via water separation, bio-oil can be fractionated into a water-insoluble fraction (pyrolytic lignin, i.e. PL) that accounts for ~20 wt.% of the bio-oil and a water-soluble fraction.[7]

Bio-oil has great potential to at least partially replace crude-oil.[8] However, bio-oil suffers from several key drawbacks including high water content, high acidity and incompatible with conventional fuels, severely limiting its application in practice.[9] Phase instability during storage and transportation is a major issue that limits the bio-oil utilisation as transport fuels.[10] Phase-separated bio-oils can cause severe operating problems, such as blockages, pumping problems and irregular combustion issues.[10] To date, there has been no universal tool for predicting the phase separation of bio-oils.

The study on predicting bio-oil phase separation is scarce. Only one study from Oasmaa[10] developed a ternary phase diagram of PL, a solvent mixture (i.e., the water-soluble and ether-soluble bio-oil), and a mixture of polar components (i.e., water and sugars), and a phase stability index was developed for bio-oils. However, there are at

least two limitations for that ternary phase diagram. One is that the ternary phase diagram does not cover the entire range of the three fractions. The other is that sugars should be separated from the mixture of polar components since sugars are not solvents.

1.2 Scope and Objectives

Therefore, this PhD thesis aims to carry out systematic research on ternary phase diagrams for predicting the phase stability of bio-oil. The specific objectives of this thesis are to:

- to study the effect of single/mixed model solvents on the ternary phase diagrams of pyrolytic lignin, model solvent and water;
- to develop a five-component mixed solvent (MS) based on the compositions of fast pyrolysis bio-oils and build phase diagrams of pyrolytic lignin, mixed solvent and water;
- to investigate the effect of ageing on the phase diagrams of pyrolytic lignin, mixed solvent and water;
- to assess the effect of minor components on the phase diagrams of pyrolytic lignin, mixed solvent and water;
- to evaluate the effect of temperature on the ternary phase diagrams of pyrolytic lignin, mixed solvent and water.

1.3 Thesis Outline

This thesis contents 9 chapters (this chapter included) which are listed below, with the thesis map demonstrated in Figure 1-1.

- Chapter 1 Introduction
- Chapter 2 Literature review
- Chapter 3 Research methodology

- Chapter 4 Effect of single/mixed model solvents on the phase diagrams of pyrolytic lignin, model solvent and water
- Chapter 5 Ternary system of pyrolytic lignin, mixed solvent, and water: phase diagram and implications
- Chapter 6 Effect of ageing on the phase diagrams of pyrolytic lignin, mixed solvent and water
- Chapter 7 Effect of bio-oil minor components on the phase diagrams of pyrolytic lignin, mixed solvent and water
- Chapter 8 Effect of temperature on ternary phase diagrams of pyrolytic lignin, mixed solvent and water
- Chapter 9 Conclusions and recommendations

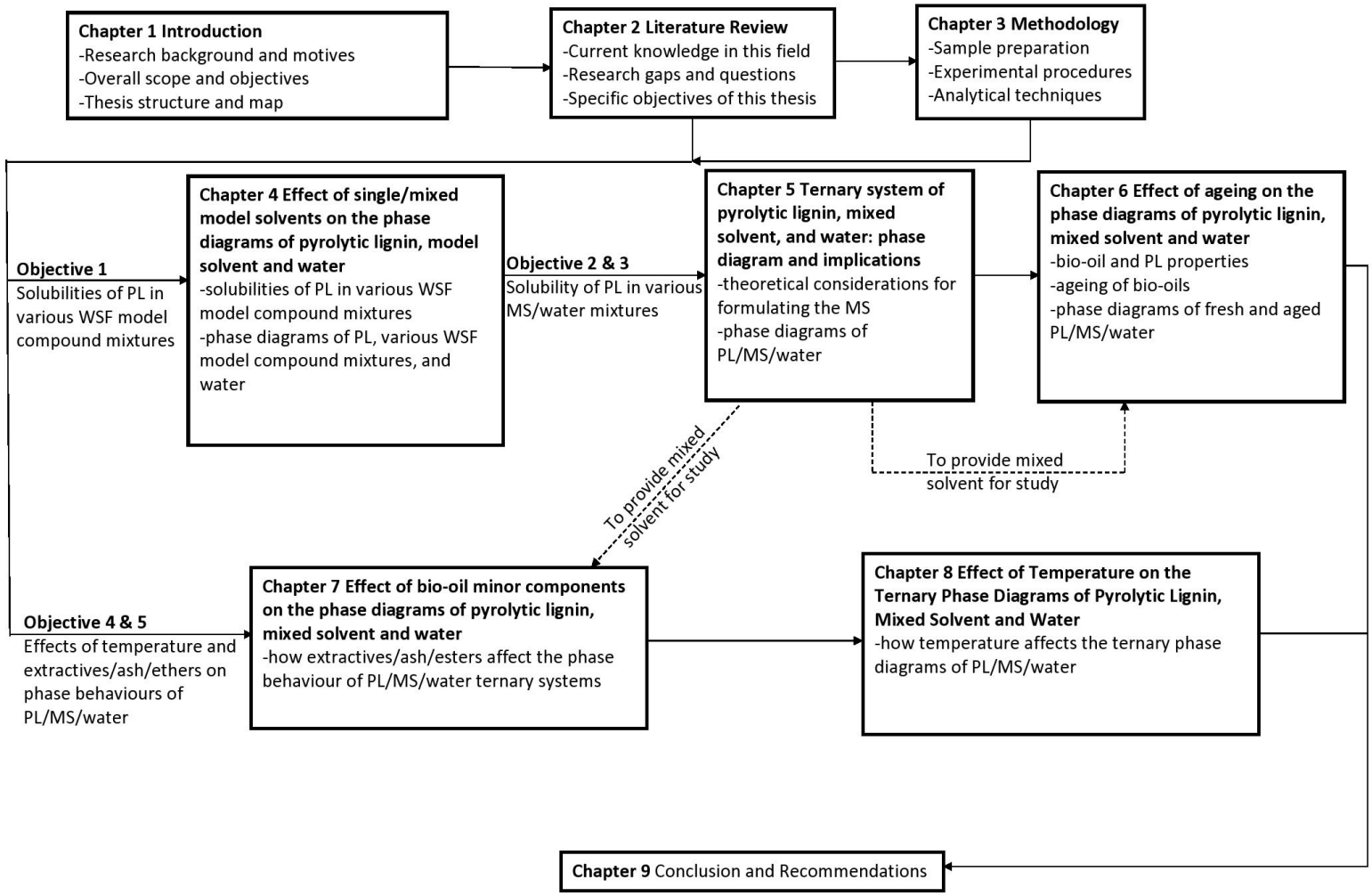

Figure 1-1 Thesis map.

Chapter 2 Literature Review

2.1 Introduction

World energy consumption has increased significantly over the past decade in contrast to the continued depletion of fossil fuel reserves.[11] Fast pyrolysis is an attractive technology to convert biomass into bio-oil, which can be used as a source for biofuels and value-added chemicals production.[4, 12] However, bio-oils have several undesired properties (e.g. high water content, high acidity, and phase instability), which hinder the commercial application of bio-oils.[13] Among these, phase instability during storage and transport could lead to severe operational problems, such as blockage, irregular combustions and pumping difficulties[10] Therefore, it is crucial to understand the phase behaviour of bio-oils before handling bio-oils and researchers should make efforts to improve the phase stability of bio-oils.

The literature review starts with the introduction of biomass fast pyrolysis, then the chemical and physical properties of pyrolysis liquids (bio-oils) are discussed, followed by the utilization of bio-oils. Also, the factors affecting the phase stability of bio-oils and strategies to improve the phase stability of bio-oils are discussed. This chapter concludes with identifying research gaps and research objectives of this PhD project.

2.2 Biomass fast pyrolysis

2.2.1 Biomass utilization

Climate change has adverse health effects globally; in 2030, many deaths will be caused by climate change according to a WHO report.[14] A feasible method to promote global decarbonisation to accomplish the climate goals of The Paris Agreement (Accord de Paris) in 2015 is to use renewable energies.[15] Bioenergy, such as biofuels, is one type of renewable energy. However, bioenergy still highly relies on direct combustion that will contribute to air pollution.[16]

Traditionally, biomass is utilized for heat generation, which accounted for 18 % of global energy consumption for heating in 2011.[17] Renewable, relatively cheap and most importantly carbon-neutral are the advantages of biomass utilization as a fuel.[18] However, some undesirable properties of biomass limit its practical application, such

as lower heating value than that of fossil fuels.[19] In addition, biomass has a poor grind ability due to its fibrous structure, which affects milling, feeding and further handling process.[20]

Biomass can be biochemically or thermochemically converted into liquid fuels to mitigate the undesirable characteristics of biomass as a direct fuel.[21] The thermochemical process is expected to have a shorter reaction time and higher yield of liquid products, in contrast to biochemical conversion.[22]

2.2.2 Thermal conversion of biomass

As shown in Figure 2-1, the thermal conversion of biomass includes pyrolysis, liquefaction, gasification and combustion.[23] Typically, the direct biomass combustion process is to generate electricity. Similarly, gas products produced by biomass gasification can also be used for heat generation. The liquefaction and pyrolysis of biomass are designed for producing liquid products. Compared to the biomass liquefaction process that requires catalysts and pressurized gas (e.g. CO, carbon monoxide) [24], biomass pyrolysis has many advantages, such as low operating cost.[25]

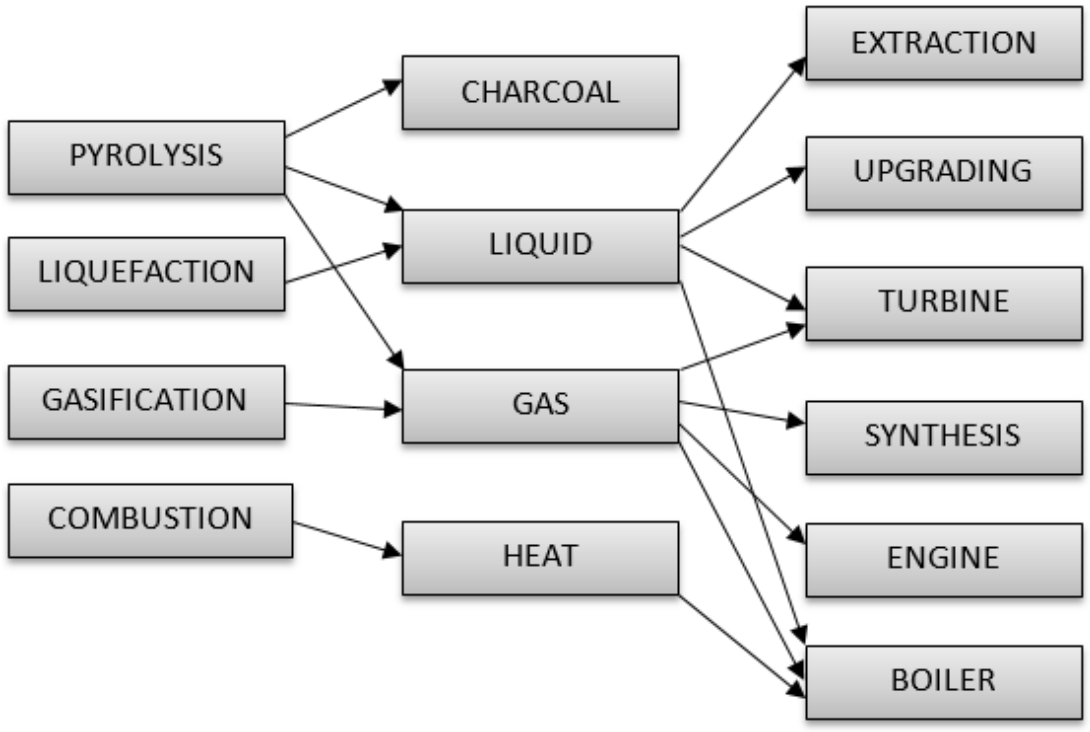

Figure 2-1 Thermal conversion of biomass and products.[23]

2.2.3 Biomass fast pyrolysis

As shown in Figure 2-2, biomass pyrolysis process converts samples to vapours, chars and gases.[26] After being condensed, the pyrolysis vapours are collected as a dark brown bio-oil. Compared with other biomass pyrolysis processes, fast pyrolysis maximizes liquid product yields.

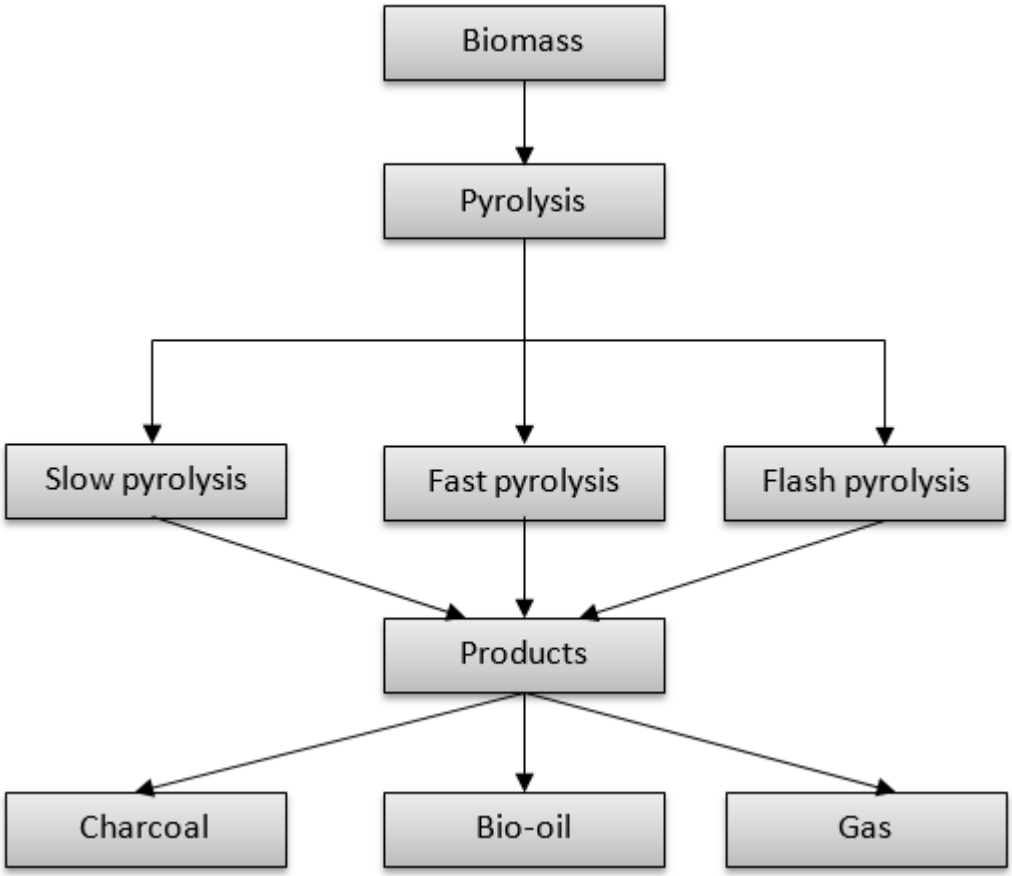

Figure 2-2 Different types of pyrolysis process.[27]

High heating and heat transfer rate. Typically, to archive high heat transfer and rates in the process of fast pyrolysis, sample particle sizes must be small (usually < 3 mm).[12]

Reaction temperature at ~500 °C. Typically, fast pyrolysis reactions for the production of bio-oils operate at 425–600 ˚C.[28, 29] Higher liquid product yields of woody biomass fast pyrolysis can be achieved around 500 °C.[23]

Short vapour residence times. Typically, the vapour residence times of fast pyrolysis should be less than 2 seconds to minimize the secondary reaction. When the residence

time is >2 s, cracking reactions of vapours can take place that significantly reduces liquid product yields.[23]

2.3 Properties of fast pyrolysis bio-oil

The compositions of fast pyrolysis bio-oils are complex, depending on biomass feedstock (e.g., softwood and hardwood),[30, 31] pre-treatment methods (e.g., particle size and moisture),[32-34] pyrolysis conditions (e.g., pyrolysis temperature)[28, 29] and collection methods (e.g. hot filtration or condensation).[35-37] A typical composition of a fast pyrolysis bio-oil sample is shown in Table 2-1. [10]

Table 2-1 Typical composition of fast pyrolysis samples.[10]

Fraction/compound	Amount (wt. %)
water	25
acids	3-7
alcohols	< 1
phenols	2-6
aldehydes, ketones	22-27
anhydro sugars	20-30
pyrolytic lignin	20

Water content

Water contents in fast pyrolysis bio-oil are usually analysed by KF titration followed by a standard procedure ASTM D1744.[38] Water in bio-oils has both positive and negative effects on the storage and utilization of bio-oil. On the one hand water in bio-oil can reduce viscosity and promote atomization,[39] On the other water reduces heating values rendering bio-oil a low-value fuel for energy use. In addition, high water contents may lead to phase separation during bio-oil storage.

Elemental composition

A CHNS/O analyser (Perkin-Elmer 2400 Elemental Analyzer or equivalent) can be used to analyse elemental compositions of fast pyrolysis bio-oils. The most important difference between fossil oils and fast pyrolysis bio-oils is that the oxygen contents of fast pyrolysis bio-oils are much higher.[40]

Chemical composition

As mentioned above, bio-oil has a very complex composition[31] A classical method, GC-MS is usually used to analyse the volatile and semi-volatile components of bio-oils.[31] Based on the percentage contribution to total detectable chromatographic areas of bio-oils, the relative contents of components can be detected. A standard analytical procedure for the characterisation of bio-oil using GC-MS has been developed by National Renewable Energy Laboratory (NREL).[41] Although GC-MS is a feasible method to identify and quantify bio-oil components, only ~50 wt % of bio-oil can be detected with GC-MS methods based on the volatilities of compounds.[42] In addition, around 15 wt % non-volatiles of bio-oils can be detected by high-performance liquid chromatography (HPLC).

Molecular weight distribution

The number average and weight average molecular weight distribution of bio-oil can be determined by gel permeation chromatography.[43] The bio-oil samples are dissolved in organic solvents and then are filtered using syringe filterers to avoid plugging of the columns from insoluble impurities.[31] Differential refractometer (RI) and ultraviolet-visible (UV) detectors are the most commonly used detectors for GPC analysis of bio-oils.[43] GPC calibration is usually made with monodisperse polymers (e.g. polystyrene and polyethylene glycol).[31]

Chemical groups in bio-oils

^{13}C NMR provides information on the carbon shifts of bio-oil components. Due to a broader chemical shift range, the most important advantage of ^{13}C NMR technique is less spectral overlap.[44] Typical ^{13}C NMR chemical shift integration regions of bio-oils were detailed reviewed by Joseph et al.[45] Methoxy/hydroxyl groups are assigned to 70-54 ppm, while carbohydrates and aromatics, alkenes are assigned to 103-70 and 163-103 ppm respectively. The carbonyl groups in bio-oils are the most distinguished between 215-163 ppm and do not overlap with the rest of the chemical groups in bio-oils.

Table 2-2 Chemical-Shift Assignments ^{13}C NMR Measurements.[45]

^{13}C NMR assignments	Chemical shift ranges
carbonyls	215-163
aromatics, alkenes	163-103
carbohydrates	103-70
methoxy/hydroxyl	70-54
alkyl	54-0

Multiphase behaviour of bio-oils

The multiphase behaviour of fast pyrolysis bio-oil is mainly attributed to complicated solubilities and reactivities of the chemicals in it.[46] Typically, bio-oil is produced in a single-phase liquid containing a small number of solids (e.g. ash and chars.).[7, 47] However, bio-oils produced from feedstocks with a high ash content usually have two phases or even three phases, because the presence of biomass ash will catalyse secondary reactions between pyrolysis vapours to give more water as by-products during the pyrolysis process, thereby promoting phase separation of bio-oil.[10] An optical microscope is the easiest method that can detect the phase behaviour of bio-oil.

Chemical and thermal stability

Due to the presence of a large number of reactive compounds, fast pyrolysis bio-oil is less stable (chemically and thermally) than fossil fuels.[48] Bio-oil is not a thermodynamic equilibrium product, and a wide range of chemical reactions may occur during the long-term storage of bio-oil that is regarded as bio-oil ageing.[49] Typical chemical reactions are listed in

Table 2-3.[49] A**s** a result, the average molecular weight and water content of bio-oil will increase during the ageing process.[50] In addition, the enhanced temperature will promote the ageing process, for example, bio-oil being stored at 80 ℃ for 24 hours equals to that after being stored at room temperature for one year.[48]

Table 2-3 Typical reactions in bio-oils related to ageing. [49]

Chemical groups	Possible reactions
organic acids	esterification
aldehydes, ketones	hydration, acetalization, oxidation
furans	polymerization
phenolic compounds	resin formation
alcohols	esterification, oxidation

Bio-oil water-soluble fraction and water-insoluble fraction

When the water content reaches 30%, the phase separation of bio-oil may occur.[43] After phase separation, there are usually two fractions: a top layer that is a water-soluble fraction and a bottom layer that is also known as pyrolytic lignin fraction. There are two methods to separate bio-oil by water addition: adding bio-oil to water and adding water to bio-oil. The first method with high water to bio-oil ratio is suitable for obtaining the PL fraction.[51] The latter one, with low water to bio-oil, is often used to collect WSF for utilization or research purposes.[43, 51] The water-insoluble fraction (PL) can be further separated into CH_2Cl_2-soluble (LMW) and CH_2Cl_2-insoluble (HMW) fractions via CH_2Cl_2 extraction.[52]

Moreover, pyrolytic lignin has some reactive functional groups that can react with other chemicals in water-soluble fraction and with pyrolytic lignin itself (water-insoluble fraction) to form polymers during storage, and pyrolytic lignin has been regarded as the major contributors to the bio-oil phase instability.[53] In the open literature, the study on the phase stability of bio-oil based on the concentrations of water, pyrolytic lignin (water-insoluble fraction), and the light organics (water-soluble fraction) is scarce. Oasmaa et al. used water-soluble fraction model compounds and pyrolytic lignin extracted from bio-oil to build phase diagrams for studying the phase behaviour of fresh and aged bio-oils. [10] However, in this study, some parts of the phase diagrams are not covered, which means the study is not

comprehensive enough.

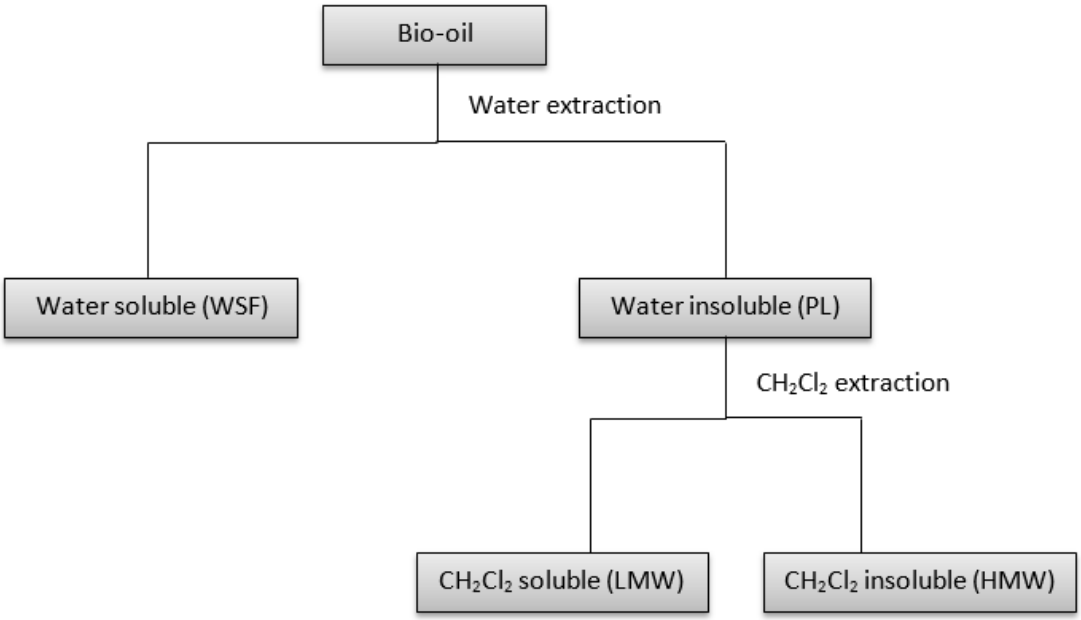

Figure 2-3 Extraction of pyrolytic lignin and its fractions from bio-oil.[52]

2.4 Bio-oil utilization

Bio-oils have a wide range of applications, including valuable chemical production, liquid fuels, heat and power generation.[5] The existing boilers need to be modified to accommodate the viscous bio-oils as fuel.[46] Although bio-oils have many applications, it is not suitable to be directly used as transportation fuels due to some undesirable properties: high viscosity, and phase instability.[54] Therefore, bio-oil upgrading is necessary for transport fuel applications.[5, 25, 55]

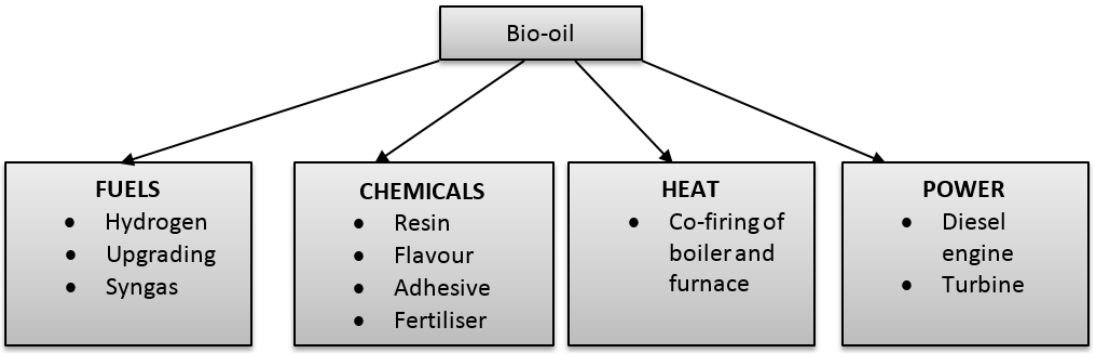

Figure 2-4 The potential applications of the bio-oils.[5]

2.4.1 Bio-oil combustion

Combustion tests were carried out by Neste in Finland to show that it is possible to partially replace light and heavy fuel oils in industrial boilers with bio-oils.[56] The combustion performance of fast pyrolysis bio-oil is similar to that of light fuels.[46]

2.4.2 Catalytic upgrading of bio-oil to transport fuels

The two main bio-oil upgrading methods are hydrotreating and catalytic vapour cracking, as discussed below.[5]

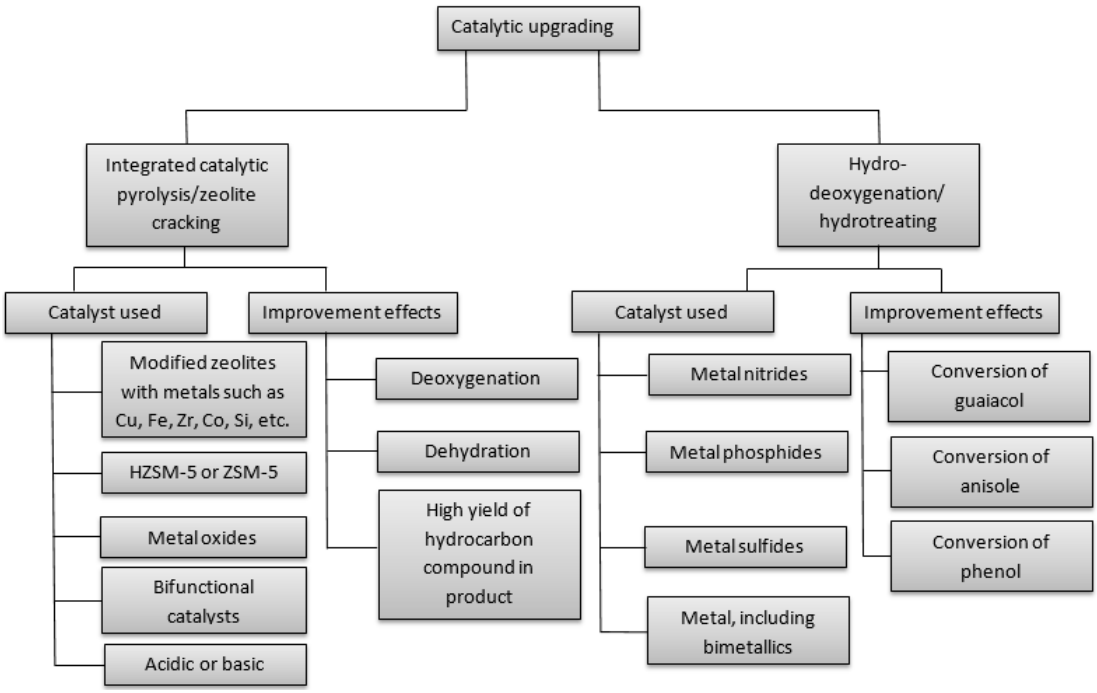

Figure 2-5 Different techniques for fast pyrolysis bio-oil upgrading. [57]

With a source of hydrogen, oxygen from bio-oil will be removed during the catalytic hydrotreating process.[5] Hydrotreating process is usually carried out at ~400 °C, and pressurized hydrogen (up to 20 MPa) with catalysts.[58] The process conditions and catalysts for hydrotreating are similar to those used in petroleum refining processes.[59] The further refining process is required to turn the hydrotreating products to transport fuels.[60] The total yield of naphtha-like products is approximately 25 wt % equivalent from biomass feedstock.[61]

Catalytic cracking aims to remove oxygen from bio-oil under mild conditions (~500 °C, 1 atm) in the presence of catalysts, which is similar to the cracking process in the petroleum industry.[5] ZSM-5 and other similar zeolite catalysts have been wildly used in the catalytic cracking process.[62, 63] The main concerns for the catalytic cracking process are coke formation, low product yield and poor product quality.[64]

2.4.3 Synthesis gas production

Bio-oil gasification is a relatively new method to produce "green" hydrocarbons. There are two major gasification types, according to gasification agents used during the process.[65] The first one is a non-catalytic partial oxidation process that produces syngas ($CO + H_2$) with oxygen (O_2) as gasification agent; and the other one is steam gasification process, which produces hydrogen (H_2) with only steam as gasification agent.[66] Water in bio-oil can be fully converted *via* the latter method. Therefore, studies have been carried out on optimizing operating conditions for bio-oil steam gasification (i.e., temperature, catalyst), to achieve higher hydrogen (H_2).[67, 68] In addition, a relatively new two-stage biomass pyrolysis/reforming (catalytic or non-catalytic) process has been used for the production of hydrogen or syngas.[69] This process has several advantages, such as it can produce syngas with the lowest tar yield, reaction temperatures in the pyrolysis and reforming process can be independently optimized and fast pyrolysis vapours can be utilized inline.[70]

2.4.4 Value-added chemicals

Over 300 chemicals have been detected in fast pyrolysis bio-oils, which are fragments originated from biomass constituents (cellulose, hemicellulose and lignin derivatives).[49] Although there are many separation methods have been reported, water addition seems to be the most feasible option.[71] As shown in Table 2-5, Ren et al. reported a case on the production of chemical groups from bio-oil by organic solvent extraction.[72] It can be seen that four fractions/groups were fractioned, including pyrolytic lignin (extracted by water), furans, ketones, phenolics (extracted by CHCl3), organic acids and levoglucosan(extracted by EtOAc).

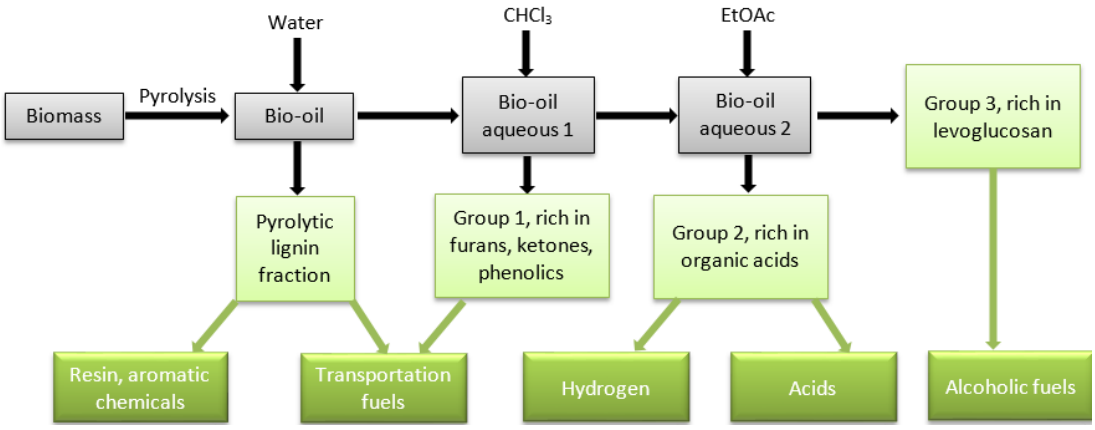

Figure 2-6 Procedures for the separation of chemical groups from the water-soluble fraction of bio-oil.[72]

Companies have commercialized the water-soluble fraction of fast pyrolysis bio-oil for more than ten years.[5] Phenolic compounds that can provide smoke flavours and as well as low molecular aldehydes (especially glycolaldehyde) that can be used as meat browning agents.[73] Red Arrows have successfully commercialized a series of food flavours.[74] Another potential utilization of the water-soluble fraction is the production of environmentally friendly road de-icers.[75] Although it may be toxic to some plants and animals depending on concentration, inorganic salts like $CaCl_2$ (calcium chloride) and NaCl (sodium chloride) are much cheaper and still be widely used as de-icer.[76] It is technically feasible to commercialize de-icers from bio-oil, but not economical at present.

Pyrolytic lignin fraction (water-insoluble fraction of bio-oil), usually accounts for 20-25 wt % of the total bio-oil.[77] Pyrolytic lignin is the oligomers derived from lignin degradation, and it has shown the potential of being utilized as an adhesive extender for waterproof coating.[78] Compared with phenol, pyrolytic lignin has lower toxicity and lower cost, which makes PL a very attractive adhesive component. Consequently, there are some resin manufacturers, such as A.C.M. Wood chemicals companies in England and Louisiana Pacific in North America have been successful in the commercialization of adhesives derived from bio-oils.[79, 80]

2.5 Factors affecting bio-oil stability

Fast pyrolysis of woody biomass usually produces a single-phase product. However, the liquid product of pyrolysis (bio-oil) can be formed of two or even more phases,

depending on pyrolysis and condensation conditions and as well as the composition of biomass feedstock.[7]

2.5.1 Biomass feedstock

The properties of biomass feedstock, for example, water contents, have a significant influence on the phase stability of bio-oil.[7, 81] Fast pyrolysis of biomass feedstock with high moisture content (> 15 wt %) usually produce bio-oil with high water content (> 25 wt %), which can easily separate into two phases.[82] The low-polarity and low-density chemicals derived from the biomass extractives can be found at the top of the bio-oil. If the content of extractives in the feedstock is high, for example, the bio-oil produced from bark biomass fast pyrolysis usually suffers from phase separation.[83] Because of the high content of extractives, there is a significant difference between the properties of the top layer and the bottom layer of bio-oil.[30] The viscosity, ash, solid content and heating value of the top layer are higher, while the contents of water and oxygen are lower.[30]

The ash content of grass biomass is usually higher, in contrast to woody biomass.[84] Although the composition of ash in biomass varies from biomass types, ash usually contains a large amount of AAEM and Si.[85] The presence of ash content in biomass samples can significantly affect the composition of bio-oil,[86] because ash can catalyse the pyrolysis reactions under some circumstances to produce more water, which will lead to the formation of an extra phase.[10] Proximate and ultimate analysis of some biomass samples for bio-oil production are listed in Table 2-4.[7]

Table 2-4 Elemental and proximate analyses of biomass used in fast pyrolysis studies.[7]

		proximate analyses (wt %, dry basis)			ultimate analysis (wt %, dry basis)				
references	biomass	ash	volatiles	fixed carbon	C	H	N	S	O (by diff.)
Garcia-Perez et al.[87]	pine	0.2-0.5	80.3	19.5	46.6-50.3	6.0-6.3	0.04-0.1	N.A.	43.3-47
Garcia-Perez et al.[87]	eucalyptus	0.5	81.9	17.6	48.4	6.3	0.1	N.A.	45.2
Jones et al. [88]	hybrid poplar	N.A.	N.A.	N.A.	50.6	6.1	0.6	N.A.	40.7
Demirbas et al.[84]	corn stover	5.1	84.0	10.9	42.5	5.0	0.8	0.2	42.6
Demirbas et al.[84]	poplar	1.3	N.A.	16.4	48.4	5.9	0.4	0.001	39.6
Demirbas et al.[84]	rice husk	22.6	61.0	16.7	47.8	5.1	0.1	N.A.	38.9
Garcia-Perez et. al[89]	sugar cane	11.3	N.A.	15.0	44.8	5.4	0.4	0.01	39.6
Demirbas et al.[84]	peach pit	1.0	N.A.	19.9	53.0	5.9	0.3	0.05	39.1
Demirbas et al.[84]	switchgrass	8.9	76.7	14.4	46.7	5.9	0.8	0.19	37.4
Demirbas et al.[84]	read oak wood	0.5	77.6	21.9	50.0	4.0	1.2	N.A.	42.4
Demirbas et al.[84]	wheat straw	13.7	66.3	21.4	41.8	5.5	0.7	N.A.	35.5
Demirbas et al.[84]	beech wood	0.5	82.5	17.0	49.5	6.2	0.3	N.A.	41.2
Demirbas et al.[84]	spruce wood	1.7	80.2	18.1	51.9	6.1	0.3	N.A.	40.9
Oasmaa et al.[90]	forest residues	2.1-3.8	73.2-76.7	N.A.	51.1-51.4	5.9-6.0	0.5	N.A.	42-32

2.5.2 Pyrolysis condition

Pyrolysis conditions (e.g. heating rate and temperature) also have a great influence on bio-oil phase stability.[87, 91] Phase separation of bio-oil can occur once the vapours are condensed due to specific pyrolysis conditions. The bio-oil produced from biomass fast pyrolysis is usually in a single-phase state, while slow pyrolysis using the same biomass tends to produce a two-phase bio-oil because more water is generated during the slow pyrolysis process.[92, 93]

High Water content (> 30 wt %) and high content of water-insoluble compounds in bio-oil have been recognized as the two factors significantly affecting the phase instability of bio-oil.[94] The other influence on phase instability of bio-oil is the concentration of water-soluble fraction of bio-oil (light organic fraction).[95] Increase in pyrolysis temperature may reduce the content of such bio-oil light organic fraction due to fragmentation reactions [96], thus increasing bio-oil instability.[49]

2.5.3 Ageing during storage and transportation

Phase separation can easily occur during storage or transportation.[30] The average molecular weight of bio-oil increases during ageing, indicating that polymerisation and condensation reactions are undergoing to form polymers.[47] Diebold detailed reviewed the reactions during ageing.[49] The carbonyl groups are the most active functional groups in bio-oil. During ageing, carbonyl groups and light molecules react with other compounds in bio-oil, resulting in the formation of water and insoluble compounds and as well as the reduction in the total amount of light molecules.[95] The increase of water content and the decrease of light molecular content during ageing will lead to phase instability of bio-oil.[93] As mentioned earlier, the polymerisation of pyrolytic lignin can also cause phase-instability during storage and transportation.[53] However, little work has been done on predicting phase stability of bio-oil based on bio-oil composition (water, water-insoluble and water-soluble fraction).

2.6 Strategies to improve phase stability of bio-oil

Most researchers focused on improving phase stability of bio-oil via hydroprocessing methods (e.g. hydrogenation, hydrocracking), which needs severe reaction condition, such as high temperature or high pressure.[55, 97, 98] However, there are also feasible

strategies to enhance phase stability of bio-oil by simply adding solvents and/or mixing with other fuels.[99]

2.6.1 Organic Solvents addition

As shown in Table 2-5,[7] it is clear that the addition of solvents is a feasible way to improve the phase stability of bio-oil. The effect of organic solvent on the physical and chemical properties of bio-oil has been studied by researchers.[99, 100] Some of these studies focused on improving the phase stability of bio-oil by using simple dilution effects.[101] Others were trying to reduce the effects of reactive chemicals (e.g. ketones, acids) by adding stabilizers (mostly alcohol) to enhance the thermal and chemical stability of bio-oil.[100] Considering the positive effects on the bio-oil properties and its feasibility, solvent addition has been treated as one of the most useful methods for upgrading bio-oils.[102-104] Recently, some papers on the combustion of bio-oils with organic solvents were published, such as VTT bio-oil blends with diglyme tested using a diesel engine by CNR - Engine Institute in Italy,[105] bio-oils blends with ethanol tested in a gas turbine combustor to generate electricity.[106] The combustion and injection characteristics of bio-oil organic solvents blends were compared with those of standard petroleum fuel. The spray characteristics of bio-oil/ethanol blends were similar to those of petroleum fuel.

Table 2-5 Effect of adding solvents on bio-oil phase stability

bio-oil	solvent used	Observation
forest residue oil	alcohols	The rate of bio-oil ageing is drastically decreased with the presence of alcohols, as measured by the viscosity of the bio-oil. [103]
wood oil	ethyl acetate, methanol, acetone, methanol, etc.	Solvents were used for stabilizing the whole bio-oil during long-term storage.[103]
forestry residue oil	isopropanol	The solubility of water-insoluble fractions has been significantly increased with the addition of alcohols into bio-oil.[35, 99]
BTG oil	alcohols	Alcohols are used as catalytic esterification reagents at 60 °C in the presence of an acid catalyst and a dehydrating agent.[107, 108]
an anonymous commercial supplier	glycerol and methanol	During ageing, the viscosity and acidity of the bio-oil decreased while water content increased.[109]
mallee wood oil	methanol in the presence of acid catalysts	Formation of esters and ethers during the acid catalysed reactions. [110, 111]
wood chips oil produced from a circulating bed unit	methanol in the presence of acid catalysts	No phase separation was observed during ageing. The acidity and viscosity of the oils decreased while thermal stability improved significantly.[112]

Recently, substantial research was carried out by A. Oasmaa *et al.* on adding a model solvent mixture into both fresh and aged bio-oils.[10] In this study, bio-oil was regarded as a mixture of three pseudo-components: a solvent fraction (light oxygenated compounds), a polar fraction (water and sugars), and a nonpolar water-insoluble fraction (PL fraction). Phase diagram describing the compositions of bio-oils are developed by the authors, as shown in Figure 2-7.[10] However, there are at least two limitations for that ternary phase diagram. One is that the ternary phase diagram does not cover the entire range of the three fractions. The other is that sugars should be separated from the mixture of polar components since sugars are not solvents.

Consequently, the phase diagrams are not suitable for predicting the phase stability of bio-oils, and more work in this field is required to bridge the knowledge gap.

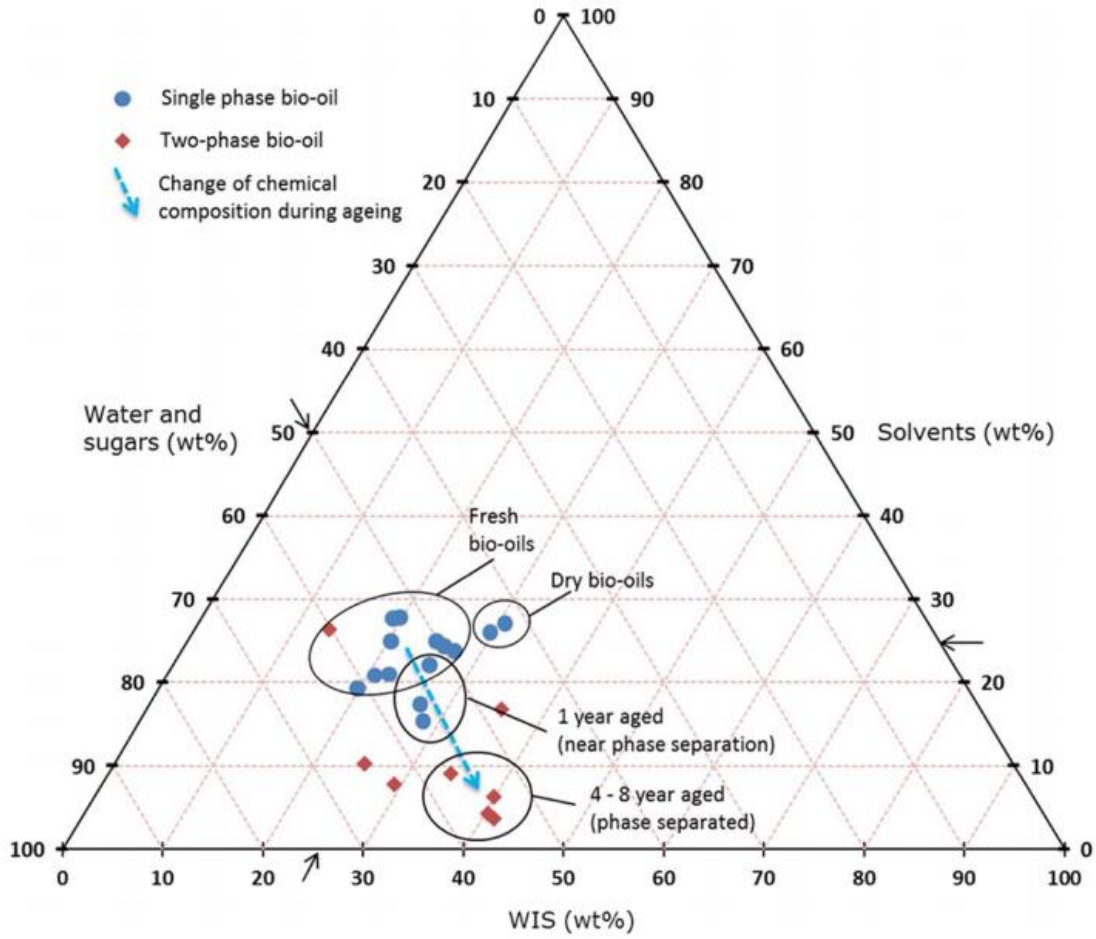

Figure 2-7 Ternary-phase diagram of phase stability based on chemical composition and homogeneity of fresh and aged bio-oils.[10]

2.6.2 Bio-oil blends with other Fuels

Due to its high water and oxygen content, the solubility of bio-oil in mineral oil is very low. However, if co-solvents are used, it is possible to prepare homogeneous blends of bio-oil and other fuels. Adjaye and Bakhshi examined the solubility of bio-oil with diesel, with the aid of organic solvents at different temperatures.[113] The diesel tend to have the best solubility in bio-oil/methanol mixtures (bio-oil/methanol=9:1), with a ratio of 3: 7 (bio-oil/methanol mixtures: diesel). However, the diesel layer was

eventually separated after 4h. The stability time of the blends increased as the proportion of diesel was decreased.

Weeracahnci et al. had studied phase behaviours and fuel properties of bio-oil/diesel/alcohol blends.[114] Phase diagrams were involved in that study to determine the area of complete solubility. Butanol is a better co-solvent than ethanol, but a large number of alcohols are required to achieve a homogeneous bio-oil/diesel/alcohol mixture.

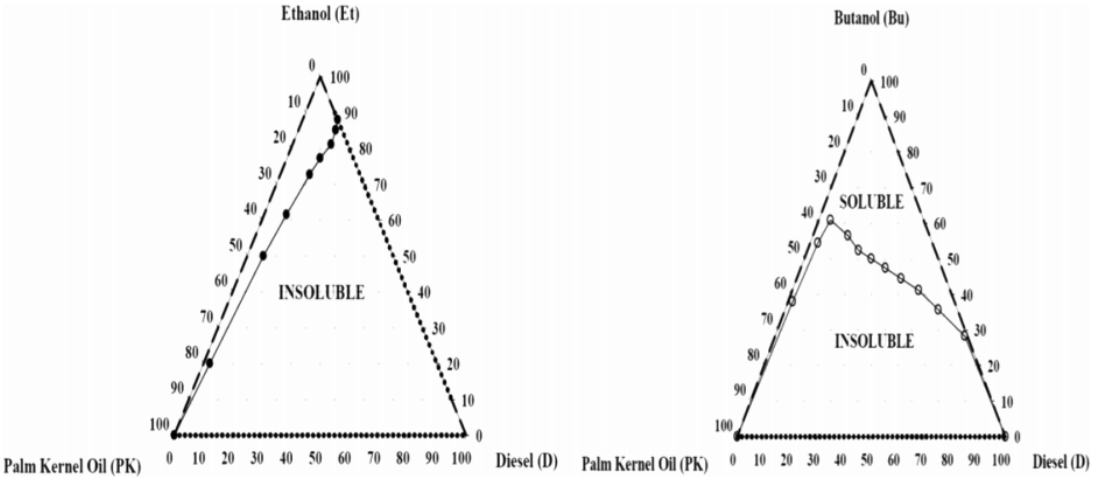

Figure 2-8 Phase behaviour of three-component system.[114]

Recently, PYTEC has successfully achieved the application of bio-oils and diesels blended before combustion for a diesel engine.[115] The injector and pumps were specially designed only for this blend. The bio-oil/diesel oil blends, with a volume ratio of 96: 4, was fed into a special designed high-pressure engine and up to twelve hours of operation were recorded.

2.6.3 Bio-oil based emulsions with other fuels

Although bio-oils are not completely soluble in mineral oils, or vice versa, due to the considerable difference in chemical and physical properties, they can form emulsions. Bio-oil based emulsions with other fuels were a promising method for stabilizing bio-

oil and as well as the introduction of bio-oils into fuel markets. Chiaramonti et al. developed emulsified bio-oils (with diesel) in the proportion of 25%, 50% and 75%, and found that the emulsions were stable than raw bio-oils.[116, 117] The viscosity of the emulsion increases with the increase of bio-oil content. The range of emulsifiers should be 0.5-2.0 % to provide acceptable viscosity. Ikura et al. prepared an emulsion of bio-oil light fractions (obtained by centrifugation) and No.2 Diesel with the aid of surfactants.[118] The cost of preparing a stable emulsion was around 2.6 cents per Litre for 10% emulsion. The viscosity of 10% emulsion is much lower than that of raw bio-oil, and its corrosiveness is about half that of raw bio-oil. Emulsification does not require complex chemical reactions. However, high energy consumption cannot be ignored, and corrosiveness to engines is evitable.

2.7 Conclusion and Research Gaps

Based on the above literature review, it could be summarized that:

1) Fast pyrolysis is a promising technology converting biomass into liquid products (bio-oil) that can partially replace non-renewable fossil fuels. However, the undesired features (i.e., phase-instable, incompatible with traditional fuels.) hinder the utilization of bio-oils.
2) Phase separated bio-oil may cause some serious problems including blockages and irregular combustions. As bio-oil is a relatively new product in the global energy market, there are no guidelines on how to handle bio-oil properly and prevent bio-oil phase separation.
3) The studies on how to predict bio-oil phase stability are insufficient. The only existing tool based on the compositions of pyrolytic lignin/a mixture of light compounds/a mixture of polar components for predicting bio-oil phase separation has its limitations. It does not cover the whole range of the three fractions, which means this is an incomplete tool.

4) Fast pyrolysis bio-oil is not thermodynamic stable, and various chemical reactions can take place during transport and storage — for example, condensation reactions and self-aggregation of functional groups on the water-insoluble fractions (pyrolytic lignin). The ageing reactions lead to an increase in the content of pyrolytic lignin fraction, which may further cause phase instabilities of bio-oils. Moreover, the study on how the water-insoluble fractions affect the bio-oil phase stability is scarce.

Therefore, further research and development should be carried out in the above research area, including:

1) Developing a mixed solvent based on the composition of bio-oils in the existing literature to represent the water-soluble fractions. As bio-oil can be considered as a mixture of three pseudo-components: water-insoluble fraction (PL), water-soluble fraction, and water. It is important to understand the composition of the water-soluble fractions and develop a mixed solvent to represent the water-soluble fractions.
2) Preparation of various PL samples. The pyrolytic lignin is cracked polymer (derived from lignin pyrolysis) with broad molecular weight distribution, containing all kinds of phenolic compounds, and even large lignin polymers. Due to this, different pyrolytic lignin samples may have different effects on phase behaviour.
3) Phase diagrams of various PLs (pyrolytic lignin)/MS (mixed solvent)/water ternary systems. A ternary phase diagram shows three variables that sum to a fixed value (usually 100 %.), which is widely used to exhibit the phase behaviour of a ternary system containing the three components. Therefore, ternary phase diagrams can also be used in this case to predict the phase behaviours of bio-oil samples.

2.8 Research objectives

As identified by the previous literature review and discussion, there are several research gaps in this field. However, it is unlikely to fill all the gaps in the study within the limited time of this PhD study. Therefore, this study will focus on the following objectives:

(1) To study the effect of single/mixed model solvents on the ternary phase diagrams of pyrolytic lignin, model solvent and water
(2) To develop a five-component mixed solvent (MS) based on the compositions of fast pyrolysis bio-oils and build phase diagrams of pyrolytic lignin, mixed solvent and water
(3) To investigate the effect of ageing on the phase diagrams of pyrolytic lignin, mixed solvent and water
(4) To assess the effect of minor components on the phase diagrams of pyrolytic lignin, mixed solvent and water
(5) To evaluate the effect of temperature on the ternary phase diagrams of pyrolytic lignin, mixed solvent and water

Chapter 3 Research Methodology and Analytical Techniques

3.1 Introduction

This chapter presents the research methodologies applied for the study targeting at the objectives outlined in Chapter 2. The experimental and analytical techniques are detailed in the following sections.

3.2 Methodology

To achieve the main research objectives outlined in Section 2.8, a series of experiments had been carried out, including:

1) Solubilities of PL in various model compound mixtures, and the construction corresponding phase diagrams of PL/model compound mixtures/water;
2) Preparation of MS (mixed solvent) to construct phase diagrams of PL/MS/water;
3) Phase diagrams of PL (from both fresh and aged bio-oil), mixed solvent and water were constructed;
4) Addition of bio-oil minor compounds into phase diagrams of PL/MS/water mixtures;

Figure 3-1 presents the overall research methodology with the methodology description of each research objective detailed below.

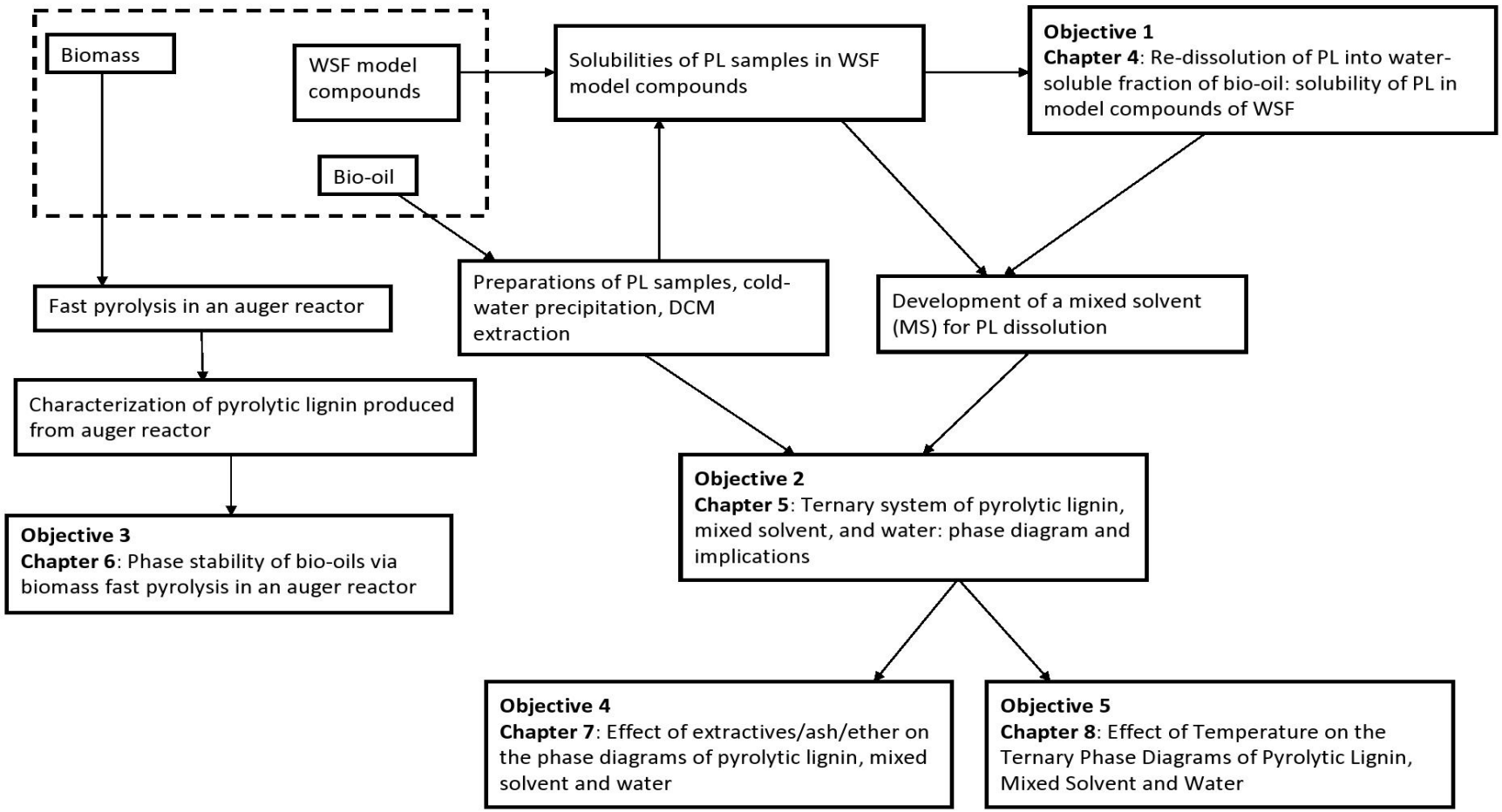

Figure 3-1 Research methodology

3.2.1 The solubility of pyrolytic lignin in model compounds of the water-soluble fraction

The PL sample was prepared from bio-oils via cold-water precipitation. The solvent mixtures were prepared by mixing bio-oil water-soluble fraction model compounds. Properties of the PL sample were also analysed, such as ultimate and proximate, molecular weight distribution (Mw). The homogeneity of the PL/solvent mixtures/water mixtures were quantified using an optical microscope (Olympus SL 60/61). The results and discussions of this work are detailed in chapter 4.

3.2.2 Developing phase diagrams of PL and its fractions, mixed solvent, water systems.

The used PL samples (PL and its fractions) and a mixed solvent (denoted as "MS") were produced accordingly. A series of phase diagrams of PL and its fractions, mixed solvent and water were then constructed. The effect of free sugar (represented by levoglucosan) on phase diagrams of PL/MS/water was also studied. Chapter 5 describes the results and discussions of this work.

3.2.3 Phase diagrams of PL samples from fresh bio-oils, mixed solvent and water systems.

The fresh bio-oil samples were produced via biomass fast pyrolysis in an auger reactor. A set of bio-oil accelerated ageing experiments were conducted. The PL samples (from both fresh and aged bio-oils) were prepared accordingly. Then phase diagrams of PL samples/MS/water were constructed. Chapter 6 clarifies the results and discussions about this work.

3.2.4 Effect of extractives/ash/esters on phase diagrams of PL, mixed solvent and water

To investigate the effect of extractives/ash/esters on phase diagrams of PL/MS/water, model compounds representing extractives/ash/esters were selected and their contents were based on open literature. All the chemicals were purchased from Sigma−Aldrich and used without further purification, if not stated otherwise. Further phase diagrams of PL/MS/water with the addition of extractives/ash/esters were constructed. The results and discussions about this work are presented in chapter 7.

3.2.5 Effect of temperature on phase diagrams of PL, mixed solvent and water

The solubility parameters of PL and as well as MS at different temperatures were calculated. Further phase diagrams of PL/MS/water at different temperatures were constructed. The effects of levoglucosan on phase diagrams of PL/MS/water at different temperatures were also studied. The results and discussions about this work are presented in chapter 8.

3.3 Experimental Section

3.3.1 Sample preparation

Bio-oil. The bio-oil sample used in this thesis was provided by an anonymous company. The obtained bio-oil sample was stored at ~4 °C before used for further experiments.

Mallee and pine biomass. The mallee and pine wood biomass were cut and sieved into size fraction of 250-500 μm and then stored in a fridge at ~4 °C before further experiments.

Fresh bio-oils. The fresh bio-oil samples were produced from biomass fast pyrolysis via auger reactor. The obtained bio-oil sample was stored at ~4 °C before used for future experiments.

Pyrolytic lignin and its fractions. The PL sample used in this study was prepared from bio-oil via cold water precipitation.[119, 120] Briefly, bio-oil was added dropwise to ice-cooled water, and magnetic stirring was used for mixing. The bio-oil to water ratio was

kept at 100 to 1. Subsequently, the pyrolytic lignin was filtered, transferred into DI water, and slowly stirred for overnight in order to wash out water-soluble products. Finally, the mixture was filtered again and the pyrolytic lignin was dried carefully under vacuum at room temperature. The PL sample was further separated into CH_2Cl_2-soluble fraction (denoted as "PL-LMW" sample) and CH_2Cl_2-insoluble fraction (denoted as "PL-HMW" sample) *via* CH_2Cl_2 extraction (m:m = 1:1).[119, 120] After extraction, the solvent was evaporated at 40 °C and the PL and its fractions were stored in a lab desiccator at room temperature before further analysis.

Water-soluble model compound mixtures. The model compounds and their solvent mixture ratios are selected based on compositions of bio-oils from a wide range of feedstocks and reactors used for fast pyrolysis reviewed in previous works.[121] Acetic acid, hydroxyacetone, furfural, phenol and methanol are selected as model compounds to represent a water-soluble fraction of bio-oils, and their ratios are selected based on extreme conditions of their compositions in various bio-oils.

3.3.2 Theoretical Considerations for Formulating the MS

The MS was formulated based on major compositions of bio-oils from a wide range of feedstocks and reactor systems in literature [6, 13, 26, 49, 122-135] (as listed in Table 3-1.). The key idea is to use the MS to substitute the light organic fraction that bridges water and PL in bio-oil. Table 3-1 lists the light fraction of bio-oil that is categorized into several chemical families with the respective average compositions. It can be seen that there are five major chemical families (i.e., acids, phenols, aldehyde and ketones, furans and alcohols, respectively) that represent approximately 80 wt % of the light fraction of bio-oil (excluding PL and water). It is, therefore, possible to develop an MS based on the five major chemical families via calculating the average compositions of different chemical families on water and PL free basis. To further simplify the solvent mixture, the five chemical families are represented by five model compounds (i.e., acetic acid, phenol, hydroxyacetone, furfural, methanol, respectively) in the

Table 3-1 Literature data on the compositions of fast pyrolysis bio-oils.[6, 13, 26, 49, 122-135]

fraction/main compounds	content (wt %, dry basis)	content (wt %, on water and PL free basis)	average content (wt %, on water and PL free basis)	average content in five major chemical families
pyrolytic lignin	16.0-35.0	N.A.	N.A.	N.A.
acids	12.5-25	18.5-36.5	27.5	35.0
acetic acid	3.0-15.0			
formic acid	0.9-7.6			
propionic acid	0.2-1.3			
butanoic acid	0.2-0.5			
pentanoic acid	0.1-0.8			
isocrotonic acid	0.1-1.2			
butanoic acid, 2-hydroxy-	0.1-1.0			
phenol and phenol derivates	5.0-10.0	7.5-14.5	11.0	14.0
phenol	0.1-5.0			
cresol (o-cresol, m-cresol and p-cresol)	0.3-1.5			
catechol	0.6-3.0			
guaiacol	0.8-2.5			
aldehydes and ketones	8.5-25	12.5-36.5	24.5	31.5
hydroxyacetone	1.2-9.5			
glycolaldehyde (unstable, exist as dimers)	0.5-8.0			
acetaldehyde	0.1-2.0			
acetone	0.1-3.0			
linear ketones (pentanone, octanal etc.)	0.1-2.0			
cyclic ketones (c5 and c6 cyclic ketones)	0.5-5			
furan and furan derivates	5.0-10.0	7.5-14.5	11.0	14.0
furfural	1.0-5.0			
2(5h)-furanone	0.1-1.5			
furfural alcohol	0.1-1.0			
methylfurfural	0.1-0.8			
alcohols	1.0-5.0	1.5-7.5	4.5	6.0
methanol	0.5-3.5			
ethanol	0.2-1.5			
ethylene glycol	0.2-1.0			
sugars	3.0-7.0	4.5-10.0	7.3	N.A.
levoglucosan	0.5-3.0			
cellobiosan	0.2-3.0			
glucose	0.4-1.3			
esters and ethers	1.0-2.0	1.5-3.0	2.3	N.A.
methyl butanoate	0.1-1.3			
acetic anhydride	0.1-1.3			
methyl pyruvate	0.1-0.5			
propane, 1-ethoxy-2-methyl-	0.3-1.0			
alkene and alkane	1.0-2.0	1.5-3.5	2.5	N.A.
decane	0.1-0.2			
octadecane	0.1			
2-hexene	0.1			
cyclic alkanes and alkenes	<1.0			
nitrogen compounds	<1.0	<1.0	<1.0	N.A.
aniline	0.1			
pyridine	0.1			
2-hydroxypyridine	trace			
aromatics	<1.0	<1.0	<1.0	N.A.
benzene	trace			
tolune	trace			
naphthalene	trace			

N.A.: Not applicable

formulated MS. Therefore, the weight percentages of five model compounds in the MS are chosen based on the average weight percentages of each chemical family in the mixture of five major chemical families. This leads to the development of an MS with the composition of 33.3 wt % of acetic acid, 33.3 wt % of hydroxyactone, 13.3 wt % of phenol, 13.3 wt % of furfural and 6.8 wt % of methanol. Therefore, based on the composition of the MS and the solubility parameter of each model compound in Table 3-2, the solubility parameter of the MS can be estimated, i.e. δ_{MS} = 11.99 $cal^{1/2}$ $cm^{-3/2}$.

Table 3-2 Composition of the formulated MS in this study.

selected compound for the solvent	content (wt %)	solubility parameter (δ, $cal^{1/2}$ $cm^{-3/2}$)[136]
acetic acid	33.3	10.45
hydroxyacetone	33.3	13.08
phenol	13.3	11.78
furfual	13.3	12.14
methanol	6.8	14.48

3.3.3 Development of Ternary Phase Diagrams

Development of ternary phase diagram follows a previous method.[109] Briefly, the experiment starts with the insoluble PL/water mixture of different concentrations followed by progressively adding small amounts of the solvent into the mixture until a homogeneous mixture is recorded with an optical microscope (Olympus SL 60/61). As PL cannot dissolve instantaneously, ultrasonic mixing for approximately 30 minutes was introduced to ensure the dissolution equilibrium. The standard deviation of the experiments is within 1.0 % of the whole mixture (based on the weight percentage of MS in the mixture system). It is also noted that the phase diagrams reported in this study are constructed at room temperature (25 ℃).

3.3.4 Accelerated ageing of bio-oil

Fresh bio-oil samples were sealed in Pyrex glass containers and left in an oven at 80 °C for 24 h, following the method detailed elsewhere.[50] Phase separation of both bio-oil samples occurred after 24h accelerated ageing. After ageing experiments, the samples were cooled in an ice bath. The weight of these samples was recorded before and after the accelerated ageing process in order to detect any weight loss. Only when no measurable weight loss was detected, the aged samples were then stored in a lab fridge at ~4 °C for further experiments.

3.3.5 Catalytic esterification of bio-oils

The catalytic esterification of bio-oils were performed at 170 °C in a batch reactor, following a previous method [137]. Briefly, ~30 g of the reaction mixture (methanol and bio-oil in a mass ratio of 0.9:1) and 6 wt% solid acid catalyst (Amberlite, strongly acidic) were added into the batch reactor. After purging with helium to remove air in the reactor, the reactor was placed vertically in a fluidized sand bath (model: Techne SBL-2) and preheated the reactor to desired reaction temperature in 3 min. After holding at the reaction temperature for 1 hour, the reactor was immediately transferred into an ice-water bath for rapid cooling.

3.3.6 Calculation of solubility parameters of MS/water mixtures at different temperatures

The solubility parameter δ is defined as the square root of the cohesive energy density (E_{CED}, the evaporative internal energy of a volume unit of molecular) [138], according to Equation (3-1):

$$\delta = \sqrt{E_{CED}} = \sqrt{\frac{\Delta H_{vap} - RT}{V_m}} \qquad (3\text{-}1)$$

where enthalpy of vaporization (ΔH_{vap}) and molar volume (V_m) are both affected by the temperature.

To determine the solubility parameter of MS at different temperatures, the values of ΔH_{vap} and V_m for five model compounds are required. The ΔH_{vap} and V_m values at different temperatures were obtained either from literature (i.e., ΔH_{vap} of acetic acid [139], furfural[140], methanol[141] and water[142], and V_m of furfural [143], methanol [144], phenol[145] and water [146]) or calculated based on the Joback/Reid group contribution method [147]. As shown in Table 3-3, the values of the solubility parameter of the MS at 0, 25 and 40 °C are determined to be 12.36, 11.99 and 11.66 $cal^{1/2}\ cm^{-3/2}$, respectively.

Table 3-3 Solubility parameter of the chemicals at different temperature.

	solubility parameter at 0 °C, δ ($cal^{1/2}\ cm^{-3/2}$)	solubility parameter at 25 °C,[a] δ ($cal^{1/2}\ cm^{-3/2}$)	solubility parameter at 40 °C, δ ($cal^{1/2}\ cm^{-3/2}$)
acetic acid	10.78	10.45	10.18
hydroxyacetone	13.71	13.08	12.80
phenol	12.04	11.78	11.57
furfural	12.52	12.14	11.94
methanol	14.89	14.48	14.01
water	23.84	23.37	23.17
MS	12.36	11.99	11.66

3.4 Instruments and Analytical Techniques

3.4.1 Ultimate and proximate analysis

The proximate analysis was conducted using a thermogravimetric analyser (Mettler-Toledo Star 1). The elemental compositions of all PL samples were determined using an elemental analyser (PerkinElmer 2400 Series II).

3.4.2 UV-fluorescence Spectroscopy

The proximate The UV fluorescence spectra of all PL samples were obtained using a fluorescence spectrometer (Perkin-Elmer LS 55). The analysis was carried out using synchronous scan mode with a slit width of 2.5 nm and a constant energy difference of −2800 cm^{-1}, following a method detailed elsewhere.[135] Each PL sample was dissolved in methanol to a final concentration of 10 ppm and filtered through a 0.45 um filter paper for analysis.

3.4.3 Molecular weight distributions

Molecular weight distributions of PL and its fractions were analysed by gel permeation chromatography (GPC), following a previous method. Different samples were dissolved in 1000 ppm tetrahydrofuran (THF) solution, then filtered by a 0.45 μm polyvinylidene difluoride (PVDF) syringe filter (Thermo Scientific). Subsequently, the dissolved samples were analyzed by a GPC system (Varian 380-LC) equipped with an ultraviolet (UV) detector, using a set of two PLgel columns (Agilent, PLgel, 3 μm, 100 A, 300 × 7.5 mm). THF was used as the eluent at a flow rate of 1.0 mL/min for GPC analysis. Phenol and polystyrene with the molecular weight range of 94− 4120 Da were used as standards.

3.4.4 G/H/S ratios

It is known that PL contains three different types of phenolic units, i.e., guaiacyl (G), p-hydroxyphenyl (H), and syringyl (S), respectively. The G/H/S ratios for the PL and its fractions were determined using a ^{13}C nuclear magnetic resonance (NMR) spectrometer (Bruker AV500) at 125.771 MHz according to a method detailed elsewhere. In each analysis, ∼100 mg of PL (or its fractions) was dissolved in ∼0.55 mL of dimethyl sulfoxide (DMSO)-d_6. The ^{13}C NMR spectrometric data were recorded at a pulse angle of 90°, a relaxation delay of 1.5 s, and an acquisition time of 0.08 s for a total of 48 scans.

3.4.5 Solubility parameters

The solubility parameters are known for the three different types of phenolic units, i.e., δ_G = 13.52 $cal^{1/2}$ $cm^{-3/2}$ for guaiacyl, δ_H = 14.12 $cal^{1/2}$ $cm^{-3/2}$ for p-hydroxyphenyl, and δ_S = 14.23 $cal^{1/2}$ $cm^{-3/2}$ for syringyl. Based on the G/H/S ratios determined using the ^{13}C NMR method, the solubility parameter of the PL can be calculated.

3.4.6 Optical imaging

Optical images of selected mixtures were acquired using an optical microscope (Olympus SL 60/61).

3.4.7 IC analysis

The contents of sugar were quantified by a high-performance anion-exchange chromatography with a pulsed amperometric detector (HPAEC-PAD) *via* a Dionex ICS-3000 ion chromatography (IC) system equipped with CarboPac PA20 analytical and guard columns. The water-soluble fraction of bio-oils were directly analysed by HPAEC-PAD using a special gradient program developed in our previous work for achieving a good separation of sugars.[148]

3.5 Summary

Bio-oil is produced from pine and mallee wood biomass fast pyrolysis in a lab-scale auger reactor, and bio-oil accelerated ageing experiments were also conducted. Pyrolytic lignin (PL) samples were obtained from various bio-oil samples (including both fresh and aged) via cold-water precipitation. Properties of PL samples were investigated according to the analytical techniques presented in section 3.4, such as ultimate and proximate analysis, average molecular weight, G/H/S ratio, and solubility parameter etc. The sugar contents of some fresh and aged bio-oils were also quantified using the method described in section 3.4. A series of phase diagrams of pyrolytic lignin, mixed solvent and water were constructed. The results from experiments led to a better understanding of the phase stability of bio-oils.

Chapter 4 Effect of Single/Mixed Model Solvents on the Phase Diagrams of Pyrolytic Lignin, Model Solvent and Water

4.1 Introduction

As reviewed in section 2, ternary phase diagram is a useful, straightforward, and important tool to understand, predict and control the phase behaviour of bio-oil. Chiaramonti et al. constructed phase diagrams of bio-oil/diesel fuel/emulsifier to examine the best ratios for phase stability, engine performance and operating cost. [117] Recently, Oasmma et al. reported adding a solvent mixture into bio-oils to improve phase stability and constructing phase diagrams to propose an index that can be used to represent the phase stability of bio-oils.[10] However, little work has been done on the PL solubilities in different solvent mixture/water systems.

Therefore, this study focuses on the PL solubilities in various model solvent/water systems and the ternary phase diagrams of PL, model solvents and water, taking into account various model solvents that are formulated from single to multiple components. The C, H, N and O (by difference) contents of the PL sample used in this chapter were determined to be 67.1, 6.2, 0.2, 26.5 wt % on a dry basis, respectively. The average molecular weight of the PL sample was determined to be 660 g/mol on a GPC system. The δ value of the PL used in this study is determined to be 13.95 $cal^{1/2}cm^{-3/2}$. Model solvents selected in this study is detailed in Table 4-1.

Table 4-1 Model solvents selected in this study

model solvent	ratios selected	solubility parameter, [a] δ ($cal^{1/2}$ $cm^{-3/2}$)
single-component model solvent		
acetic acid (denoted as “AA”)	N.A. [b]	10.45
hydroxyacetone (denoted as “HA”)	N.A. [b]	13.08
furfural (denoted as “FU”)	N.A. [b]	12.14
phenol (denoted as “PH”)	N.A. [b]	11.78
methanol (denoted as “ME”)	N.A. [b]	14.48
two-component model solvent		
acetic acid-furfural (denoted as “AA-FU”)	1:1, 2.5: 1, 5:1	11.30, 10.93, 10.73
acetic acid-phenol (denoted as “AA-PH”)	1:1, 2.5: 1, 5:1	11.12, 10.83, 10.67
hydroxyacetone-furfural (denoted as “HA-FU”)	1:1, 2.5 : 1, 5:1	12.61, 12.81, 12.92
hydroxyacetone-phenol (denoted as “HA-PH”)	1:1, 2.5 : 1, 5:1	12.43, 12.71, 12.86
methanol-furfural (denoted as “ME-FU”)	1:1	13.31
methanol-phenol (denoted as “ME-PH”)	1:1	13.13
three-component model solvent		
acetic acid-hydroxyacetone-methanol (denoted as “AA-HA-ME”)	5:5:1	12.01
acetic acid-hydroxyacetone-furfural/phenol (denoted as “AA-HA-FU/PH”)	5:5:2	11.83/11.77
acetic acid-methanol-furfural/phenol (denoted as “AA-ME-FU/PH”)	5:1:2	11.38/11.29
hydroxyacetone-methanol-furfural/phenol (denoted as “HA-ME-FU/PH”)	5:1:2	13.02/12.93
four-component model solvent		
acetic acid-hydroxyacetone-methanol-furfural/phenol (denoted as “AA-HA-ME-FU/PH”)	5:5:1:2	12.03/11.98
acetic acid-hydroxyacetone-furfural-phenol (denoted as “AA-HA-FU-PH”)	5:5:2:2	11.82
acetic acid-methanol-furfural-phenol (denoted as “AA-ME-FU-PH”)	5:1:2:2	11.46
hydroxyacetone-methanol-furfural-phenol (denoted as “HA-ME-FU-PH”)	5:1:2:2	12.77

[a] For chemical compounds, data are taken from the literature[149] while those for mixed model solvent are calculated based on the composition of the mixed solvent.[149] [b] not applicable.

4.2 Phase Stabilities of Model Solvent/Water Mixtures

To investigate the PL solubilities in various model solvent/water mixtures and construct the ternary phase diagrams of various PL/model solvent/water systems, it is important to understand the phase stabilities of various model solvent/water mixtures. Among the five components in the MS solvent, acetic acid, hydroxyacetone and methanol are miscible with water, but phenol and furfural are generally immiscible with water depending on the content. Therefore, the phase stabilities of phenol and furfural in AA/water, HA/water, and ME/water mixtures were first studied. The ternary phase diagrams of various FU(or PH)/model solvent/water systems were constructed, and the results for furfural and phenol are shown in Figures 4-1 and 4-2, respectively. Several important findings can be observed from those results.

First, the binary solvent/water systems confirm that acetic acid, hydroxyacetone and methanol are completely miscible with water. Furfural is miscible with acetic acid, hydroxyacetone and methanol. It can form two different homogeneous binary systems with water, i.e., organic-rich system at low water contents (i.e., <5 wt%) and water-rich systems at high water contents (i.e., >96 wt%). This indicates the low solubility of furfural in water to form a homogeneous water-rich system and the low solubility of water in furfural to form a homogeneous organic-rich system. Phenol forms homogeneous binary systems in water only at high water contents (i.e., >93 wt%). It can also form homogeneous binary systems in acetic acid, hydroxyacetone and methanol, with vert high solubilities in those solvents (i.e., >95 wt%).

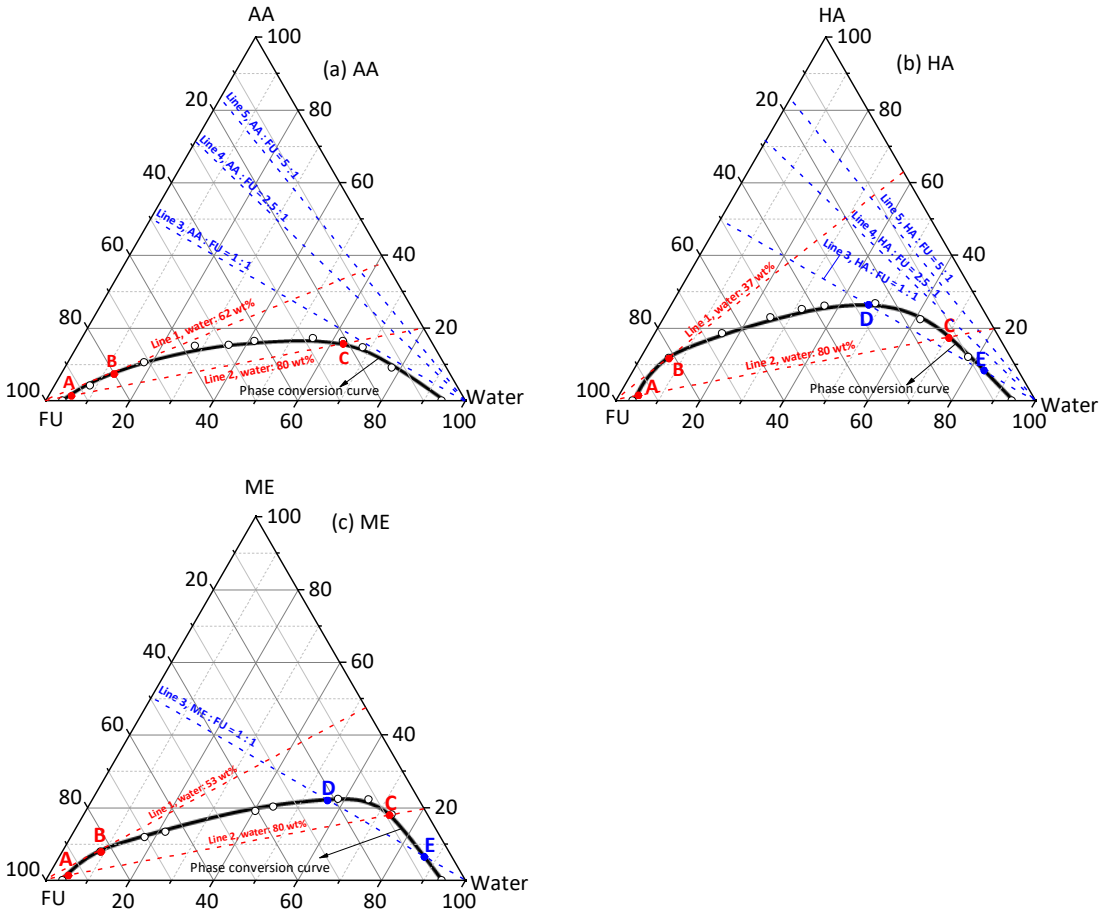

Figure 4-1 Ternary phase diagrams of furfural, solvent and water systems. Line 1 in each figure represent the critical water content of solvent/FU/water system. Line 2 in each figure represent that the water content in solvent/water mixture being 80 wt%. Panel (a): FU/AA/water system, lines 3–5 represent the ratio of AA to FU being 1:1, 2.5:1 and 5:1, respectively. Panel (b): FU/HA/water system, Lines 3–5 represent the ratio of HA to FU being 1:1, 2.5:1 and 5:1, respectively. Point D and E in Figure 4-1b represent the water contents in the HA/FU/water ternary system being ~47 and ~83 wt %, respectively. Panel (c): FU/ME//water systems. Line 3 represents the ratio of ME to FU being 1:1. Point D and E in Figure 4-1c represent the water contents in the ME/FU/water ternary system being ~56 and ~88 wt %, respectively.

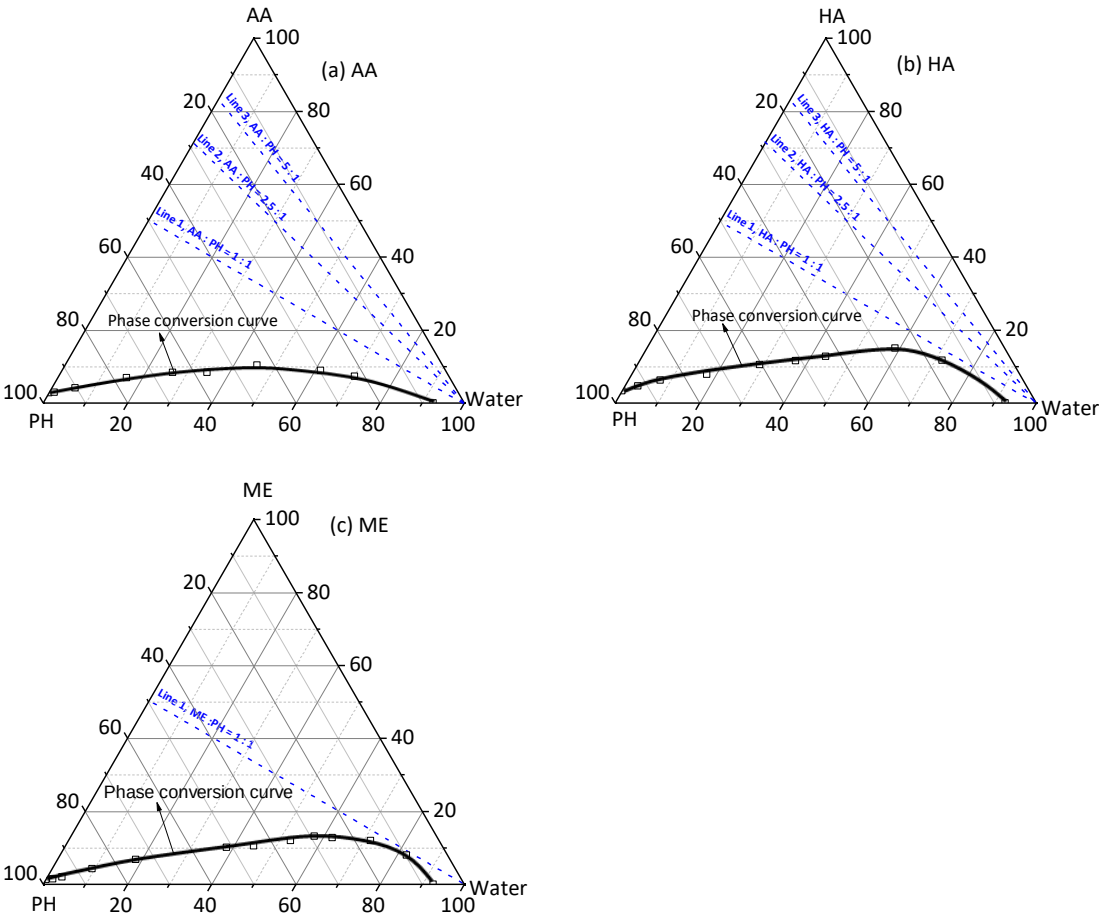

Figure 4-2 Ternary phase diagrams of phenol, solvent and water systems. Panel (a) PH/AA/water system, lines 1–3 represent the ratio of AA to PH being 1:1, 2.5:1 and 5:1, respectively. Panel (b): PH/HA/water system, Lines 1–3 represent the ratio of HA to PH being 1:1, 2.5:1 and 5:1, respectively. Panel (c): PH/ME/water system, Line 1 represents the ratio of ME to PH being 1:1.

Second, it is noted that the ternary systems of furfural/solvent/water (i.e., FU/AA/water, FU/HA/water and FU/ME/water systems) always form two different homogeneous ternary systems, i.e., organic-rich system at low water contents or water-rich systems at high water contents. To further understand the phase behaviour of furfural in various solvent/water mixtures, the boundary of the furfural content to form heterogeneous systems in various solvent/water mixtures are determined and presented in Figure 4-3. When the water content in the solvent/water mixture is lower than a critical value (see line 1 in Figure 4-3a–4-3c), the FU/solvent/water ternary systems

are always homogenous. However, when the water content in the solvent/water mixture is higher than the critical value, it can form two possible homogeneous ternary systems: one is the organic-rich system and the other is the water-rich system. For example, as shown in Figure 4-3a, if the water content in the AA/water mixture is lower than 62 wt%, the FU/AA/water systems are always homogeneous. If the water content in the AA/water mixture is higher than 62 wt%, two possible homogeneous ternary systems can be formed. For example, line 2 shows the water content of 80 wt% in the AA/water mixture. When the furfural content in the FU/AA/water system is higher than ~93 wt% (point A, equivalent to ~1370 g per 100 g model AA/water) or smaller than 22 wt% (point C, equivalent to ~30 g per 100 g model AA/water), the ternary system will become a homogenous organic-rich system or water-rich system, respectively. Similarly, when the furfural content in the FU/AA/water system is between 22 and 93 wt%, the ternary system will become heterogeneous. Such a phenomenon can be also found in other FU/solvent/water systems, but the critical water content and the furfural boundary are different for different ternary systems. For example, the critical water content reduces to 37 and 53 wt% for the FU/HA/water and FU/ME/water systems. At a water content of 80 wt% in the solvent/water, the ternary system will be heterogeneous when the furfural content is in the range of 12-94 wt% and 9-94 wt% (see line 2 in Figure 4-1b and 4-1c) for the HA/water and ME/water mixtures, respectively. Moreover, the FU/solvent/water system is always homogeneous when the solvent content in the ternary system is above a critical value, i.e., ~17, ~27, and ~22 wt% for AA, HA and ME, respectively. It is also interesting to see that the FU/AA/water, FU/HA/water and FU/ME/water mixtures are always homogeneous at a low furfural content (i.e., <4 wt%).

In contrast, the ternary systems of PH/solvent/water show different phase behaviors to those for furfural. As shown in Figure 4-4a–4-4c, the phenol solubilities in the AA/water, HA/water and ME/water mixtures all reduce with increasing water content. The phenol solubility in three solvent/water mixtures follows an order of ME/water

mixture > AA/water mixture > HA/water mixture. However, when the water content in the solvent/water mixture increases to >93 wt%, the PH/solvent/water systems are always homogeneous. Similarly, the PH/solvent/water system is always homogeneous when the solvent content is above ~10, ~15, and ~13 wt% for AA, HA and ME, respectively. Also, the PH/AA/water, PH/HA/water and PH/ME/water mixtures are always homogeneous at a low phenol content (i.e., <6 wt%).

Third, to study the phase behaviour of PL/model solvent/water systems, it is important to ensure that the model solvent/water mixtures are homogenous. Lines 3-5 in Figure 4-1 represents the different solvent-to-FU ratios of 1, 2.5 and 5 in the FU/solvent/water systems. For the AA/water mixtures, it can be seen that line 3 in Figure 4-1a, representing a AA-to-FU ratio of 1, does not pass through the phase conversion curves for furfural, indicating that the FU/AA/water systems are always homogeneous when the ratio of AA-to-FU is larger than 1. However, line 3 in Figures 4-1b and 4-1c does pass through the phase conversion curve for the FU/HA/water and FU/ME/water systems at points D and E. This means the FU/HA/water and FU/ME/water systems at a solvent-to-FU ratio of 1 are not homogeneous when the water contents are between ~47–83 wt% and ~56–88 wt%, respectively. At higher solvent-to-FU ratios of 2.5 and 5 (see lines 4 and 5 in Figures 4-1a–4-1c), the FU/HA/water and FU/ME/water systems are all homogeneous. For phenol, lines 1-3 in Figures 4-2a–4-2c do not pass through the phase conversion curves for the PH/AA/water, PH/HA/water and PH/ME/water systems, indicating that the PH/AA/water, PH/HA/water and PH/ME/water systems are always homogenous when the solvent-to-PH ratio is >1. Therefore, the ternary phase diagrams of FU(or PH)/solvent/water systems have important applications in determining the phase stability of model solvent/water system for two-component solvents. In order to guarantee a homogenous system for the FU/solvent/water system, the solvent-to-FU ratio should be higher than ~1, ~1.7 and ~2.1 for AA, HA and ME, respectively. However, if the solvent-to-FU ratio is smaller than the critical value for this solvent, the phase stability of the FU/solvent/water system depends on the water

content in the ternary system. For example, the FU/HA/water system at a HA-to-FU ratio of 1 is still homogeneous if the water content in the ternary system is <46 wt% or >82 wt% (see line 3 in Figure 4-1b). Similarly, the solvent-to-PH ratio should be higher than ~0.4, ~0.7 and ~0.8 for AA, HA and ME, respectively, to guarantee the PH/solvent/water system homogeneous.

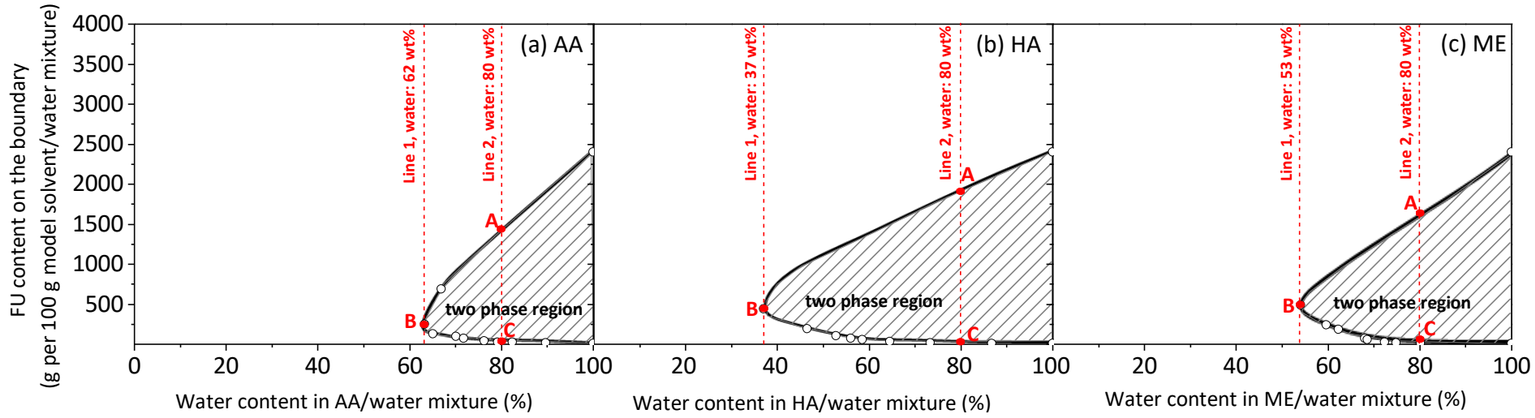

Figure 4-3 Furfural content on the phase conversion curve: (a) AA/water, (b) HA/water and (c) ME/water mixtures. Line 1 and 2 in panel (a), (b) and (c) correspond to points A, B and C in Figure 4-1a, 4-1b and 4-1c, respectively.

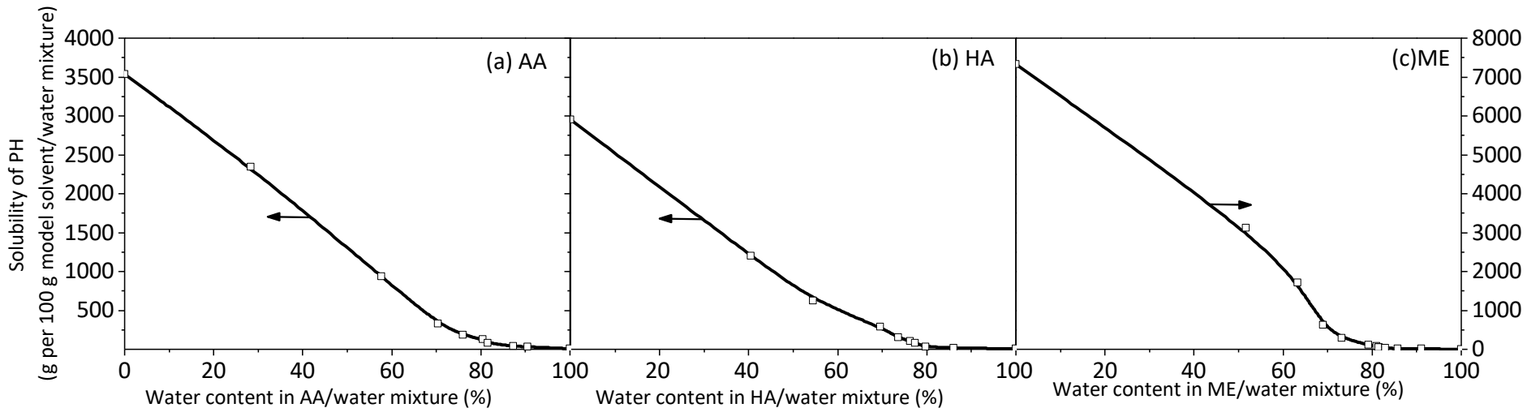

Figure 4-4 Solubilities of phenol in (a) AA/water, (b) HA/water and (c) ME/water mixtures

4.3 Ternary Phase Diagrams of PL/Model Solvent/Water Systems for Single-Component Solvents

The PL/model solvent/water systems for single-component solvent include five different systems. However, although the furfural/water and phenol/water binary systems can form homogeneous mixtures, the ratios of furfural-to-water (i.e., <0.05 or >24, see Figure 4-1) and phenol-to-water (i.e., <0.08, see Figure 4-2) are not practical in bio-oil systems. Therefore, the ternary phase diagrams of the PL/FU/water and PL/PH/water systems were not considered in the program. Figure 4-5 illustrates the ternary phase diagrams of PL/model solvent/water systems for the three single-component solvents (i.e., AA, HA and ME) while Figure 4-6 presents the PL solubilities in the three model solvent/water mixtures. It can be seen from Figure 4-5 that the maximal PL contents are ~68, ~70 and ~86 wt % (see point A in Figure 4-5a–4-5c) in the PL/AA, PL/HA and PL/ME binary systems, respectively, corresponding to the PL solubilities of ~214, ~239 and ~615 g per 100 g of model solvents (see point A in Figure 4-6a–4-6c), respectively. It is noteworthy that the PL solubility in methanol is more than double of those for acetic acid or hydroxyacetone, indicating that methanol is the best solvent for PL dissolution among the three solvents. Previous studies[150-152] have reported that the formation of hydrogen bonds between PL and solvent are mainly responsible for PL dissolution, indicating the hydrogen bonding capacity of the solvent plays an important role for PL dissolution. According to Hansen hydrogen bonding parameter (δ_h),[149] the hydrogen bonding capacity of three solvents follows an order of ME (10.9 $cal^{1/2}cm^{-3/2}$) > HA (8.8 $cal^{1/2}cm^{-3/2}$) > AA (6.6 $cal^{1/2}cm^{-3/2}$). This can explain why the PL solubility in single solvent follows the same order of ME (~615 g per 100 g of solvent) > HA (~239 g per 100 g of solvent) > AA (~214 g per 100 g of solvent).

However, a slight increase in water content slightly increases the PL solubility in the AA/water and HA/water mixtures but largely reduces that in the ME/water mixture. For example, point B in Figure 4-5a and 4-5b represent the maximal PL contents are

~73 wt% for the PL/AA/water system (equivalent to a PL solubility of ~269 g PL per 100g of AA/water mixture) and ~75 wt% for the PL/HA/water system (equivalent to a PL solubility of ~297 g PL per 100g of HA/water mixture), while the PL content in the PL/ME/system continuously reduces with increasing the water content. This is because the solubility parameter values (δ) of the AA/water mixture and the HA/water mixture are close to that of the PL sample (see Figure 4-6) as the water contents in the model solvent/water mixtures increase, thus increasing the PL solubility in the AA/water and HA/water mixtures.[149] In contrast, the δ value of methanol is 14.48 $cal^{1/2}cm^{-3/2}$, which is already in the optimal δ range for PL dissolution.[149] As the water content in the ME/water mixture increases, the δ value of the ME/water mixture shifts out of the optimal δ range for PL dissolution, leading to a continuous reduction in the PL solubility in the ME/water mixture. Further increasing the water content in the PL/model solvent/water systems leads to continuous reductions in the PL solubilities in the model solvent/water mixtures. For example, the PL content in the PL/AA/water mixture reduces to ~71 wt% (equivalent to a PL solubility of ~248 g PL per 100g of AA/water mixture) at a water content of 10 wt% (point C in Figure 4-5a), and to ~58 wt % (equivalent to a PL solubility of ~138 g PL per 100g of AA/water mixture) at a water content of 18 wt% (point D in Figure 4-5a), then further to only ~4 wt % (equivalent to a PL solubility of ~4 g PL per 100g of AA/water mixture) at a water content of 54 wt% (point E in Figure 4-5a). Similarly, the PL content in the PL/HA/water reduces to ~72 wt % (equivalent to a PL solubility of ~255 g PL per 100g of HA/water mixture) at a water content of 9 wt% (point C in Figure 4-5b), and to ~59 wt % (equivalent to a PL solubility of ~146 g PL per 100g of HA/water mixture) at a water content of 17 wt% (point D in Figure 4-5b), then further to only ~5 wt % (equivalent to a PL solubility of ~6 g PL per 100g of HA/water mixture) at a water content of 53 wt% (point E in Figure 4-5b). It should be mentioned that Point C in Figure 4-5a and 4-5b represents minimal model solvent content needed to homogenize the PL/model solvent/water mixtures, while Point E in Figure 4-3a and 4-3b represents

that minimal model solvent contents above which homogeneous PL/model solvent/water mixtures are always formed. Therefore, the PL/model solvent/water systems are always phase-separated if the AA (or HA) content is lower than ~19 (or 20) wt%, while PL/model solvent/water systems is always homogeneous if the AA (or HA) content is higher than ~41 (or 42) wt%.

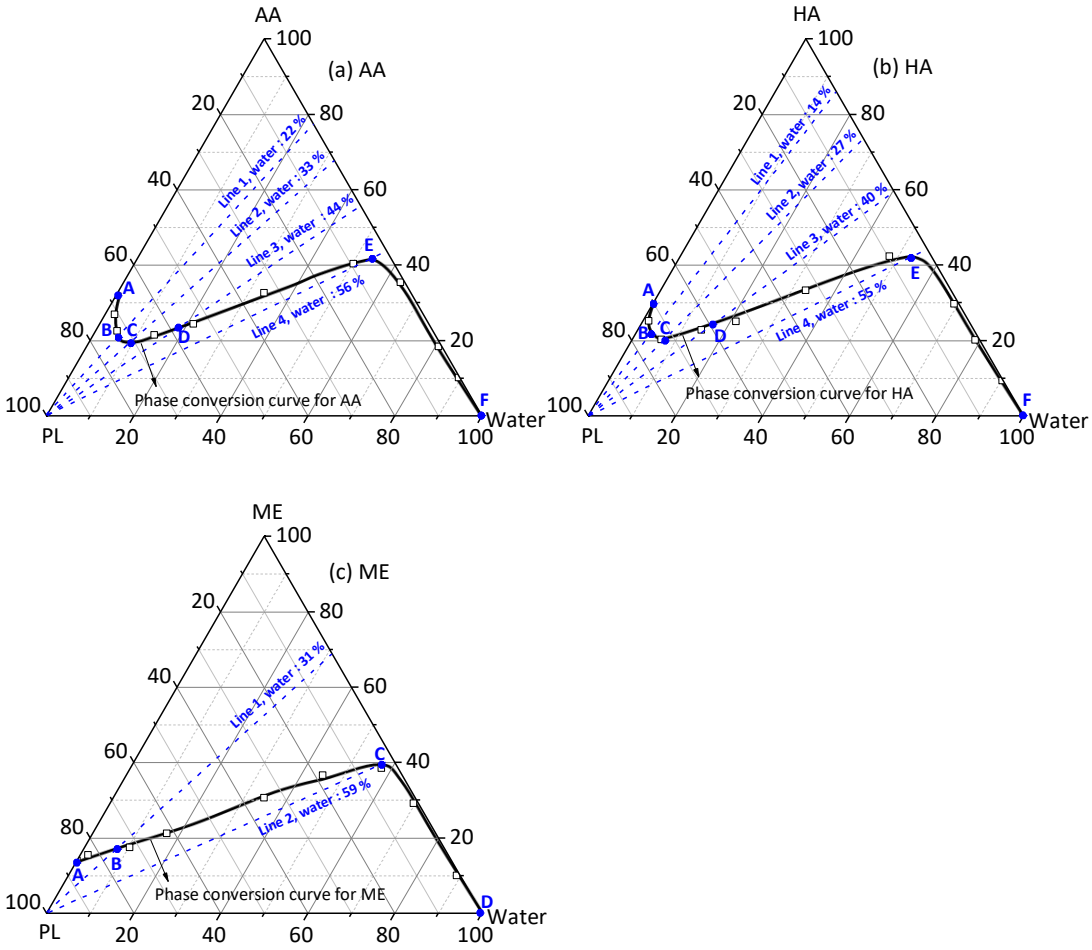

Figure 4-5 Ternary phase diagrams of PL/AA/water, PL/HA/water and PL/ME/water systems: (a) Lines 1–4 represent the AA/water mixtures with water contents of ~22,~33, ~44, and ~49, respectively; (b) Lines 1–4 represent the HA/water mixtures with water contents of ~14,~27, ~40, and ~55, respectively; (c) Lines 1 and 2 represent the ME/water mixtures with water contents of ~31 and ~59, respectively. Point A in

figure 4-5a and 4-5b represent maximal solubilities of PL in model solvents. Point B in figure 4-5a and 4-5b represent maximal solubilities of PL in model solvent/water mixtures. Point C in figure 4-5a and 4-5b represent minimal model solvent contents needed to homogenize PL/model solvent/water mixtures. Point D in figure 4-5a and 4-5b represent the half of the maximal solubilities of PL in model solvent/water mixtures. Point E in figure 4-5a and 4-5b represent that minimal model solvent contents above which homogeneous PL/model solvent/water mixtures are always formed. Point A in figure 4-5c represents the maximal solubility of PL in methanol. Point B in figure 4-5c represents the half of the maximal solubility of PL in the ME/water mixture. Point C in figure 4-5c represents the minimal model solvent content above which a homogeneous PL/ME/water mixture is always formed.

The PL content in the PL/ME/water system also reduces to ~75 wt % (equivalent to a PL solubility of ~300 g PL per 100g of ME/water mixture) at a water content of 9 wt% (point B in Figure 4-5c), and further to only ~3 wt % (equivalent to a PL solubility of ~4 g PL per 100g of ME/water mixture) at a water content of 57 wt% (point C in Figure 4-5c). It is worth noting that ~39 wt% of methanol (Point C in Figure 4-5c) is the minimal ME content required to guarantee a homogeneous PL/ME/water system. The above results clearly demonstrate that methanol is the best solvent for PL dissolution, achieving the highest PL solubility of ~615 g per 100 g of methanol. However, the PL solubility in the ME/water mixture reduces significantly as the water content increases. Compared to those in the AA/water or HA/water mixtures, the PL solubilities in the ME/water mixtures are still higher at the same water content. Therefore, methanol addition is considered as one of most effective strategies to enhance the phase stability of bio-oil.

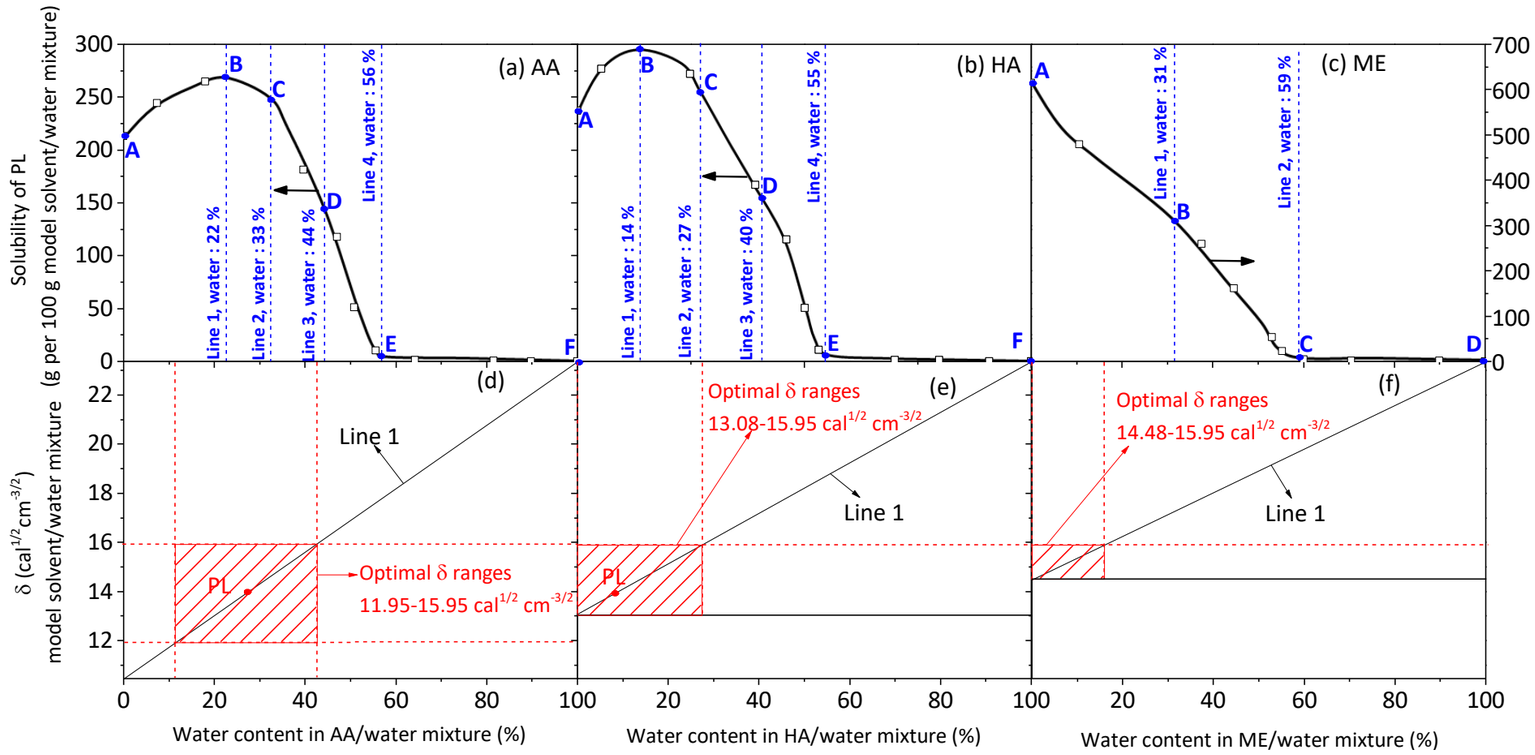

Figure 4-6 Solubilities of PL in AA/water, HA/water and ME/water mixtures: Panel (a): Lines 1–4 represent the AA/water mixtures with water contents of ~22,~33, ~44, and ~49, respectively; panel (b): Lines 1–4 represent the HA/water mixtures with water contents of ~14,~27, ~40, and ~55, respectively; panel (c): Lines 1 and 2 represent the ME/water mixtures with water contents of ~31 and ~59, respectively. Panel (d, e and f): line 1 represents the δ values of single model solvent/water mixtures at different water contents. Key points in panel (a), panel (b) and panel (c) correspond to the key points in figure 4-5a, 4-5b and 4-5c, respectively.

4.4 Ternary Phase Diagrams of PL/Model Solvent/Water Systems for Two-Component Solvents.

4.4.1 Ternary Phase Diagrams of PL/AA-FU/water and PL/AA-PH/water systems

Panels a and b of Figure 4-7 illustrate the ternary phase diagrams of the PL/AA-FU/water and PL/AA-PH/water systems at different AA-to-FU(or PH) ratios of 1, 2.5 and 5 while Figure 4-8 presents the corresponding PL solubilities in the AA-FU/water and AA-PH/water mixtures. According to the results in Figures 4-1 and 4-2, all the AA-FU(or PH) two-component solvent mixtures at a AA-to-FU(or PH) ratio > 1 are homogeneous. Point A_1–A_3 in Figure 4-7a and 4-7b represent the maximal PL content that can be achieved for homogeneous PL/AA-FU and PL/AA-PH binary systems, respectively. For example, the maximal PL contents in the PL/AA-FU and PL/AA-PH binary systems are ~46 and ~51 wt % (equivalent to PL solubilities of ~87 and ~104 g PL per 100 g of AA-FU and AA-PH solvents) at a AA-to-FU(or PH) ratio of 1, respectively. As the AA-to-FU ratio increases, the maximal PL content increases to ~52 wt% (equivalent to a PL solubility of ~113 g PL per 100 g of AA-FU solvent) at a AA-to-FU ratio of 2.5, and further to ~58 wt% (equivalent to a PL solubility of ~145 g PL per 100 g of AA-FU solvent) at a AA-to-FU ratio of 5. Similarly, as the AA-to-PH ratio increases, the maximal PL content increases to ~57 wt% (equivalent to a PL solubility of ~132 g PL per 100 g of AA-PH) at a AA-to-PH ratio of 2.5, and further to 61 wt% (equivalent to a PL solubility of ~158 g PL per 100 g of AA-PH) at a AA-to-PH ratio of 5. Obviously, the observed PL solubilities are considerably lower than those in AA, indicating both furfural and phenol addition shows negative effect on PL dissolution in AA. The more furfural (or phenol) in the two-component AA-FU(or PH) solvent system, the lower the PL solubility is. Compared to phenol, furfural has stronger effect to suppress the PL dissolution, since the PL solubility in the AA-FU solvent is lower than that in the AA-PH solvent at the same AA-to-FU(or PH) ratio.

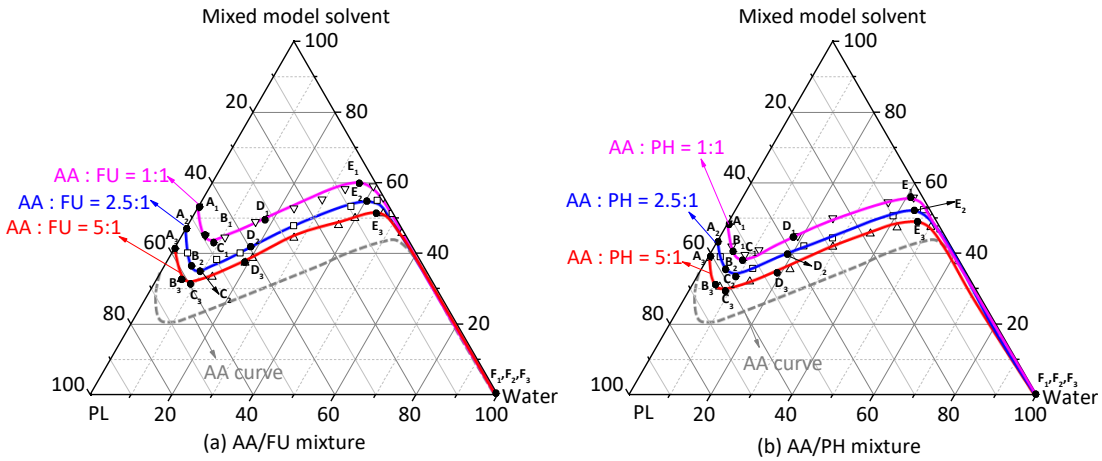

Figure 4-7 Ternary phase diagrams of PL/AA-FU/water and PL/AA-PH/water systems. Points A_1, A_2 and A_3 in each figure represent the maximal solubility of PL in the mixed model solvent. Points B_1, B_2 and B_3 in each figure represent the maximal solubility of PL in the mixed model solvent/water mixture. Points C_1, C_2 and C_3 in each figure represent the minimal mixed model solvent content needed to homogenize the PL/model solvent/water mixture. Points D_1, D_2 and D_3 in each figure represent the half of the maximal solubility of PL in the model solvent/water mixture. Points E_1, E_2 and E_3 in each figure represent that the minimal MS content above which a homogeneous PL/model solvent/water mixture is always formed.

Point B_1–B_3 in Figure 4-7a and 4-7b represent the maximal PL contents that can be achieved for homogeneous PL/AA-FU/water and PL/AA-PH/water ternary systems at different AA-to-FU(or PH) ratios of 1, 2.5 and 5, when a small amount of water is added into the PL/AA-FU and PL/AA-PH mixtures. As the AA-to-FU ratio increase, the maximal PL contents increases from ~49 wt% (equivalent to a PL solubility of ~97 g PL per 100 g of AA-FU/water mixture) at a AA-to-FU ratio of 1, to ~57 wt% (equivalent to a PL solubility of ~132 g PL per 100 g of AA-FU/water mixture) at a AA-to-FU ratio of 2.5, further to ~61 wt % (equivalent to a PL solubility of ~158 g PL per 100 g of AA-FU/water mixture) at a AA-to-FU ratio of 5. Similarly, as the AA-to-PH ratio increases, the maximal PL contents increases from ~54 wt% (equivalent to a PL solubility of ~119 g PL per 100 g of AA-PH/water mixture) at a AA-to-PH ratio

of 1, to ~58 wt% (equivalent to a PL solubility of ~143 g PL per 100 g of AA-PH/water mixture) at a AA-to-PH ratio of 2.5, further to ~63 wt % (equivalent to a PL solubility of ~172 g PL per 100 g of AA-PH/water mixture) at a AA-to-FU ratio of 5. Such PL solubilities are also much lower than those in the AA/water mixtures, demonstrating the negative effect of both furfural and phenol addition on PL dissolution in the AA/water mixture.

The PL content in the PL/AA-FU/water system reduces as the water content in the ternary system further increases. For an AA-to-FU ratio of 1, the PL content decreases to ~48 wt% (point C_1 in Figure 4-7a) at a water content of 9 wt%, then to ~32 wt% (Point D_1 in Figure 4-7a) at a water content of 18 wt%, finally to ~4 wt% (point E_1 in Figure 4-7a) at a water content of 36 wt%. It should be mentioned that Point C_1 in Figure 4-7a represents that the minimal AA-FU solvent content (~42 wt%) needed to homogenize the PL/AA-FU/water system, while Point E_1 in Figure 4-7a represents that the minimal AA-FU content (~60 wt%) above which homogenous PL/AA-FU/water mixtures are always formed. As the AA-to-FU ratio increases from 1 to 5, the phase conversion curve shifts downwards, indicating an increase in the PL solubility in the AA-FU/water mixture. This also leads to decreases in the minimal AA-FU solvent content needed to homogenize the PL/AA-FU/water system (to ~32 wt%, Point C_3 in Figure 4-7a) and the minimal AA-FU content above which homogenous PL/AA-FU/water mixtures are always formed (to 52 wt%, Point E_3 in Figure 4-7a).

Similar trends can be found for the PL content in the PL/AA-PH/water system. However, at the same AA-to-PH(or FU) ratio, the PL content in the PL/AA-PH/water system at the same water content is slightly higher that in the PL/AA-FU/water system. For example, at an AA-to-PH ratio of 1, the PL content is ~55 wt% (Point B_1 in Figure 4-7b) at a water content of 5 wt%. Also, the minimal AA-PH solvent content needed to homogenize the PL/AA-PH/water system slightly reduces to ~38 wt% (Point C_1 in Figure 4-7b), while the minimal AA-PH content above which homogenous PL/AA-

PH/water mixtures also reduces to ~56 wt% (Point E_1 in Figure 4-7b). As the AA-to-PH ratio increases, the phase conversion curve shifts downwards, leading to an increase in the PL solubility in the AA-PH/water mixture. This is because both furfural and phenol have low solubilities in water. To make the PL/AA-FU/water or PL/AA-PH/water system homogeneous, a certain amount of acetic acid is required to dissolve furfural or phenol first, thus reducing the PL solubility in the AA-FU/water or AA-PH/water mixtures.

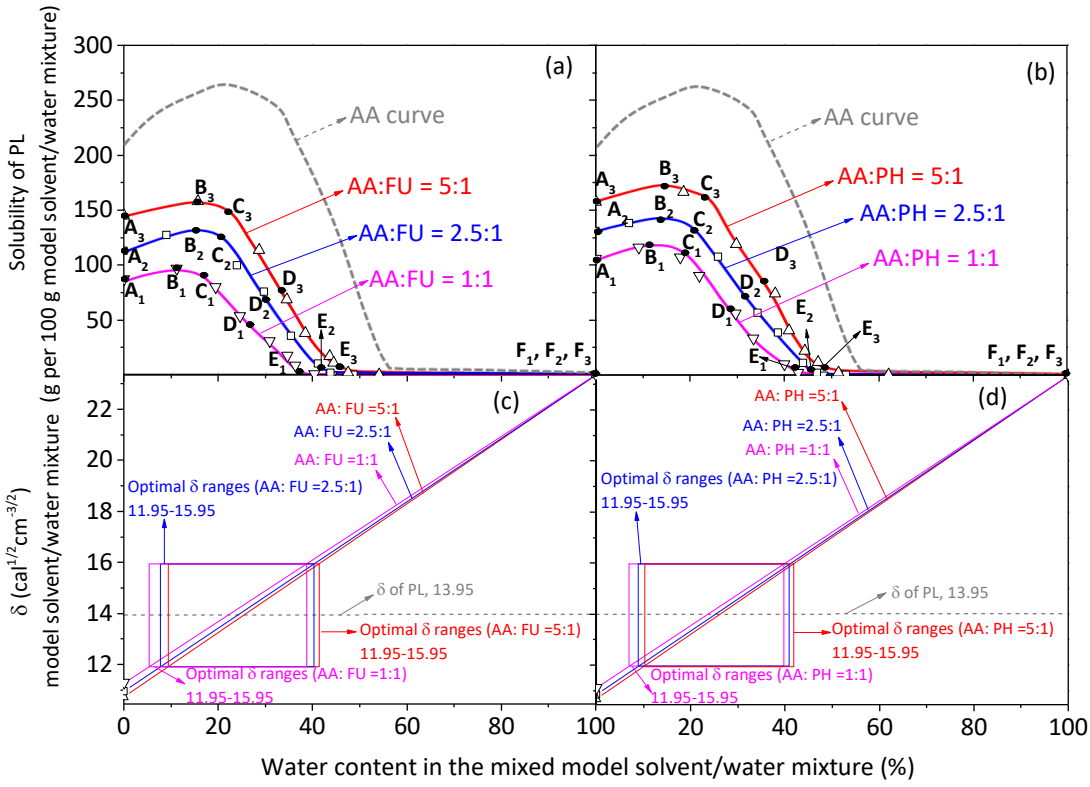

Figure 4-8 Solubilities of PL in AA-FU/water and AA-PH/water mixtures. Points A-F in panel (a) and panel (b) correspond to points A-F in Figure 4-7a and 4-7b, respectively. Panel (c) and (d): The colour area represents the optimal δ range of the mixed model solvent/water mixtures for the dissolution of PL.

4.4.2 Ternary phase diagrams of PL/HA-FU/water and PL/HA-PH/water systems

Figure 4-9a and 4-9b compare the ternary phase diagrams of the PL/HA-FU/water and PL/HA-PH/water systems at different HA-to-FU(or PH) ratios of 1, 2.5 and 5, and

the corresponding PL solubilities in the HA-FU/water and HA-PH/water mixtures are shown in Figure 4-10a and 4-10b, respectively. It is interesting to see that the phase conversion curve of PL/HA-FU/water system at a HA-to-FU ratio of 1 intersects with the side of model solvent/water at point F_1, instead of intersecting with the side of model solvent/water at vertex "water". This is because the HA-FU/water mixture at a HA-to-FU ratio of 1 is inhomogeneous when the water content is between ~47–83 wt% (see Figure 4-1b). It is true that the HA-FU/water mixture is homogeneous when water content is > 83 wt%, but the PL content is very low at such a high water content. Therefore, after point F_1, the ternary system of PL/HA-FU /water is not studied at a HA-to-FU ratio of 1.

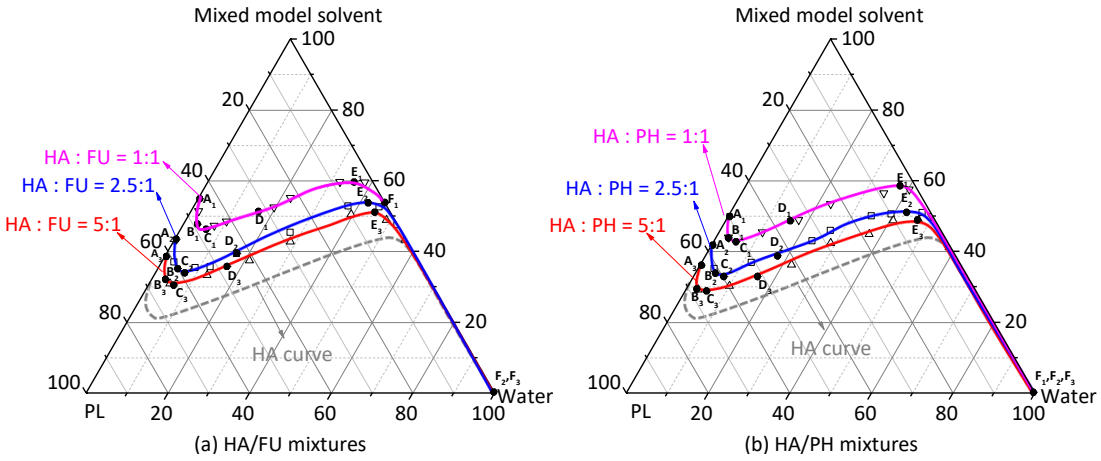

Figure 4-9 Ternary phase diagrams of PL/HA-FU/water and PL/HA-PH/water systems. Points A_1, A_2 and A_3 in each figure represent the maximal solubility of PL in the mixed model solvent. Points B_1, B_2 and B_3 in each figure represent the maximal solubility of PL in the mixed model solvent/water mixture. Points C_1, C_2 and C_3 in each figure represent the minimal mixed model solvent content needed to homogenize the PL/model solvent/water mixture. Points D_1, D_2 and D_3 in each figure represent the half of the maximal solubility of PL in the model solvent/water mixture. Points E_1, E_2 and E_3 in each figure represent that the minimal MS content above which a homogeneous PL/model solvent/water mixture is always formed.

Apart from above difference, the phase conversion curves at different HA-to-FU(or PH) ratios exhibit similar trends. Similarly, the PL solubilities in the HA-FU/water and HA-PH/water mixtures increase as the furfural and phenol contents decrease. For example, the maximal PL contents for the PL/HA-FU binary system (see Points A_1-A_3 in Figure 4-9a) are ~45, ~56, and ~61 wt% (equivalent to PL solubilities of ~81, ~132 and ~157 g PL per 100 g of model solvent/water mixture) at a HA-to-FU ratio of 1, 2.5 and 5, respectively. While the maximal PL contents for the PL/HA-PH binary system (see Points A_1-A_3 in Figure 4-9b) are ~50, ~58, and ~64 wt% (equivalent to PL solubilities of ~100, ~137 and ~176 g PL per 100 g of model solvent/water mixture) at a HA-to-PH ratio of 1, 2.5 and 5, respectively. In the ternary PL/HA-FU/water system, the maximal PL contents (see Points B_1-B_3 in Figure 4-9a) are slightly higher, i.e., ~49, ~60, and ~65 wt% (equivalent to PL solubilities of ~95, ~153 and ~184 g PL per 100 g of model solvent/water mixture) at a HA-to-FU ratio of 1, 2.5 and 5, respectively. Whereas in the ternary PL/HA-PH/water system, the maximal PL contents (see Points B_1-B_3 in Figure 4-9b) are ~53, ~62, and ~68 wt% (equivalent to PL solubilities of ~112, ~156 and ~215 g PL per 100 g of model solvent/water mixture) at a HA-to-PH ratio of 1, 2.5 and 5, respectively. Points C_1–C_3 in Figure 4-9a and 4-9b represent the minimal HA-FU and HA-PH contents required to possibly form homogeneous PL/HA-FU/water and PL/HA-PH/water systems, i.e., ~47, ~34, and ~30 wt% for the PL/HA-FU/water system at a HA-to-FU ratio of 1, 2.5 and 5, respectively, and ~43, ~33 and ~29 wt% for the PL/HA-PH /water system at a HA-to-PH ratio of 1, 2.5 and 5, respectively. In addition, points E_1–E_3 in Figure 4-9a and 4-9b represent the minimal HA-FU and HA-PH contents above which homogeneous PL/HA-FU/water and PL/HA-PH/water systems can be always formed, i.e., ~60, ~54, and ~51 wt% for the PL/HA-FU/water system at a HA-to-FU ratio of 1, 2.5 and 5, respectively, and ~59, ~51 and ~49 wt% for the PL/HA-PH /water system at a HA-to-PH ratio of 1, 2.5 and 5, respectively. The results clearly indicate that furfural or phenol addition greatly

reduces the PL solubility in the HA/water mixtures. As the HA-to-FU(or PH) ratio increases, the phase conversion curve shifts upwards.

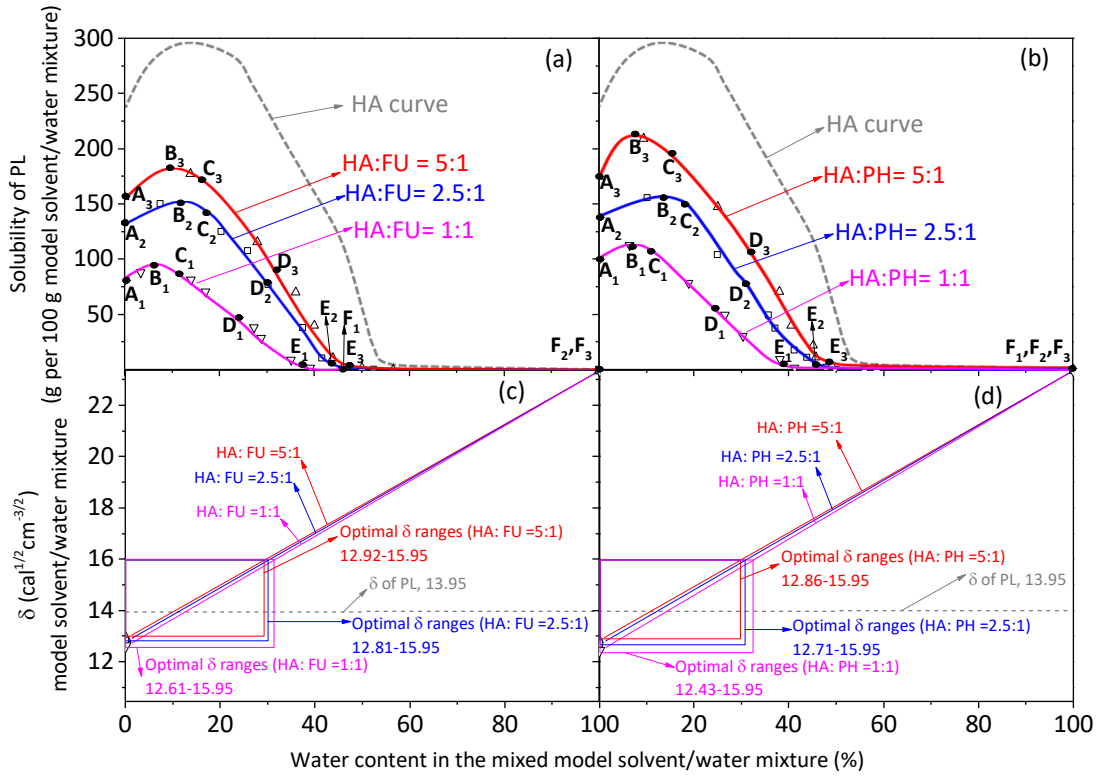

Figure 4-10 Solubilities of PL in HA-FU/water and HA-PH/water mixtures. Points A-F in panel (a) and panel (b) correspond to points A-F in Figure 4-9a and 4-9b, respectively. Panel (c) and (d): The colour area represents the optimal δ range of the mixed model solvent/water mixtures for the dissolution of PL.

4.4.3 Ternary phase diagrams of PL/ME-FU/water and PL/ME-PH/water systems

Figure 4-11 compares the ternary phase diagrams of the PL/ME-FU/water and PL/ME-PH/water systems, while the PL solubilities in the ME-FU/water and ME-PH/water mixtures are compared in Figure 4-12. It can be found that the addition of furfural or phenol into the PL/ME binary system largely reduces the maximal PL content. For example, the maximal PL content reduces from ~85 wt% for the PL/ME binary system, to ~63 (or 67) wt% for the PL/ME-FU(or ME-PH) binary system with a ME-to-FU(or PH) ratio of 1.

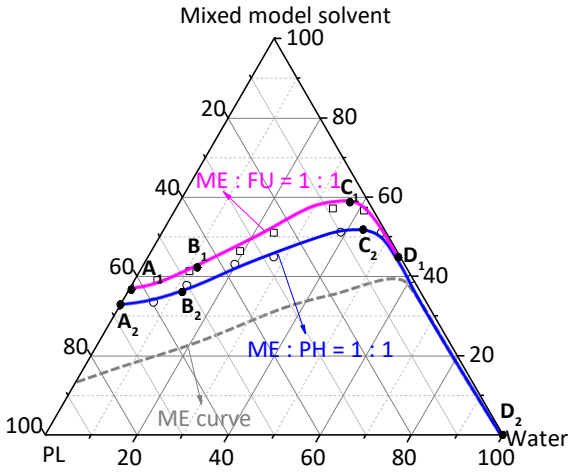

Figure 4-11 Ternary phase diagrams of PL/ME-FU/water and PL/ME-PH/water systems. Points A_1 and A_2 represent the maximal solubility of PL in ME-FU and ME-PH, respectively. Points B_1 and B_2 represent the half of the maximal solubility of PL in the ME-FU/water and ME-PH/water mixture. Points C_1 and C_2 represent that the minimal MS content above which homogeneous PL/ ME-FU/water and PL/ME-PH/water mixtures are always formed.

Accordingly, the maximal PL solubility reduces drastically from ~615 g per 100 g of methanol, to ~171 (or ~207) g per 100 g of ME-PU(or PH) solvent with a ME-to-FU(or PH) ratio of 1. As the water content in the PL/ME-FU/water and PL/ME-PH/water ternary systems increases, the PL solubilities in the ME-FU/water and ME-PH/water mixtures continue to reduce. In addition, the minimal ME-FU and ME-PH contents required to guarantee homogenous ternary mixtures are ~59 and ~52 wt % (points C_1 and C_2 in Figure 4-11) for the PL/ME-FU/water and PL/ME-PH/water systems, respectively, compared to that of ~39 wt% (point C in Figure 4-5c) for the PL/ME/water system.

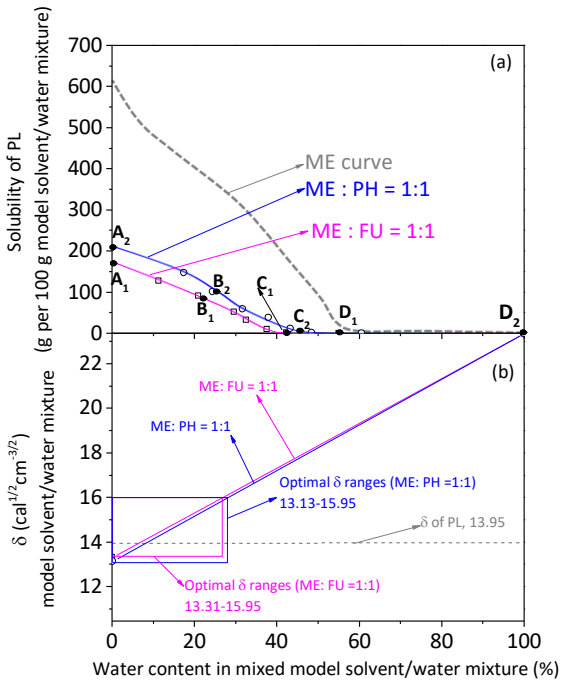

Figure 4-12 Solubilities of PL in ME-FU/water and ME-PH/water mixtures. Panel (a): points A-D correspond to points A-D in Figure 4-11. Panel (b): The colour area represents the optimal δ range of the mixed model solvent/water mixtures for the dissolution of PL.

4.5 Ternary Phase Diagrams of PL/Model Solvent/Water Systems for Three-Component Solvents

Figure 4-13 presents the ternary phase diagrams of PL/model solvent/water systems for various three-component solvents, including the AA-HA-ME (with a ratio of 5:5:1), AA-HA-FU/PH (with a ratio of 5:5:2), AA-ME-FU/PH (with a ratio of 5:1:2) and HA-ME-FU/PH (with a ratio of 5:1:2) solvents. The PL solubilities in those three-component model solvent/water mixtures are also compared in Figure 4-14. All phase conversion curves follow the similar trends as discussed in above sections. Among all the three-component solvents, the PL solubility is the highest for the AA-HA-ME (with a ratio of 5:5:1) solvent. For example, the maximal PL content for a homogeneous PL/AA-HA-ME binary system is ~70 wt % (equivalent to a PL solubility of ~238 g PL per 100 g of model solvent/water mixture), and the maximal

PL content in the PL/AA-HA-ME/water ternary system is achieved when a small amount of water is added, i.e., ~72 wt % (equivalent to a PL solubility of ~259 g PL per 100 g of AA-HA-ME/water mixture) at a water content of ~6 wt %.

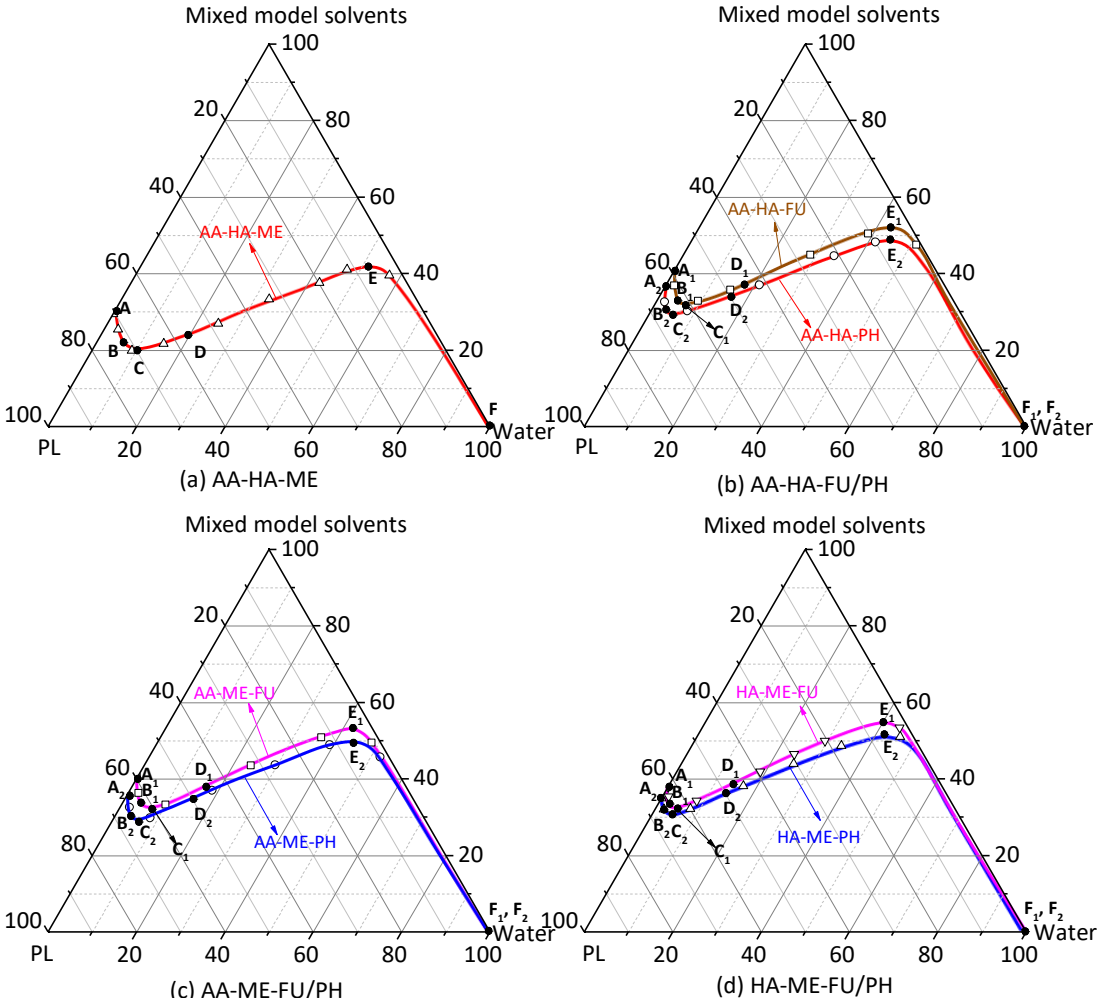

Figure 4-13 Ternary phase diagrams of PL/AA-HA-ME/water, PL/AA-HA-FU (or PH)/water, PL/AA-HA-FU (or PH)/water and PL/HA-ME-FU (or PH)/water systems. Point A in each figure represents the maximal solubility of PL in the mixed model solvent. Point B in each figure represents the maximal solubility of PL in the mixed model solvent/water mixture. Point C in each figure represents the minimal mixed model solvent content needed to homogenize the PL/model solvent/water mixture. Point D in each figure represents the half of the maximal solubility of PL in the model solvent/water mixture. Point E in each figure represents that the minimal MS content above which a homogeneous PL/model solvent/water mixture is always formed.

For other three-component solvents, the PL solubilities for the AA-HA-PH (with a ratio of 5:5:2), AA-ME-PH (with a ratio of 5:1:2) and HA-ME-PH (with a ratio of 5:1:2) solvents are similar, but those PL solubilities are slightly higher than those for the AA-HA-FU (with a ratio of 5:5:2), AA-ME-FU (with a ratio of 5:1:2) and HA-ME-FU (with a ratio of 5:1:2) solvents. For example, the maximal PL contents for homogeneous PL/model solvent binary systems are ~63, ~64 and ~65 wt% (equivalent to PL solubilities of ~173, ~178 and ~187 g PL per 100 g of model solvent/water mixture) for the PL/AA-HA-PH, PL/AA-ME-PH and PL/HA-ME-PH binary systems, respectively. In contrast, the maximal PL contents for homogeneous PL/model solvent binary systems are ~59, ~59 and ~62 wt% (equivalent to PL solubilities of ~148, ~148 and ~164 g PL per 100 g of model solvent/water mixture) for the PL/AA-HA-FU, PL/AA-ME-FU and PL/HA-ME-FU binary systems, respectively. For the PL/model solvent/water ternary systems, the maximal PL contents are ~66, ~66 and ~65 wt% (equivalent to PL solubilities of ~198, ~196 and ~194 g PL per 100 g of model solvent/water mixture) for the PL/AA-HA-PH/water, PL/AA-ME-PH/water and PL/HA-ME-PH/water systems, respectively, higher than those of ~62, ~62 and ~64 wt% (equivalent to PL solubilities of ~167, ~165 and ~178 g PL per 100 g of model solvent/water mixture) for the PL/AA-HA-FU/water, PL/AA-ME-FU/water and PL/HA-ME-FU/water systems, respectively.

The above results have shown that, although the methanol content is small (only 12.5 wt%) in the AA-ME-FU (or HA-ME-FU) solvent, the PL solubility for the AA-ME-FU (or HA-ME-FU) solvent are similar to that for the AA-HA-FU (or AA-HA-FU) solvent. This is because PL has a much higher solubility in methanol than those in acetic acid and hydroxyacetone (see Figure 4-5), as the δ value of methanol (14.48 $cal^{1/2}$ $cm^{-3/2}$) is closer to the δ value of PL (13.95 $cal^{1/2}$ $cm^{-3/2}$) than that of acetic acid (10.45 $cal^{1/2}$ $cm^{-3/2}$) and hydroxyacetone (13.08 $cal^{1/2}$ $cm^{-3/2}$). Therefore, addition of a small amount of methanol in the model solvent can enhance PL dissolution in the model solvent/water mixture. Moreover, compared to phenol, furfural has more

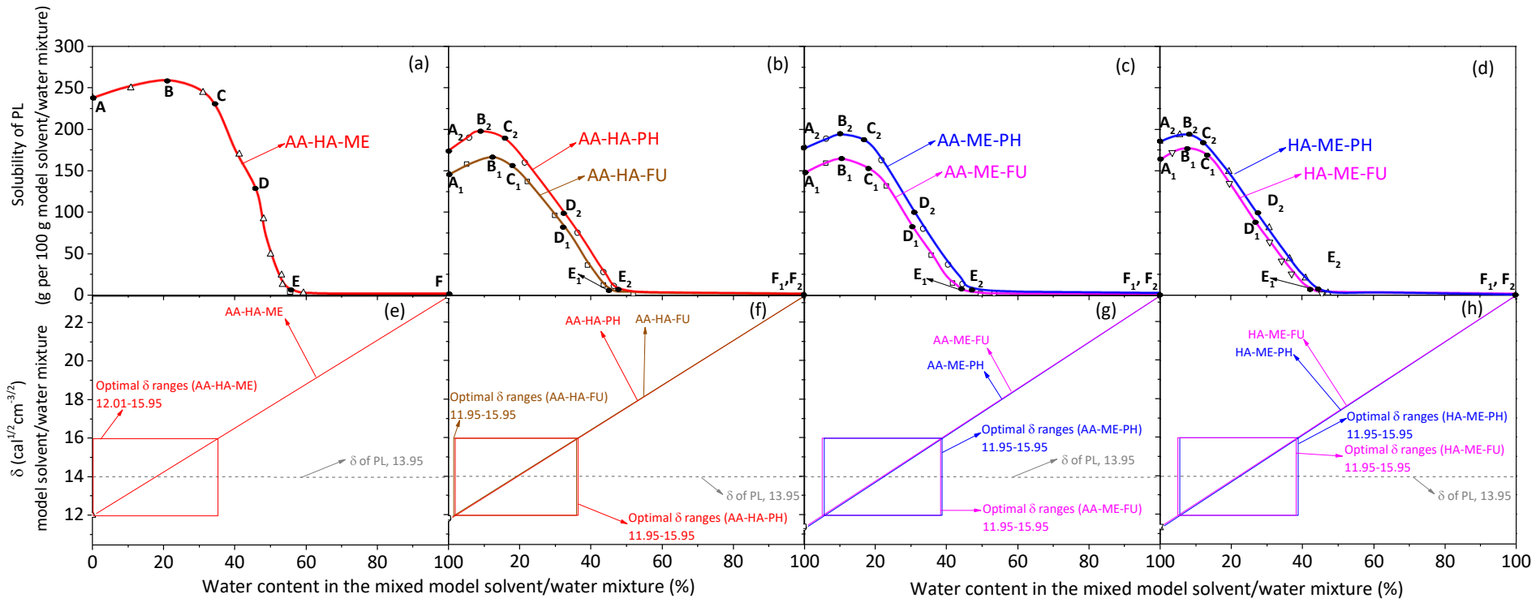

Figure 4-14 Solubilities of PL in various model solvent/water mixtures: (a) AA-HA-ME/water mixtures; (b) AA-HA-PH/water and AA-HA-FU/water mixtures; (c) AA-ME-PH/water and AA-ME-FU/water mixtures; (d) HA-ME-PH/water and HA-ME-FU/water mixtures. Points A-F in panel (a), panel (b), panel (c) and panel (d) correspond to points A-F in Figure 4-13a, 4-13b, 4-13c and 4-13d, respectively. Panel (e), (f), (g) and (h): The colour area represents the optimal δ range of the mixed model solvent/water mixtures for the dissolution of PL.

negative effects on PL dissolution in model solvent/water mixtures. This is reasonable since phenol has higher solubilities in acetic acid, hydroxyacetone and methanol than furfural.

4.6 Ternary Phase Diagrams of PL/Model Solvent/Water Systems for Four-Component Solvents

Figure 4-15 presents the ternary phase diagrams of PL/model solvent/water systems for various three-component solvents, including AA-HA-ME-FU/PH (with a ratio of 5:5:1:2), AA-HA-FU-PH (with a ratio of 5:5:2:2), AA-ME-FU-PH (with a ratio of 5:1:2:2) and HA-ME-FU-PH (with a ratio of 5:1:2:2). The PL solubilities in various four-component model solvent/water mixtures are shown in Figure 4-16. The phase conversion curve for the five-component solvent AA-HA-ME-FU-PH (with a ratio of 5:5:1:2:2, referred to as MS), which was reported previously,[153] is also plotted in Figure 4-15 for comparison. Two important findings can be observed from those results.

One is that the AA-HA-ME-FU and AA-HA-ME-PH solvents are the best solvents to dissolve PL among all four-component model solvents. As shown in Figure 4-15a, the phase conversion curves for the PL/AA-HA-ME-FU/water and PL/AA-HA-ME-PH/water systems are slightly below the curve for the PL/MS/water system, indicating that the PL solubilities in the AA-HA-ME-FU/water and AA-HA-ME-PH/water mixtures are higher than those in the MS/water mixtures. This is reasonable since both furfural and phenol have negative effects on PL dissolution in model solvent/water mixtures. The total content (26.7 wt%) of furfural and phenol in the MS is much higher than those (15.4 wt%) in the AA-HA-ME-FU (5:5:1:2) and AA-HA-ME-PH (5:5:1:2) solvents, thus reducing the PL solubilities in the five-component MS solvent. It can be seen that the maximal PL contents for homogeneous PL/AA-HA-ME-FU and PL/AA-HA-ME-PH binary systems (see Point A_1 and A_2 in Figure 4-15a) are ~65 and ~68 wt% respectively, slightly higher thant that of ~63 wt% for the PL/MS binary system.[153]

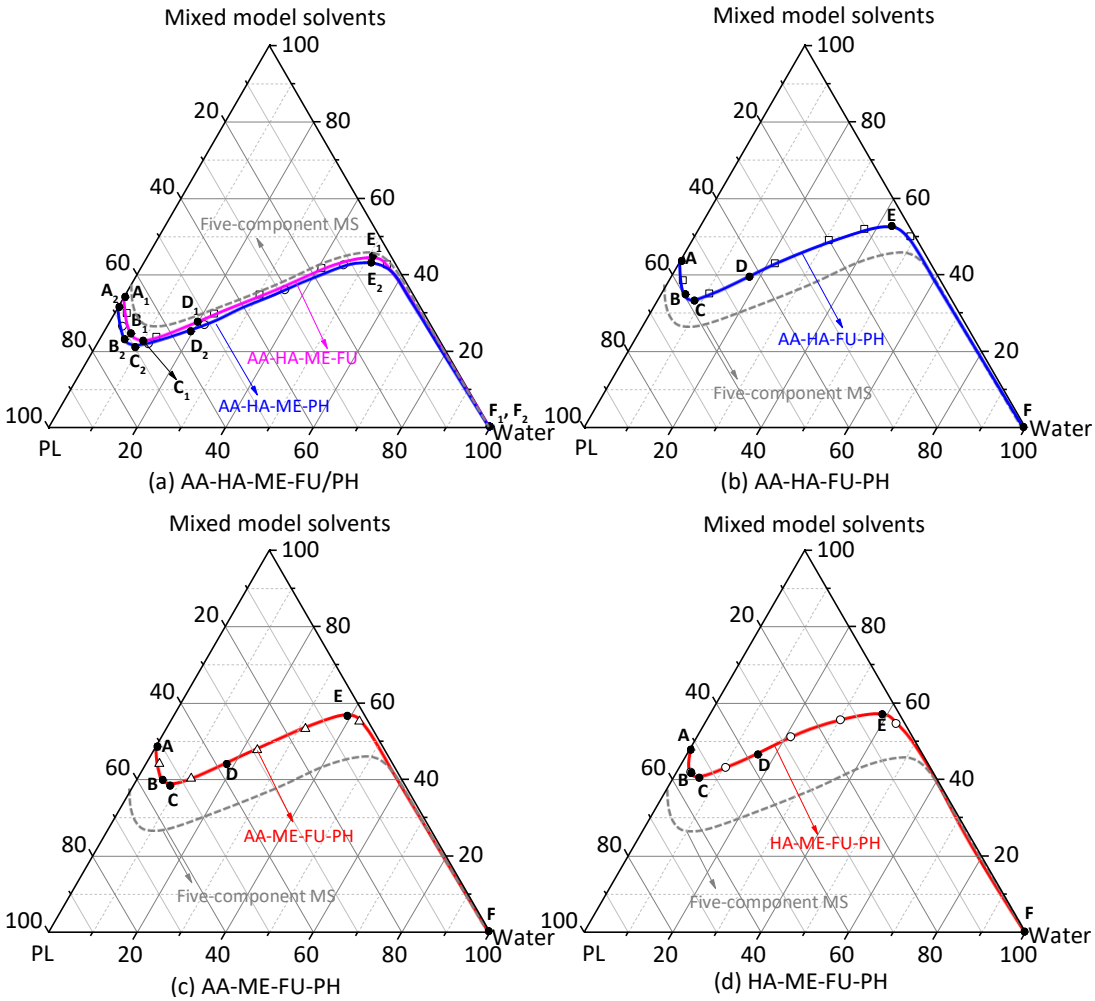

Figure 4-15 Ternary phase diagrams of PL/AA-HA-ME-FU (or PH)/water, PL/AA-HA-FU-PH/water, PL/AA-ME-FU-PH/water and PL/HA-ME-FU-PH/water systems. Point A in each figure represents the maximal solubility of PL in the mixed model solvent. Point B in each figure represents the maximal solubility of PL in the mixed model solvent/water mixture. Point C in each figure represents the minimal mixed model solvent content needed to homogenize the PL/model solvent/water mixture. Point D in each figure represents the half of the maximal solubility of PL in the model solvent/water mixture. Point E in each figure represents that the minimal MS content above which a homogeneous PL/model solvent/water mixture is always formed. The grey dashed curves represent the phase conversion curves for a PL, five-component MS and water system.[153]

The maximal PL contents in the PL/AA-HA-ME-FU/water and PL/AA-HA-ME-PH/water ternary systems (see Point B_1 and B_2 in Figure 4-15a) are ~69 and ~71 wt% (equivalent to PL solubilities of ~226 and ~246 g PL per 100 g of model solvent/water mixture), while the maximal PL content in the PL/MS/water ternary system is ~66 wt %.[153]

The other is that the phase conversion curves for the PL/AA-HA-FU-PH/water, PL/AA-ME-FU-PH/water and PL/HA-ME-FU-PH/water systems are all above the curve for the PL/MS/water system, as shown in Figure 4-15b–4-15d. This is due to the higher total content of furfural and phenol in those solvents, i.e., ~28.6 wt% for the AA-HA-FU-PH solvent, and ~40 wt% for the AA-ME-FU-PH and HA-ME-FU-PH solvents, thus reducing the PL solubilities in those four-component solvents. The maximal PL contents in the PL/AA-HA-FU-PH, PL/AA-ME-FU-PH, PL/HA-ME-FU-PH binary systems (see Point A in Figure 4-15b–4-15c) are ~56, ~51, ~52 wt % (equivalent to a PL solubility of ~128, ~106, ~109 g PL per 100 g of model solvent/water mixture), respectively. While the maximal PL contents in the PL/solvent/water ternary systems (see Point B in Figure 4-15b–4-15c) increase to ~60, ~54 and ~55 wt% (equivalent to PL solubilities of ~149, ~117, ~122 g PL per 100 g of model solvent/water mixture) for the AA-HA-FU-PH, AA-ME-FU-PH, HA-ME-FU-PH solvents, respectively.

The results above clearly show that both furfural and phenol have negative effect on PL dissolution in the four-component solvent/water mixtures. The PL solubility decreases in these mixtures as the total content of furfural and phenol in the solvent increases. Therefore, the results in this study clearly demonstrate that there are at least two effective strategies to enhance the phase stability of bio-oil: (1) addition of organic solvents (i.e., methanol, hydroxyacetone, acetic acid) into bio-oil and (2) removal of furfural and phenolic from bio-oil (i.e., via selective adsorption). In addition, it is also

noted that furfural and phenol must be included in formulating the mixed solvent, as done in our previous study,[153] for establishing ternary phase diagrams for predicting the phase stability of bio-oil.

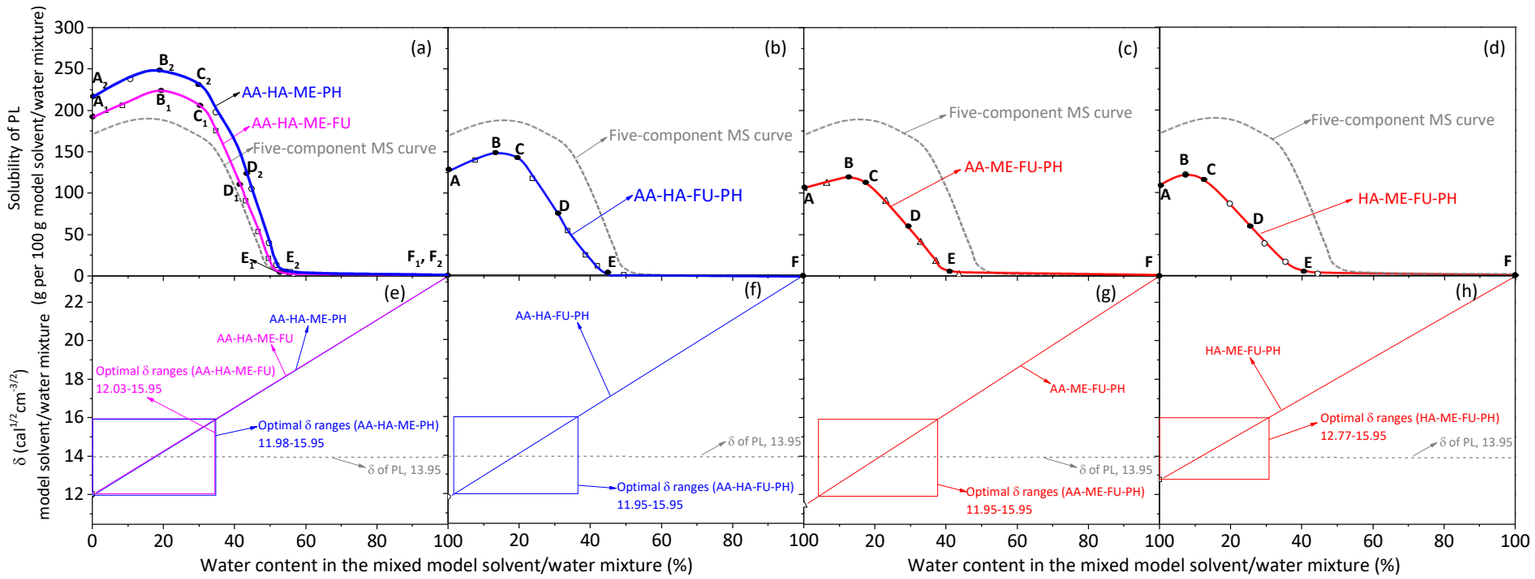

Figure 4-16 Solubilities of PL in various model solvent/water mixtures: (a) AA-HA-ME-PH/water and AA-HA-ME-FU/water mixtures; (b) AA-HA-FU-PH/water mixtures; (c) AA-ME-FU-PH/water mixtures; (d) HA-ME-FU-PH/water mixtures. Points A-F in panel (a), panel (b), panel (c) and panel (d) correspond to points A-F in Figure 4-15a, 4-15b, 4-15c and 4-15d, respectively. Panel (e), (f), (g) and (h): The colour area represents the optimal δ range of the mixed model solvent/water mixtures for the dissolution of PL. The grey dashed curves represent the solubilities of PL in mixtures of five-component MS and water.[153]

4.7 Conclusions

This study investigates the effect of single/mixed model solvents on the ternary phase diagrams of PL, model solvent and water, considering various single-component (i.e., AA, HA and ME), two-component (i.e., AA-FU/PH, HA-FU/PH, ME-FU/PH), three-component (i.e., AA-HA-ME, AA-HA-FU/PH, AA-ME-FU/PH, HA-ME-FU/PH) and four-component (i.e., AA-HA-ME-FU/PH, AA-HA-FU-PH, AA-ME-FU-PH, HA-ME-FU-PH) model solvents. The PL solubilities in various model solvent/water mixtures are also calculated. Several important conclusions can be drawn:

(1) FU is miscible with AA, HA and ME, but forms two different homogeneous binary systems with water, i.e., organic-rich system at low water contents (i.e., <5 wt%) and water-rich systems at high water contents (i.e., >96 wt%). In contrast, PH has very high solubilities (i.e., >95 wt%) in AA, HA and ME, but only forms homogeneous binary systems with water at high water contents (i.e., >93 wt%).

(2) For FU in solvent/water mixture, there exists a critical water content (i.e., ~62 , ~37 and ~53 wt% for AA, HA and ME, respectively) below which the FU/solvent/water ternary systems are always homogenous. However, when the water content in the solvent/water mixture is higher than the critical value, it can form two possible homogeneous ternary systems (one is the organic-rich system and the other is the water-rich system) depending on the water content in the solvent/water mixture. In contrast, the PU solubility is high in the solvent/water mixtures, but decreases with increasing the water content in the solvent/water mixture. It is important to make sure the solvent/water mixture is homogeneous when studying the ternary phase diagrams of PL, model solvent and water

(3) Among three single-component solvents (i.e., AA, HA and ME), ME is the best solvent for PL dissolution in solvent, followed by HA and AA. The highest

PL content of ~86 wt% is achieved in ME, equivalent to a PL solubility of ~615 g per 100 g of ME (more than doubled the PL solubilities in AA and HA). This indicates that methanol addition is the most effective strategy to enhance the phase stability of bio-oil. Increasing the water content can slightly increase the PL solubilities in the AA/water and HA/water mixtures, but a further increase in the water content leads to the reduction of PL solubilities in the AA/water and HA/water mixtures. In constrast, increasing the water content continuously reduces the PL solubilities in the ME/water mixtures.

(4) The ternary phase diagrams for the two-component solvents clearly demonstrate that both FU and PH have negative effect on PL dissolution in model solvent/water mixtures. For example, the maximal PL contents in PL/AA-FU, PL/HA-FU and PL/ME-FU binary systems reduce to ~46, ~45, and ~63 wt%, which correspond to PL solubilities of ~86, ~81, and ~ 171 g PL per 100 g of model solvent, respectively. An increase in the FU or PH content in the solvent further reduces the PL solubility in the solvent/water mixture. Compared to PH, FU has slightly stronger effect to suppress the PL dissolution in the solvent/water mixture.

(5) For the three-component solvents, the AA-HA-ME solvent has the strongest ability to dissolve PL, leading to the maximal PL content of ~70 wt% for the PL/solvent binary system (equivalent to a PL solubility of ~238 g PL per 100 g of solvent/water mixture). Similarly, addition of both FU and PL largely reduces the PL solubility in the solvent/water mixtures.

(6) The ternary phase diagrams for the four-component solvents indicate that the total content of FU and PH is an important factor to determine the PL solubility in the solvent/water mixture. The PL solubility decreases as the total content of FU and PH in the solvent increases. Therefore, removal of FU and PH from bio-oil can be another effective strategy to enhance the phase stability of bio-oil. However, FU and PH have to be included in the mixed solvent in order to

generate useful ternary phase diagrams for predicting the phase stability of bio-oil.

Chapter 5 Ternary System of Pyrolytic Lignin, Mixed-Solvent and Water: Phase Diagram and Implications

5.1 Introduction

In the open literature, the study on predicting bio-oil phase separation based on the concentrations of water, PL and the light organic fraction is scarce. Only one study from Oasmma[10] developed a ternary phase diagram of PL, solvent mixture (i.e., the water-soluble and ether-soluble bio-oil) and mixture of polar components (i.e., water and sugars), and a phase stability index was developed for bio-oils. However, there are at least two limitations for that ternary phase diagram. One is that the ternary phase diagram does not cover the entire range of the three fractions. The other is that sugars should be separated from the mixture of polar components, since sugars are not solvents.

Therefore, this work aims to develop a set of phase diagrams which may be suitable for predicting the phase stability of different bio-oils. As mentioned in section 3.3.2, a representative mixed solvent (MS) is developed to substitute the light organic fraction of bio-oil for mixing with water and PL. This chapter aims to develop ternary phase diagrams of PL (or its fraction)/MS/water system to study the phase behaviour of PL and its fractions in various MS/water mixtures. The effect of free sugars (mainly levoglucosan) on the phase behaviour of PL (or its fraction)/MS/water system is also investigated. The potential applications of phase diagram in predicting phase separation of bio-oil are further discussed.

5.2 Properties of PL and Its Fraction

PLs extracted from different bio-oils can have different characteristics in term of average molecular weight and the ratio of phenylpropane units.[154] It can be seen in Figure 5-1 that the weight average molecular weight (Mw) of the PL-HMW, PL, and PL-LMW samples are 1276, 958, and 740 Da, respectively. This is in consistent with

previous reported Mw of PL from different bio-oils and PL fractions,[9, 155] i.e., 650 – 1300 Da.[155] The proximate and ultimate analysis results of three PL samples are shown in Table 5-1. The PL-HMW sample has a higher fixed carbon content and a lower volatile content than the PL-LMW sample, because the PL-HMW has a much higher molecule weight and thus a lower volatility compared to the PL-LMW. Interestingly, the PL-HMW sample has a lower carbon content and a higher oxygen content than the PL-LMW sample. This leads to the higher atomic O/C ratio (0.37) and the lower atomic H/C ratio (1.13) for the PL-HMW sample in comparison to 0.28 and 1.20 for the PL-LMW sample, respectively. The atomic H/C and O/C ratios are widely used for estimating fuel aromaticity and polarity, respectively.[156-158] The higher O/C ratio of the PL-HMW indicates it has a higher polarity than the PL-LMW. This is not surprising because the PL-HMW is not soluble in CH_2Cl_2 (a non-polar solvent) while the PL-LMW is soluble in CH_2Cl_2. The lower atomic H/C ratio of the PL-HMW suggests its higher aromaticity. The UV fluorescence intensities of all PL samples are presented in Figure 5-2. It can be seen that the UV fluorescence spectra of these PL samples are mainly centred at ~350 nm (corresponding to two or three fused rings[159]). The UV fluorescence spectrum of the PL-HMW slightly shifts towards larger fused ring structures, which provides direct evidences for the higher aromaticity as abovementioned. For the three different types of phenolic units (i.e., G, H and S[160]), the ^{13}C-NMR analysis shows that the PL, PL-HMW and PL-LMW samples have the G/H/S ratios of 1.49/0.29/1.0, 0.81/0.1/1.0 and 1.84/0.63/1.0, respectively.

Table 5-1 Properties of pyrolytic lignin samples.

	PL-LMW [e]	PL [f]	PL-HMW [g]
moisture (wt %, ar[a])	1.1	1.8	1.8
ash (wt %, db[b])	0.6	1.5	0.9
volatile (wt %, db[b])	81.8	75.8	68.9
fixed carbon (wt %, db[b])	17.6	22.7	30.2
C (wt %, daf[c])	68.09	66.26	62.79
H (wt %, daf[c])	6.81	6.37	5.92
N (wt %, daf[c])	0.06	0.11	0.19
O (wt %, daf[c])[d]	25.04	27.26	31.1
Atomic H/C	1.20	1.15	1.13
Atomic O/C	0.28	0.31	0.37

[a] as received; [b] dry basis; [c] dry ash free basis; [d] by difference; [e] PL-LMW: CH_2Cl_2-soluble fraction of pyrolytic lignin; [f] PL: pyrolytic lignin; [g] PL-HMW: CH_2Cl_2-insoluble fraction of pyrolytic lignin.

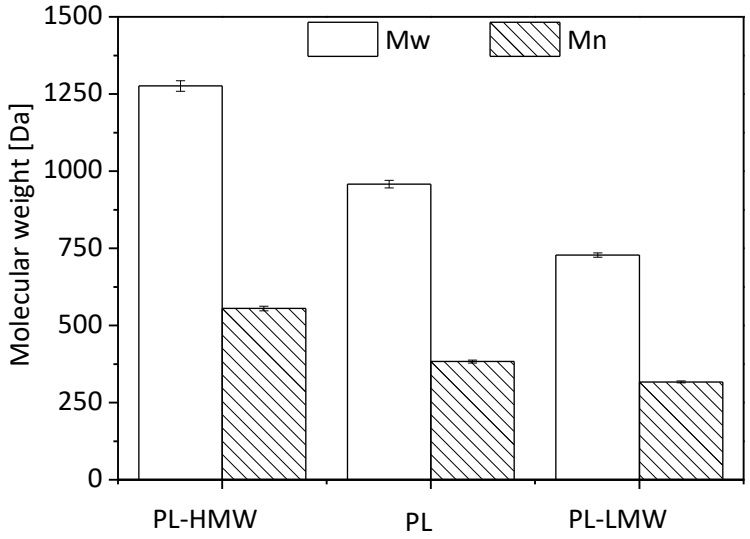

Figure 5-1 Weight average molecular weight (Mw) and number average molecular weight (Mn) of PL and its fractions. PL-HMW: CH_2Cl_2-insoluble fraction of pyrolytic lignin; PL: pyrolytic lignin; PL-LMW: CH_2Cl_2-soluble fraction of pyrolytic lignin.

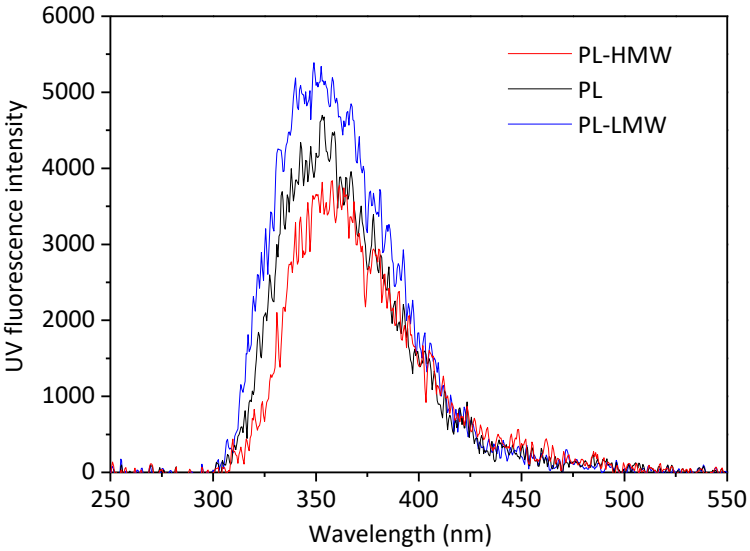

Figure 5-2 UV fluorescence spectra of PL and its fractions. PL-HMW: CH_2Cl_2-insoluble fraction of pyrolytic lignin; PL: pyrolytic lignin; PL-LMW: CH_2Cl_2-soluble fraction of pyrolytic lignin.

5.3 Ternary Phase Diagram of PL/MS/Water System

Figure 5-3 presents the ternary phase diagram of the PL/MS/water system. The phase conversion curve clearly divides the ternary phase diagram into two regions: homogeneous region (above the curve) and inhomogeneous region (below the curve). The panels a and b of Figure 5-4 illustrate the representative microscopic photographs of two PL/MS/water mixtures. Figure 5-4a shows a homogeneous mixture in a single phase at a PL/MS/water system with weight percentages of 20/70/10, corresponding to point 1 in Figure Figure 5-3. Figure 5-4b illustrates the heterogeneous structure of an inhomogeneous mixture at a PL/MS/water system with weight percentages of 20/20/60, corresponding to point 2 in Figure 5-3. The construction of the phase conversion curve in Figure 5-3 leads to several important points to be made.

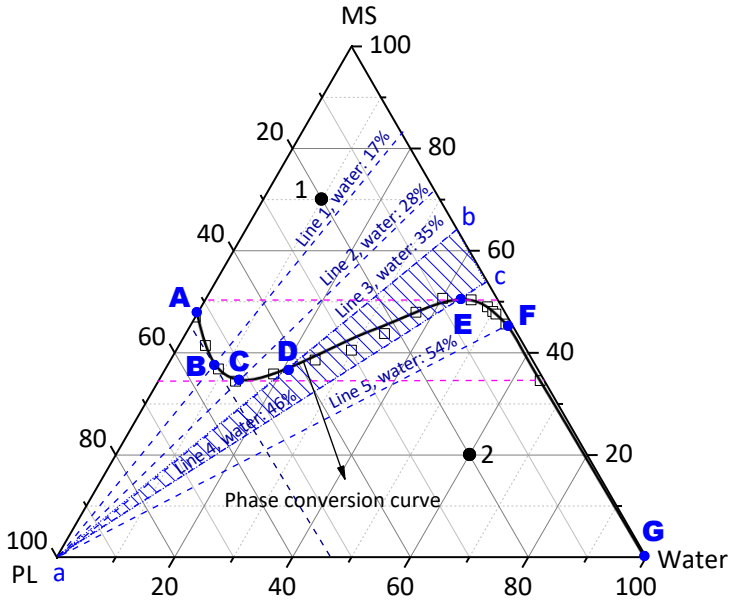

Figure 5-3 Ternary phase diagram of the PL/MS/water system. Line 1 represents the MS/water mixture passing through point B at which the maximal solubility of PL is achieved in the MS/water mixture. Point C represents the minimal solvent required to possibly form a homogeneous PL/MS/water solution, corresponding to line 2. Lines 3 and 4 represents the MS/water mixtures passing through point D and E, respectively and are the boundaries of the narrow range in water content (i.e., the range of line $\overline{bc}$ of the shaded triangle *abc*) in which a drastic reduction in the solubility of PL in the MS/water mixture is evident as the content of water increases from point D to point E. Point E represents the minimal solvent at which a homogeneous solution is always formed for the ternary system, corresponding to line 4. Line 5 passes through point F, representing the MS/water mixture which dissolves little PL. Points 1 and 2 are the representative compositions of homogeneous and inhomogeneous mixtures for microscopic photographs presented in Figure 5a and 5b, respectively. PL: pyrolytic lignin; MS: mixed solvent

First, considering that PL is dissolvable in the MS, it is understandable that the phase conversion curve intersects with the side (at point A) of the PL/MS binary system in Figure 5-3. As PL is not dissolvable in water, the phase conversion curve does not

intersect with the side of the PL/water binary system in Figure 5-3. Furthermore, since the MS and water are fully miscible, it is expected that the phase conversion curve insects with the side of the MS/water binary system at the vertex "water" (i.e., point G).

Second, the datum points on the phase conversion curve in Figure 5-3 represent the solubilities of PL in the MS/water mixtures of various water contents. Therefore, the results on the phase conversion curve in Figure 5-3 can be plotted in the form of PL solubility in the MS/water mixture as a function of water content in the MS/water mixture, as shown in Figure 5-5a, with key points (A-F) and lines (1-5) being highlighted in both figures. In a PL/MS binary system, i.e., point A (in both Figure 5-3and Figure 5-5a) where the water content in the MS/water mixture is zero, PL has a maximal concentration of ~53 wt % (see Figure 5-3) in the PL/MS binary system, which is equivalent to a solubility of ~112 g PL per 100 g of MS (see Figure 5-5a). The shift in the composition of the PL/MS/water system from point A to point B along the phase conversion curve (in Figure 5-3) results in an increase in water content in the PL/MS/water ternary system. As shown in both Figure 5-3and Figure 5-5a, increasing water content from point A to point B enhances the solubility of PL in the MS/water mixture. However, further increasing water content in the ternary system shifts the system from point B to point C, which witnesses a reduction in the solubility of PL in the MS/water mixture. The maximal solubility of PL in the MS/water mixture is ~54 wt % in the PL/MS/water mixture (equivalent to the solubility of ~118 g PL per 100 g of MS/water mixture) at point B, which corresponds to a water content of ~17 wt % in the PL/MS/water ternary system (see line 1). Point C represents the minimal solvent (~35 wt % in the PL/MS/water system) required to possibly form a homogeneous PL/MS/water solution, corresponding to line 2 (i.e., ~28 wt % water in the MS/water mixture). The solubility of PL in the MS/water mixture further decreases to ~75 g PL per 100g MS/water mixture from point C to point D, which represents the water content of the MS/water mixture increasing from 28 (line 2) to 35 wt % (line 3).

However, a further shift from point D to point E, i.e., the water content of the MS/water mixture increasing from 35 (line 3) to 46 wt % (line 4), results in a drastic decrease in the amount of dissolved PL in the PL/MS/water system from ~43 to ~6 wt % (corresponding to a reduction in the PL solubility from ~75 to ~7 g per 100 g of MS/water mixture). Point E represents the minimal solvent (~50 wt % in the PL/MS/water system) required to guarantee a homogeneous PL/MS/water solution, corresponding to line 4 (i.e., ~46 wt % water in the MS/water mixture). When the water content in the MS/water mixture is above 54 wt % (point F, corresponding to line 5), the solubility of PL in the MS/water mixture becomes very low (<5 g per 100 g of MS/water mixture). Clearly, such a drastic reduction in the solubility of PL in the MS/water mixture demonstrates the presence of a very narrow range of water content (35−46 wt %, i.e., the range of line $\overline{bc}$ in the shaded triangle area *abc* in Figure 4 and the range in Figure 5-5, bounded by lines 3 and 4) where the water content in the MS/water mixture has a critical role in dictating the solubility of PL in the MS/water mixture.

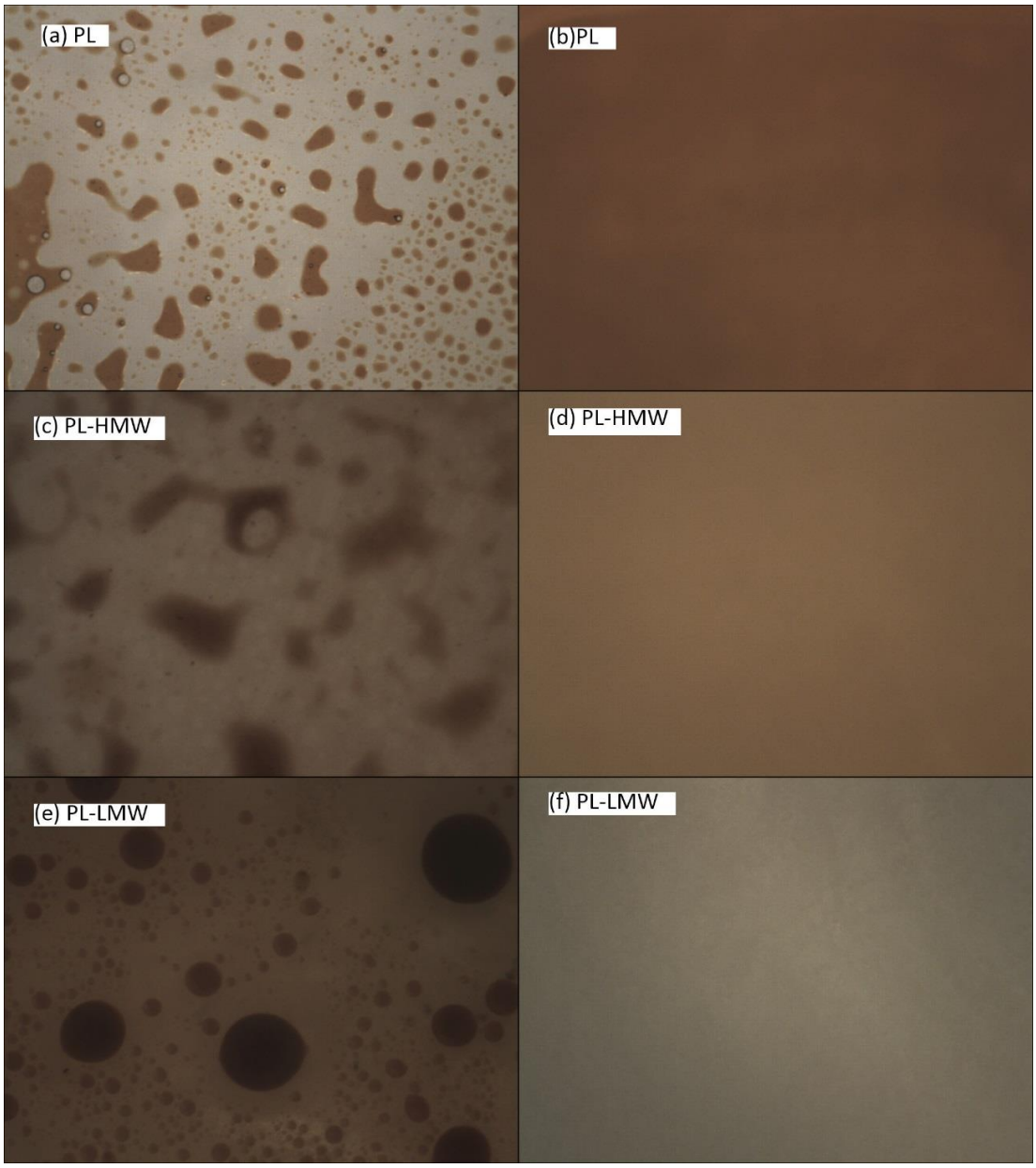

Figure 5-4 Representative microscopic photographs of inhomogeneous and homogeneous mixtures of PL and its fractions. (a) The image of the PL/MS/water system with weight percentages of 20/20/60; (b) the image of the PL/MS/water system with weight percentages of 20/70/10; (c) the image of the PL/MS/water system with weight percentages of 20/20/60; (d) the image of the PL-HMW/MS/water system with weight percentages of 20/70/10; (e) the image of the PL-HMW/MS/water system with weight percentages of 20/20/60; (f) the image of the PL-LMW/MS/water system with weight percentages of 20/70/10. PL-HMW: CH_2Cl_2-insoluble fraction of pyrolytic lignin; PL: pyrolytic lignin; PL-LMW: CH_2Cl_2-soluble fraction of pyrolytic lignin.

Third, the solubility principle can be used to interpret the ternary phase diagram of the PL/MS/water system. The changes in the solubility of PL in MS/water mixture can be explained via comparing the solubility parameter δ of the PL with those of the MS/water mixtures at different water contents. Figure 6b shows that the δ of the MS/water mixture increases linearly with the water content and also presents the optimal δ range (see the shaded area) of solvent for PL dissolution according to the discussion in Section 3.2. It is interesting to note that the observed changes in the solubility of PL in MS/water mixtures (in Figure 5-3 and Figure 5-5a) agree well with the shift in the δ value of the MS/water mixture from inside to outside of the optimal δ range in Figure 5-5b. The solubility of PL is high (>75 g per 100 g of MS/water mixture) in the optimal δ range (i.e., with a water content <35 wt %). Particularly, point B, where corresponds to the highest solubility of PL in the MS/water mixture and closely to line 1 that represents the MS/water mixture with a water content of ~17 wt%, has almost the same δ value of PL. As the water content increases to >35 wt % (outside the optimal δ area), the solubility of PL in MS/water mixture decreases drastically (see Figure 5-5a). Last, the ternary phase diagram provides some important guidelines for the phase stability of the PL/MS/water system. If some minimal requirements are met, the phase separation of the PL/MS/water system may be avoided. For example, the PL/MS/water system is always phased separated, if the PL content is >54 wt %, or the water content is >54 wt %, or the MS content is <35 wt %, while the PL/MS/water system is always stable if the MS content is >50 wt %. It is also observed that the PL has a good solubility (i.e., with the PL content of ~43−54 wt %) in the MS/water mixture, if the water content in the MS/water mixture is <35 wt %. There is also a critical range (i.e., 35–46 wt %) of the water content in the MS/water mixture, where the PL solubility is drastically affected by the water content.

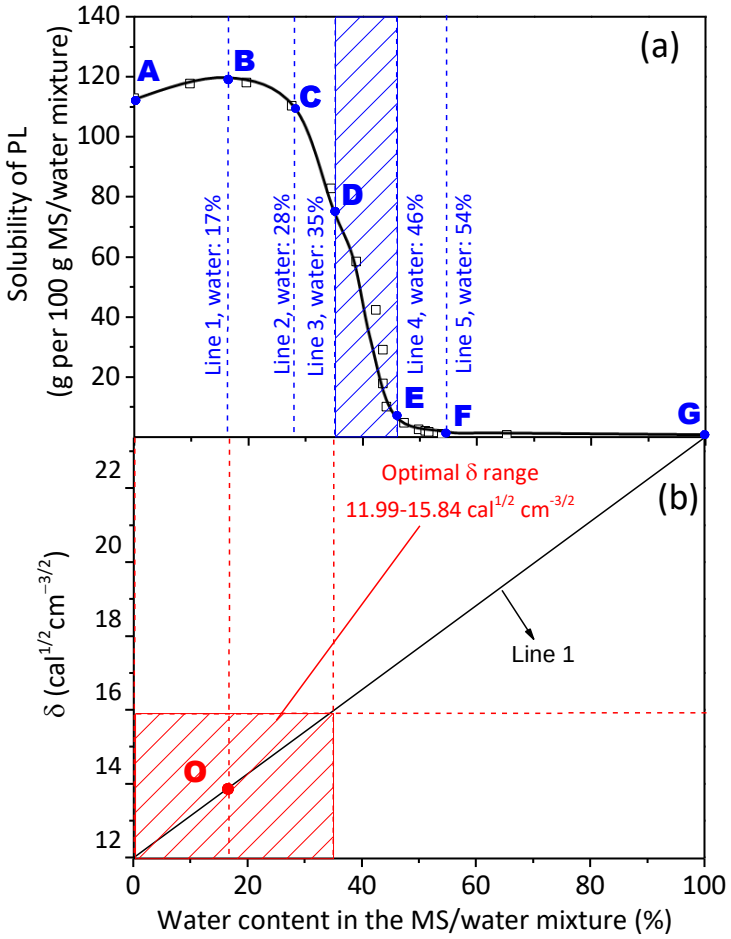

Figure 5-5 Solubilities of PL in various MS/water mixtures. Panel (a): lines 1-5 represent the MS/water mixtures with water contents of ~17, ~28, ~35, ~46 and ~54 wt %, respectively; points A-G and the shaded area correspond to points A-G and the shaded triangle *abc* in Figure 4, respectively. Panel (b): line 1 represents the δ values of the MS/water mixtures at various water contents; point O represents the δ value of PL; and the shaded area represents the optimal δ range of the MS/water mixtures for the dissolution of PL. PL: pyrolytic lignin; MS: mixed solvent.

5.4 Ternary Phase Diagrams of PL-HMW/MS/Water and PL-LMW/MS/Water Systems

The ternary phase diagrams of different PL fractions were further developed to understand the phase behaviour of different PL fractions in the MS/water mixtures. The ternary phase diagrams and the solubilities of the PL-HMW and PL-LMW are

compared in Figure 5-6 and Figure 5-7. The representative microscopic photographs for the PL-HMW and PL-LMW are also shown in the panels c-f of Figure 5-4. Two important observations can be made. One is the solubilities of different PL fractions in the same MS/water mixture follow an order of PL-LMW > PL > PL-HMW. The PL-LMW shows much a higher solubility in the same MS/water mixture, compared to other PL fractions. It appears that the solubility of PL (or its fractions) is strongly influenced by the average molecular weight, with an increased solubility for PL of a lower average molecular weight. Thus, the PL-LMW can maintain a single phase in the MS/water mixture with a lower MS content and/or a higher water content, in comparison to PL and PL-HMW. For example, the PL-LMW/MS/water system is always stable if the MS content is >48 wt %, in comparison to >54 and >57 wt % for the PL/MS/water and PL-HMW/MS/water systems, respectively. The results suggest the bio-oil phase stability can be largely improved if the content of PL-HMW in the bio-oil is low, and solvent addition is an effective strategy to improve the bio-oil stability. The other important observation is that the trends of the phase conversion curves for PL fractions follow a similar pattern to that for the PL, as highlighted with similar key points (A-F) and lines (1-5) in Figure 5-6 (also plotted as the solubilities of PL factions in the MS/water mixture in Figure 5-7). In PL-HMW/MS or PL-LMW/MS binary systems, the PL-HMW and PL-LMW has maximal concentrations of ~45 and ~58 wt % in the binary systems as shown in Figure 5-6, corresponding to the solubility of ~85 and ~138 g per 100 g of MS, respectively. As the composition of the ternary mixture shifts from point A to point B along the phase conversion curve (see Figure 5-6a and Figure 5-6b), the increase of a small amount of water also enhances the solubility of the PL-HMW or PL-LMW in the MS/water mixture. For example, the PL-HMW and PL-LMW have maximal concentrations of ~49 and ~61 wt % in the ternary system, corresponding to water contents of ~15 and ~17 wt % in the MS/water mixtures, respectively. This is equivalent to the solubilities of ~96 and ~156 g per 100 g of MS/water mixture (see Figure 5-7a and 5-Figure 5-7b),

respectively. Similar as the PL/MS/water phase diagram, further increasing of water content (from point B to point C) in the MS/water mixture results in a reduction in the solubilities of PL-HMW and PL-LMW in the MS/water mixture. At the point C, the minimal MS required to homogenize the PL-HMW/MS/water and PL-LMW/MS/water mixture is ~42 and ~29 wt %, respectively. The solubilities of the PL-HMW and PL-LMW in the MS/water mixture continue to decrease to ~50 g PL-HMW and ~120 g PL-LMW per 100 g MS/water mixture from point C to point D. Shifting from point D to point E represents the water content of MS/water mixture for the PL-HMW and PL-LMW increasing from 33 to 42 wt % and from 36 to 49 wt %, respectively. Within such narrow ranges (as shown in Figure 5-7a and 5-Figure 5-7b), the solubilities of PL-HMW and PL-LMW decrease drastically from ~44 to ~3 g and from ~120 g to ~6 g per 100 g of MS/water mixture, respectively. When the water content in the PL-HMW/MS/water and PL-LMW/MS/water system is >48 and >56 wt % (point F i Figure 5-6a and 5-Figure 5-6b), the solubilities of PL-HMW and PL-LMW in the MS/water mixture approach almost zero.

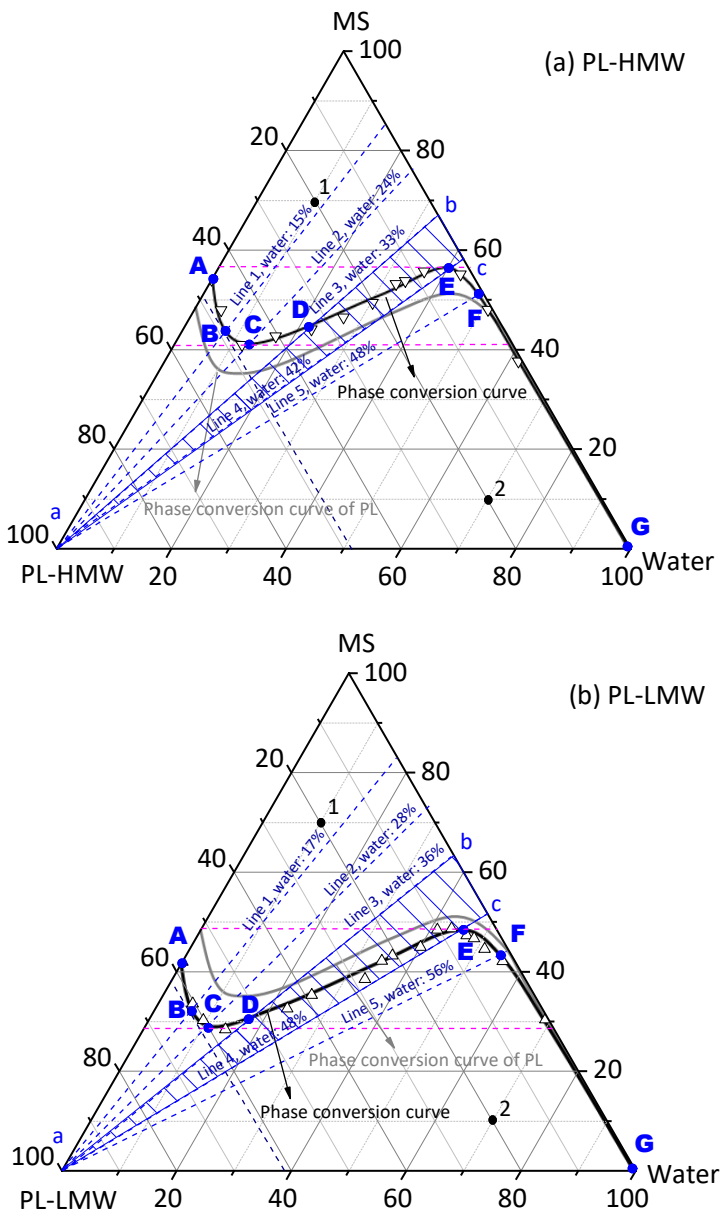

Figure 5-6 Ternary phase diagrams of PL-HMW/MS/water and PL-LMW/MS/water. Panel (a): lines 1-5 represent the MS/water mixtures with a water content of ~15, ~24, ~33, ~42 and ~48 wt %, respectively. Panel (b): line 1-5 represent the MS/water mixtures with a water content of ~17%, ~28%, ~36%, ~49 % and ~56 % respectively. Definitions of lines 1-5 and the shaded area *abc* in both panels (a) and (b) are same as those given in Figure 4. Points 1 and 2 in both panels are the representative compositions of homogeneous and inhomogeneous mixtures for microscopic photographs presented in Figure 5c and 5f, respectively. PL-HMW: CH_2Cl_2 insoluble fraction of pyrolytic lignin; PL-LMW: CH_2Cl_2 soluble fraction of pyrolytic lignin; MS: mixed solvent.

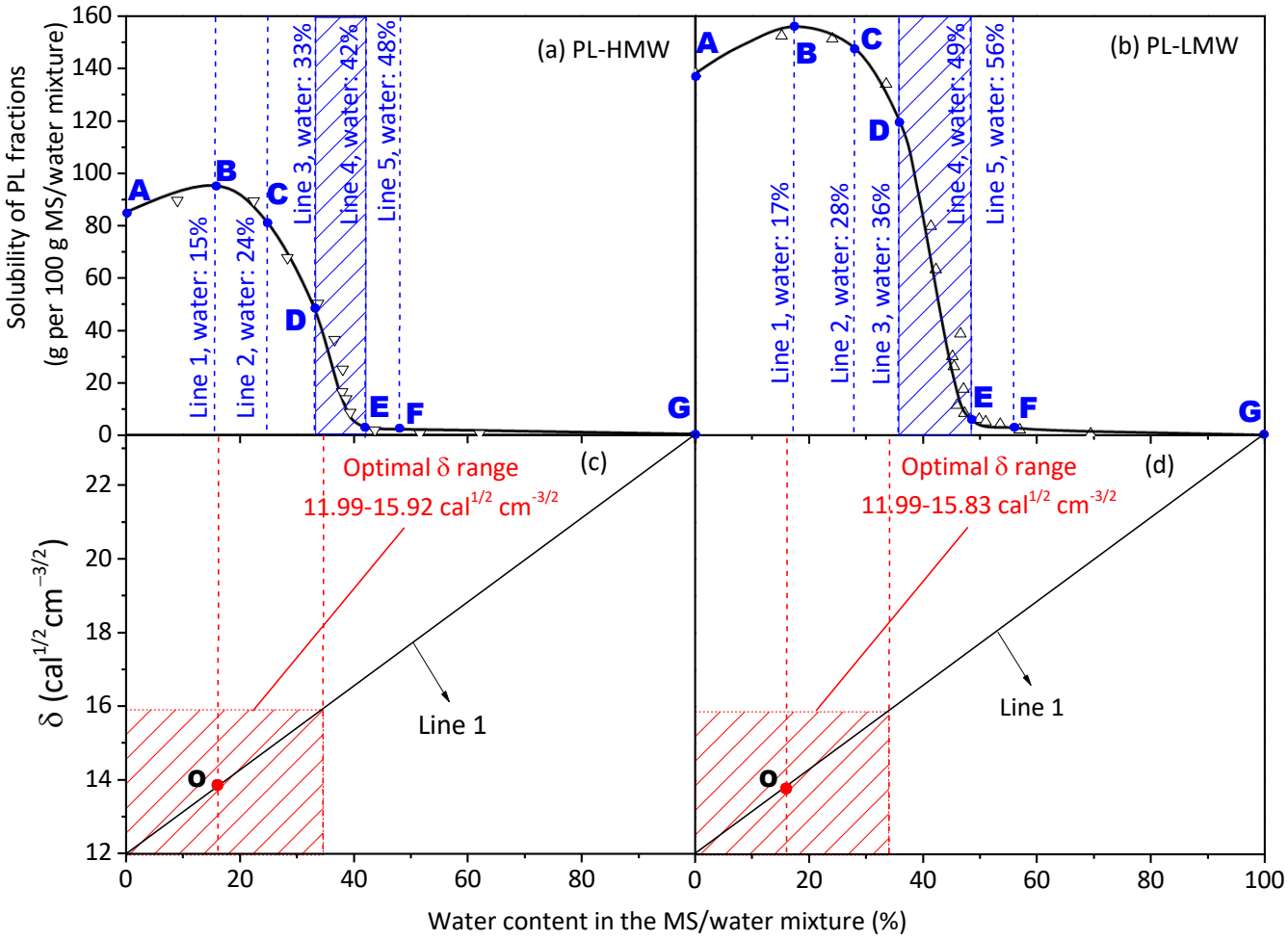

Figure 5-7 Solubilities of PL-HMW/MS/water and PL-LMW/MS/water in various MS/water mixtures. Panel (a): lines 1-5 represent the MS/water mixture with a water content of ~15, ~24, ~33, ~42 and ~48 wt %, respectively. Panel (b): Lines 1-5 represent the MS/water mixture with a water content of ~17, ~28, ~36, ~49 and ~56 wt %, respectively. Panel (c) and (d): line 1 represents the δ values of the MS/water mixtures at various water contents; point O represents the δ value of PL-HMW (or PL-LMW); and the shaded area represents the optimal δ ranges of the MS/water mixtures for the dissolution of PL-HMW (or PL-LMW). Points A-G in panel (a) and (b) correspond to points A-G in Figure 7a and 7b, respectively. The shaded areas in panel (a) and (b) correspond to the shaded triangles *abc* in Figure 7a and 7b, respectively. Definitions of lines 1-5 in panels (a) and (b) are same as those given in Figure 4. Definitions of shaded areas in panels (a) and (b) are same as that in Figure 6. PL-HMW: CH_2Cl_2 insoluble fraction of pyrolytic lignin; PL-LMW: CH_2Cl_2 soluble fraction of pyrolytic lignin; MS: mixed solvent.

The data on the solubilities of the PL-HMW and PL-LMW presented in Figures Figure 5-6a, 5-Figure 5-6b, 5-Figure 5-7a and 5-Figure 5-7b can also be interpreted based on the solubility principles. The δ values of the PL-HMW and PL-LMW are 13.92 and 13.83, respectively. At point B where the maximal solubilities of PL-HMW and PL-LMW are reached, the δ values of the MS/water mixtures (with 15 and 17 wt % of water in the MS/water mixture, corresponding to line 1 in Figure 5-6a, 5-Figure 5-6b, 5-Figure 5-7a and 5-Figure 5-7b) are 13.7 and 13.9 (see Figure 5-7c and 5-Figure 5-7b), respectively. Therefore, the δ values of the MS/water mixtures closely match those of the solutes (PL-HMW or PL-LMW), as shown Figure 5-7. Similarly, it is also understandable for the presence of the critical ranges in the water content (i.e., ~33–42 wt % for the PL-HMW and ~36–49 wt % for the PL-LMW from point D to point E) of the MS/water mixtures, where the solubilities of the PL-HMW and PL-LMW are drastically affected by the water content. This is because, as the water content of the MS/water mixture increases to that of point D (i.e. ~33 and ~36 wt % for the PL-HMW and PL-LMW), the δ values of the MS/water mixtures move out of the optimal δ ranges for the dissolution of the PL-HMW and PL-LMW, respectively. At point E (i.e., ~42 and ~49 wt % water in the MS/water mixture for the PL-HMW and PL-LMW), the δ values of the MS/water mixtures are far beyond the optimal δ ranges for dissolving the PL-HMW or PL-LMW, the solubilities of PL fractions become very low (<5 g per 100 g of MS/water mixture).

5.5 Effect of Sugar on Ternary Phase Diagrams of PL and Its Fractions

Bio-oil can be considered as a mixture of three pseudo-components: PL, water-soluble fraction (excluding water) and water. In this study, the water-soluble fraction is modelled by the MS that is formulated from the five model compounds representing the five key chemical families (i.e., acids, phenols, aldehydes and ketones, furans and alcohols, respectively). As shown in Table 3-1, sugar is another important solute in the bio-oil system, in addition to PL. Therefore, to enable the practical application of the PL/MS/water ternary phase diagram, the effect of sugar on the phase behaviour of the

ternary systems should be studied. It is important to note that the sugar as a solute refers to the free sugar in the system. It was recently reported[120] that ~5−7 wt % of sugar (mainly in the form of levoglucosan) could be present in the bio-oil used in this study. Therefore, levoglucosan was added into the PL/MS/water systems at two different contents of 5 and 7 wt % (calculated based on the whole system containing PL, MS, water and the added levoglucosan) to evaluate the effect of sugar on the phase behaviour of the PL/MS/water ternary system and generate the phase conversion curves. To evaluate the effect of levoglucosan, the ternary diagram is plotted on a levoglucosan-free basis, i.e., the contents of PL, MS and water normalized to 100% for the PL/MS/water ternary system, excluding levoglucosan that has been added into the system. Similar phase diagrams are also developed and constructed for the PL-HMW/MS/water and PL-LMW/MS/water systems, as shown in Figure 5-8.

Figure 5-8 shows that the phase conversion curves of the PL (or its fraction)/MS/water systems, which can be greatly affected by the presence of levoglucosan in the system when the water content in the ternary system is low (i.e., <20 wt %). For example, when levoglucosan is added in the PL/MS binary system at a content of 5% in the whole mixture, the maximal PL content in the PL/MS binary system for forming a homogeneous system reduces significantly from 54 to 37 wt % (on a levoglucosan free basis). While the maximal solubilities for the PL-HMW and PL-LMW in the PL fraction/MS binary system decrease from ~47 to 30 wt % and from ~60 to 44 wt % (on a levoglucosan free basis), respectively. An increase in the content of levoglucosan to 7 wt % in the whole mixture further reduces the maximal contents of the PL, PL-HMW and PL-LMW to ~25, 22 and 32 wt %, respectively. However, the maximal contents of the PL, PL-HMW and PL-LMW increase substantially with increasing the water content in the PL(PL-HMW or PL-LMW)/MS/water ternary system. The more sugar added into the system, the more water required to maintain the system homogeneous. When the water content in the ternary system (on a levoglucosan free basis) is higher than a certain value (i.e., >15 and >20 wt % at 5 and 7 wt% of

levoglucosan in the whole mixture, respectively), the sugar has no effect on the solubility of PL (or its fractions) in the MS/water mixture hence the ternary phase diagrams of the PL/MS/water, PL-HMW/MS/water and PL-LMW/MS/water systems.

5.6 Applications of the Ternary Phase Diagram

To test the applicability of the phase diagram, the data on the bio-oils with known composition of PL, MS, water and sugar are required. In the process of collecting literature, three important considerations are taken into account. First, the importance of free sugar in the system must be considered. Therefore, only the bio-oil samples in the previous studies[29, 120, 161, 162] that reported the contents of free sugars < 7 wt % are included. Second, fast pyrolysis bio-oil concerns PL in the system so that the collected literature data are replotted in the ternary phase diagram of the PL/MS/water system. Third and last, the literature data are processed and converted to be on a sugar-free basis for plotting on the phase diagram. As shown in Figure 10, coincidently, all the bio-oil samples with known compositions are within the homogenous region of the PL/MS/water phase diagram at 7 wt % levoglucosan in the whole system. It appears that such a ternary phase diagram of the PL/MS/water system may be useful in predicting the phase stability of bio-oil samples. It is known that bio-oil can be separated into two phases with excess water content.[163] This process can be clearly reflected in the phase diagram. In this study, a single-phase bio-oil was added into cold water with different water-to-oil ratios of 10−100, a two-phase bio-oil was easily formed even at a low water-to-oil ratio of 10. Therefore, it is clear that bio-oil experiences phase separation after being added into excess cold water. However, bio-oils with different PL-to-MS ratios require different amounts of water for phase separation. The phase conversion curve in Figure 5-9 indicates that when the water content is above ~40 wt %, phase separation can easily occur for most bio-oils.

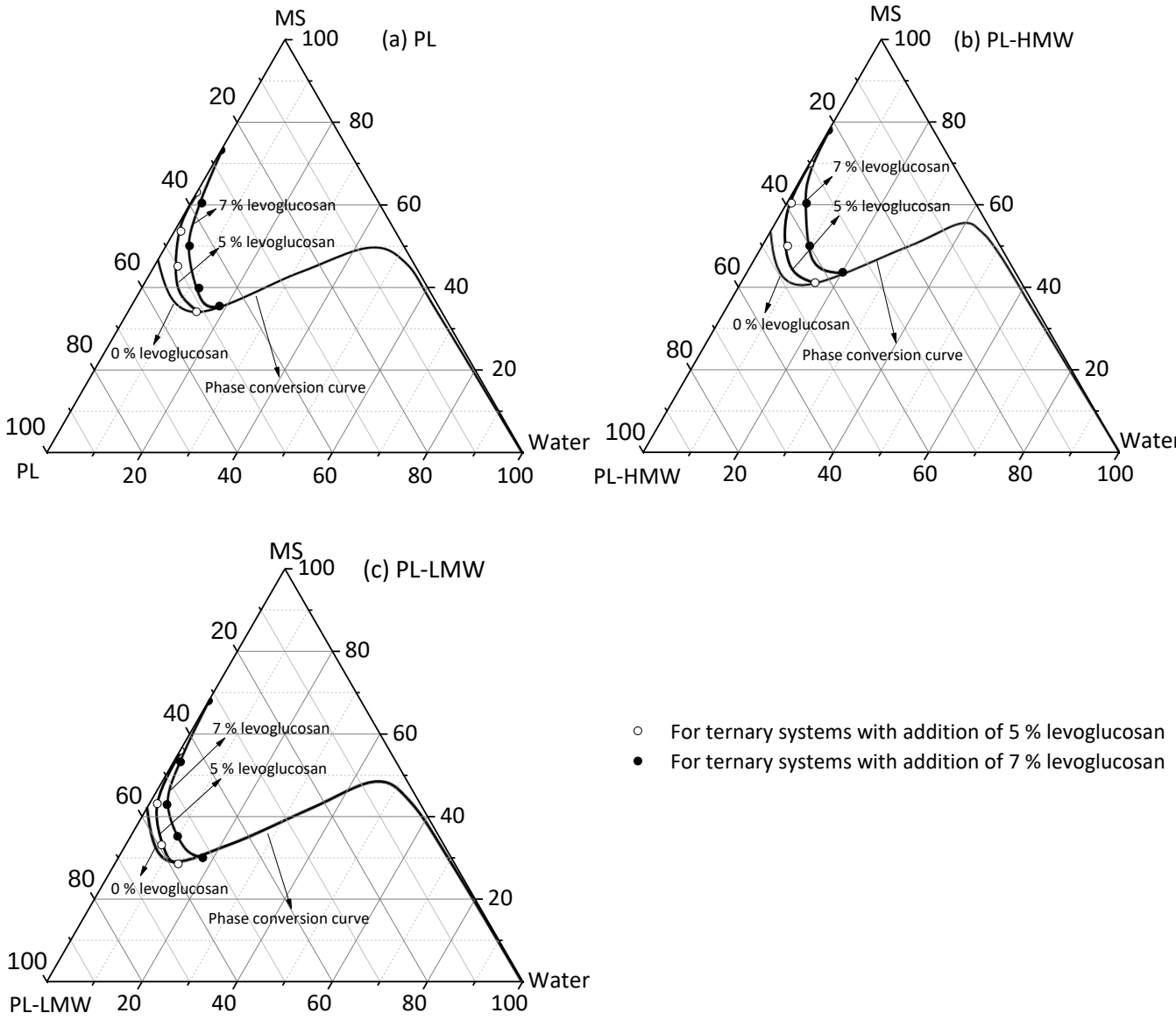

Figure 5-8 Ternary phase diagrams of the PL(its fraction)/MS/water system with the contents of sugar (represented by levoglucosan) being 5 and 7 wt % in the overall systems, respectively. The ternary diagrams are plotted with the contents of PL (or its fraction), MS and water normalized to 100 % (excluding sugar in the system).

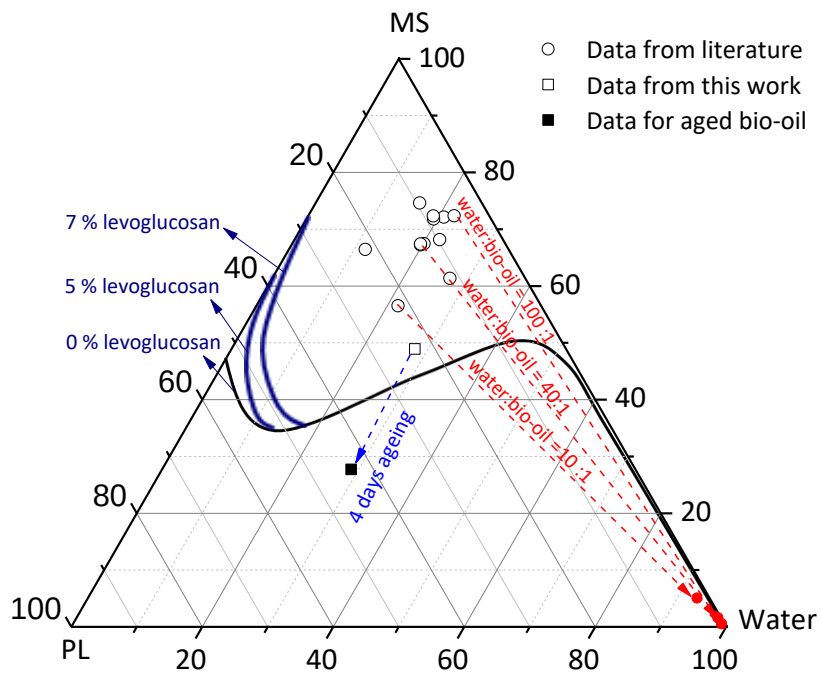

Figure 5-9 The practical applications of the phase diagram for predicting the phase stability of bio-oil samples with known compositions from the literature.[29, 120, 161, 162] The ternary diagram is plotted with the contents of PL, MS and water normalized to 100 % (excluding sugar in the system). The three red dash lines represent the cold water precipitation process at the water/bio-oil ratio of 10/1, 40/1 and 100/1, respectively.[29, 120, 162] The blue dash line represents 4-day bio-oil accelerated ageing process at 80 °C. PL: pyrolytic lignin; MS: mixed solvent.

Moreover, the ageing process of fast pyrolysis bio-oil can also be reflected in the ternary phase diagram. In this study, an accelerated ageing experiment of the bio-oils sample was also carried out at 80 °C for 4 days to generate experimental data for plotting in the phase diagram since relevant experimental data are unavailable in the literature. As clearly shown in Figure 5-9, the bio-oil sample experienced phase separation after ageing because of the drastic increase in the PL content in the aged bio-oil sample. It suggests that the bio-oil sample experienced irreversible composition changes, especially leading to significant increase in the PL content. Therefore, such ternary phase diagrams can be very useful in predicting the bio-oil ageing process. Based on the phase diagram, it may also be possible to estimate the amount of solvent required to be added into bio-oil system for avoiding the phase separation during bio-oil storage.

5.7 Conclusions

In this paper, an MS is developed based on the composition of bio-oils in existing literature for studying the phase behaviour of PL/MS/water ternary system. Several ternary phase diagrams of PL/MS/water systems are constructed for PL and its fractions, and their solubilities in various MS/water mixtures are also estimated. The phase stability of the PL/MS/water system is strongly determined by the composition of the ternary system. For example, the PL/MS/water system is always phased separated, if the PL content is >54 wt %, or the water content is >54 wt %, or the MS content is <35 wt %, while the PL/MS/water system is always stable if the MS content is >50 wt %. The ternary phase diagram can be successfully interpreted by the solubility principle. The PL solubility is high in the PL/MS binary system. An increase in the water content first leads to a slight increase in the PL solubility, followed by a gradual decrease as the water content further increases. However, there is a narrow water content range where the PL solubility is significantly affected by the water

content in the ternary system, i.e., 43−54 wt % for the PL. The solubilities of different PL fractions indicate that PL solubility is influenced by its average molecular weight, and the PL of a lower average molecular weight has a higher solubility in the same MS/water mixture. The presence of free sugar (i.e., levoglucosan) also affects the phase stability of the PL/MS/water system, but only at low water content (i.e., <20 wt %). A higher sugar content leads to the phase separation of the PL/MS/system at a lower PL content. The results suggest that the ternary phase diagram of the PL/MS/water system can be a powerful tool in predicting phase separation of bio-oil in various processes such as water precipitation and ageing.

Chapter 6 Effect of Ageing on the Phase Diagrams of Pyrolytic Lignin, Mixed Solvent and Water

6.1 Introduction

Auger reactors, with and without a heat carrier, do not require a carrier gas to move the biomass.[29, 164] Besides, auger reactors have some other features including lower operating temperatures and operating as a continuous process.[26] The main disadvantage of auger reactor is that heat transfer may be a problem if operating at large scales.[165] Velden *et al.* compared the technology strength and market attractiveness, which indicates that the auger reactor is one of the best pyrolysis technologies for commercial development.[166] Several companies: ABRI-Tech,[167] Biogreen-energy,[168] and Genesis Industries[169] have successfully commercialized the auger reactors to produce bio-oils.

Although the growing interests in developing auger pyrolysis reactors, there are very few systematic studies on the phase stability control of bio-oils.[170] Recently, a five-component mixed solvent based on the composition of fast pyrolysis bio-oils was developed in our previous studies.[121] Thus in this study, the main goal is to study the phase behaviour of fresh bio-oils produced from biomass fast pyrolysis in a lab-scale auger reactor.

6.2 Properties of PL samples

As shown in Table 6-1, PLs extracted from aged bio-oils have much higher average molecular weights, compared with those extracted from fresh bio-oils. It can be seen in Figure 6-1, both PL samples extracted from aged bio-oils centralised at ~3.0 (equivalent to ~1000 Da) while those extracted from fresh bio-oils exhibit strong peaks at ~2.5 (equivalent to ~316 Da). The proximate and ultimate analysis results of PL samples are shown in Table 6-1 . The PL samples from fresh bio-oils have higher volatile and carbon content than their counterparts, i.e., mallee oil PL has a volatile content of 77.2 % while the volatile content of PL from aged mallee oil is 73.1 %. This is because after bio-oil ageing will significantly increase the molecular weight of PLs, thus leading to a decrease in the volatile content of PL sample.

Table 6-1 Properties of the PL.

	MOPL[a]	AMOPL[b]	POPL[c]	APOPL[d]
moisture (wt %)	1.1	1.2	1.5	0.9
ash (wt %, db[e])	1.7	1.6	1.1	1.3
volatile (wt %, db[e])	77.2	73.1	84.6	75.4
fixed carbon (wt %, db[e])	21.1	25.3	14.3	23.3
C (wt %, daf[f])	64.16	61.77	68.76	65.10
H (wt %, daf[f])	7.25	6.98	6.79	5.96
N (wt %, daf[f])	0.19	0.25	0.12	0.19
O (wt %, daf[f])[g]	28.40	31.04	24.33	28.75
δ ($cal^{1/2}$ $cm^{-3/2}$)[h]	13.95	13.83	14.05	13.88
molecular weight (Da)	740	1030	550	950
polydispersity	3.4	2.9	2.4	2.7

[a] Mallee oil pyrolytic lignin. [b] Aged mallee oil pyrolytic lignin. [c] Pine oil pyrolytic lignin. [d] Aged pine oil pyrolytic lignin. [e] Dry basis. [f] Dry-ash-free basis. [g] By difference. [h] Solubility parameter values.

The authors tried to use CH_2Cl_2 extraction methods to further separate PL samples from both fresh and aged bio-oils. However, the PL samples from two fresh bio-oil samples are all soluble in CH_2Cl_2. Therefore, only four PL samples were obtain *via* CH_2Cl_2 extraction of the two PL samples produced from aged bio-oils, namely, aged mallee oil PL CH_2Cl_2-insoluble fraction (denoted as "AMOPL-HMW"), aged mallee oil PL CH_2Cl_2-soluble fraction (denoted as "AMOPL-LMW"), aged pine oil PL CH_2Cl_2-insoluble fraction (denoted as "APOPL-HMW") and aged pine oil PL CH_2Cl_2-soluble fraction (denoted as "APOPL-LMW"). The properties of the PL fractions are shown in Table 6-2. It can be seen in Figure 6-1, the molecular weights of AMOPL-HMW and APOPL-HMW are higher than those of AMOPL-LMW and APOPL-LMW respectively.

Table 6-2 Properties of the PL fractions.

	AMOPL-HMW[a]	AMOPL-LMW[b]	APOPL-HMW[c]	APOPL-LMW[d]
moisture (wt %)	1.0	1.3	0.7	1.1
ash (wt %, db[e])	1.3	1.6	1.4	0.8
volatile (wt %, db[e])	69.2	75.6	71.0	76.0
fixed carbon (wt %, db[e])	29.5	22.8	25.6	23.2
C (wt %, daf[f])	58.85	64.63	62.71	66.44
H (wt %, daf[f])	6.26	7.32	5.30	6.80
N (wt %, daf[f])	0.37	0.17	0.22	0.17
O (wt %, daf[f])[g]	34.52	27.88	31.77	26.59
δ ($cal^{1/2}$ $cm^{-3/2}$)[h]	13.93	13.99	13.90	14.01
molecular weight (Da)	1360	750	1270	770
polydispersity	2.6	2.1	2.2	2.6

[a] Aged mallee oil pyrolytic lignin CH_2Cl_2-insoluble. [b] Aged mallee oil pyrolytic lignin CH_2Cl_2-soluble. [c] Aged pine oil pyrolytic lignin CH_2Cl_2-insoluble. [d] Aged pine oil pyrolytic lignin CH_2Cl_2-soluble. [e] Dry basis. [f] Dry-ash-free basis. [g] By difference. [h] Solubility parameter values.

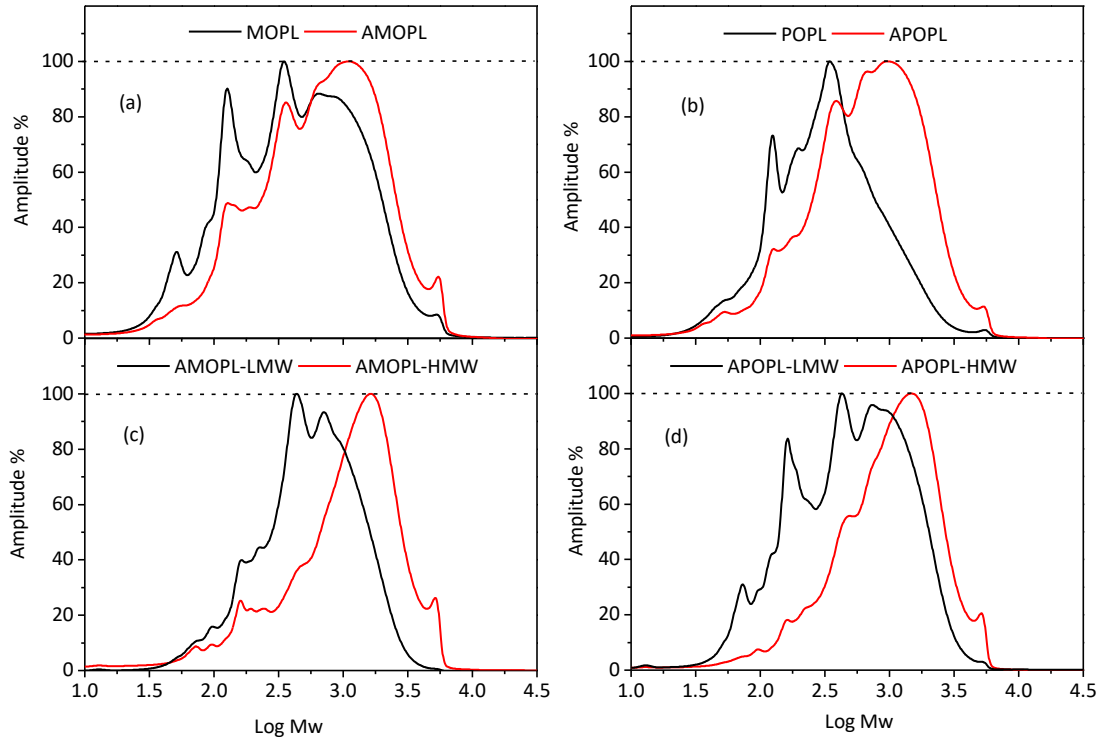

Figure 6-1 Molecular weight distributions of (a) MOPL and AMOPL, (b) POPL and APOPL, (c) AMOPL-LMW and AMOPL-HMW and (d) APOPL-LMW and APOPL-HMW. The PL samples were diluted in tetrahydrofuran at 1000 ppm for GPC analysis.

6.3 Ternary phase diagrams of PLs/MS/water

Figure 6-2 presents the ternary phase diagrams of PLs/MS/water and Figure 6-3 exhibit the solubilities of PL samples from fresh and aged bio-oils in various MS/water mixtures. Several key points (A−F) and their corresponding water contents in the MS/water mixtures (line 1−4) are highlighted in Figure Figure 6-2 and Figure 6-3. It can be seen from Figure 6-2a−6-2b and Figure 6-2c−d that the phase conversion curves of PL samples from aged bio-oils locate above those of PL samples from corresponding fresh bio-oils, indicating the solubilities of AMOPL and APOPL are lower than MOPL and POPL respectively. This is because the average molecular weight of PL samples drastically increase after 24h accelerated aging, which affects the solubilities of PL in the same MS/water mixture.[121]

Point A in Figure 6-2a−6-2b represent that MOPL, AMOPL, POPL and APOPL, when the water contents are zero, have maximal concentrations of ~59, ~50, ~65, and ~51 wt % in the PL/MS binary systems, which are equivalent to ~144, ~102, ~185 and ~107 g PL per 100 g of MS, respectively. The solubilities of MOPL, AMOPL, POPL

and APOPL in MS/water will increase to maximal values of ~160, ~114, ~221 and ~118 g PL per 100 g of MS/water mixtures when small amounts of water being added into the ternary systems. Point C in Figure 6-2a−6-2b represent the minimal MS, i.e., ~29 wt % in the MOPL/MS/water system, ~37 wt % the AMOPL/MS/water system, ~22 wt % in the POPL/MS/water system and ~35 wt % in the APOPL/MS/water system, required to possibly form homogeneous mixtures.

Further increases in the water contents of MS/water mixtures shift the systems from point C to point D, which witnesses the solubilities of PLs decrease to half of their maximal values. For example, the solubilities of MOPL, AMOPL, POPL and APOPL reduce to ~80, ~57, ~106 and ~59 g PL per 100 g of MS/water mixtures, when the water contents in MS/water mixtures are ~40, ~36, ~46 and ~38 respectively (see line 3 in Figure 6-2a−6-2b). The PL solubilities in the MS/water mixture experience dramatic reduction when the water contents of MS/water mixture further increase from point D to point E. This is because with the δ values of solutes (PLs) are not in the optimal δ ranges of solvents (MS/water mixtures), and the differences are getting greater beyond point D. In addition, point E in Figure 6-2a−6-2b represent the minimal MS contents, at which homogeneous PLs/MS/water mixtures are always formed. For example, MOPL/MS/water, AMOPL/MS/water, POPL/MS/water and APOPL/MS/water ternary systems are always in single-phase when the MS contents are >~49 wt %, >~53 wt %, >~40 wt % and >~51 wt % respectively.

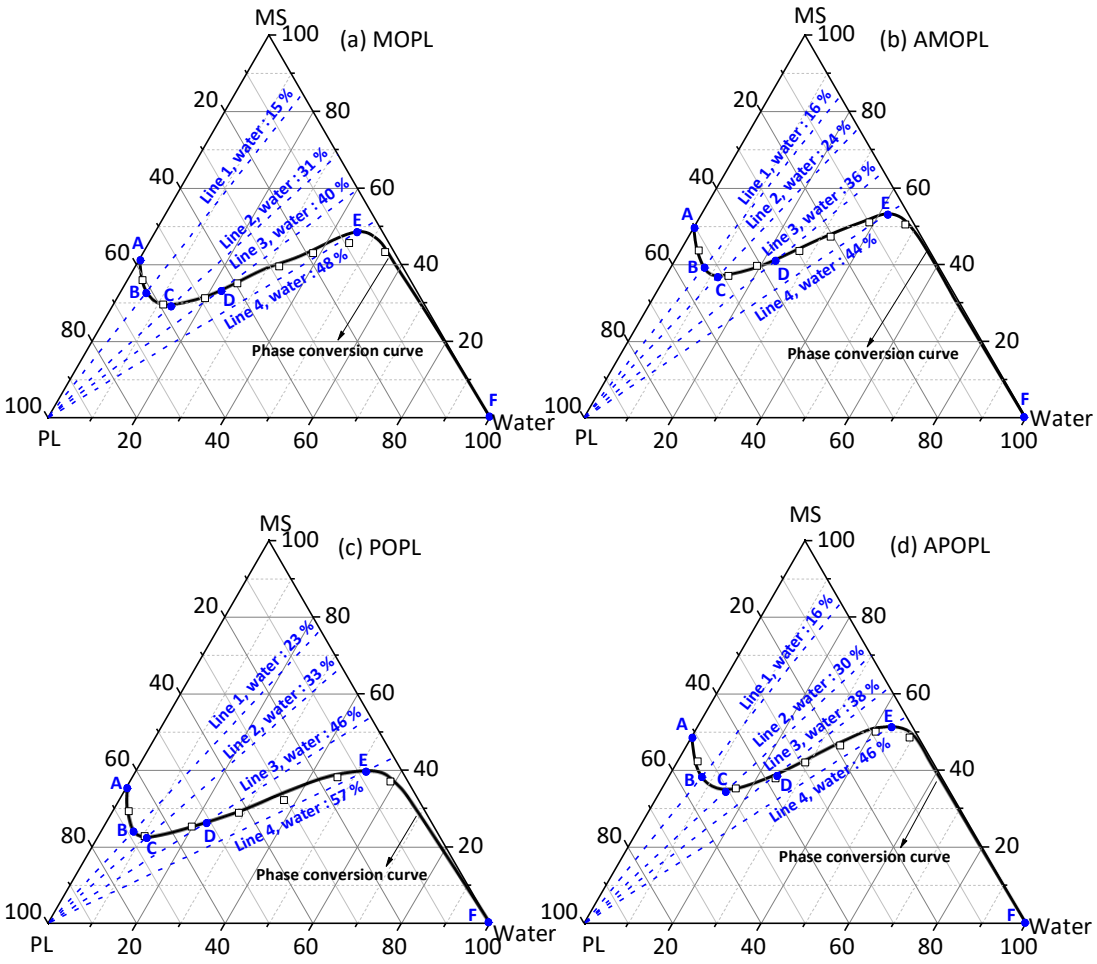

Figure 6-2 Ternary phase diagram of the PL/MS/water system for different PL samples: (a) MOPL, Line 1−4 represent the MS/water mixtures with a water content of ~15, ~31, ~40 and ~48 wt %, respectively; (b) AMOPL, Line 1−4 represent the MS/water mixtures with a water content of ~16, ~24, ~36 and ~44 wt %, respectively; (c) POPL, Line 1-4 represent the MS/water mixtures with a water content of ~23, ~33, ~46, and ~57 wt %, respectively; (d) APOPL, Line 1−4 represent the MS/water mixtures with a water content of ~16, ~30, ~38 and ~46 wt %, respectively. Point B in each figure represents the maximal solubility of PL in the MS/water mixture is achieved. Point C in each figure represents the minimal solvent needed to homogenize the PL/MS/water mixture. Point D in each figure represents that at which the solubility of PL in the MS/water mixture is half of the maximal solubility of PL in the MS/water mixture. Point E in each figure represents that the minimal solvent at which a homogeneous PL/MS/water mixture is also formed. [Legend: PL, pyrolytic lignin; MS, mixed solvent; MOPL, mallee oil pyrolytic lignin; AMOPL, aged mallee oil pyrolytic lignin; POPL, pine oil pyrolytic lignin; APOPL, aged pine oil pyrolytic lignin

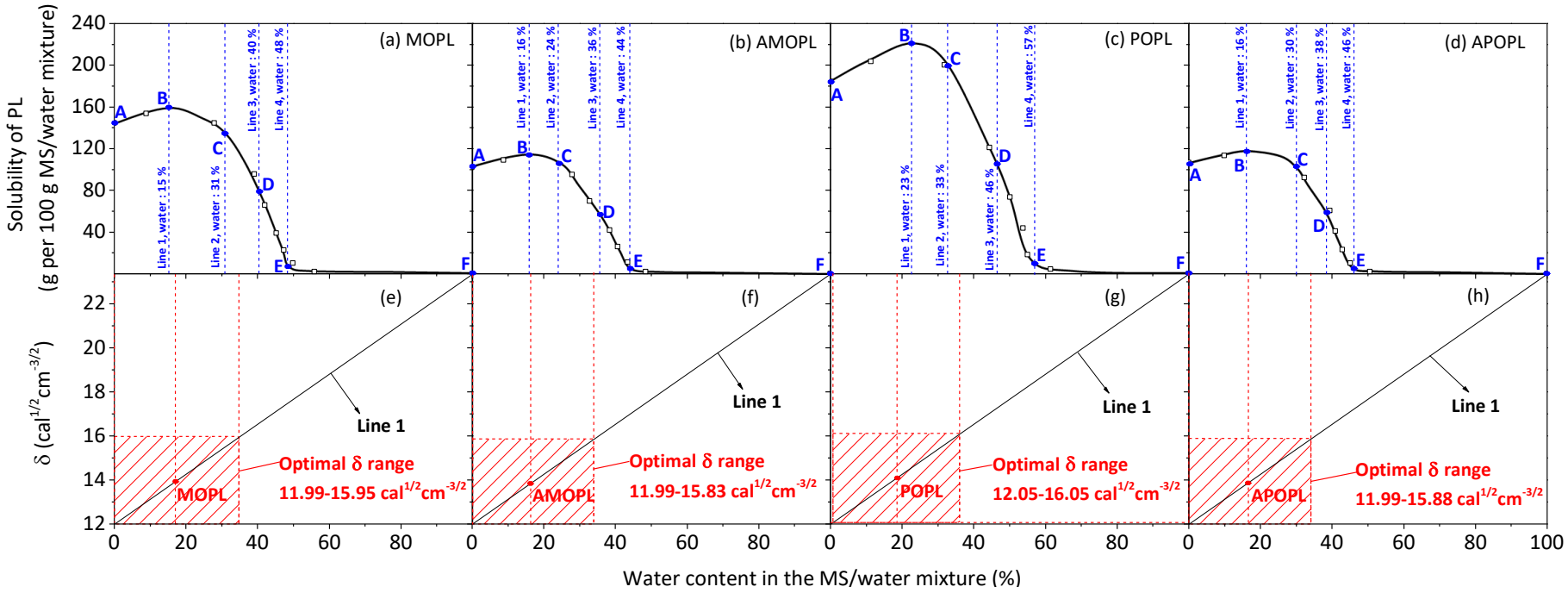

Figure 6-3 Solubilities of PL in various MS/water mixtures. Panel (a): Line 1−4 represent the MS/water mixtures with a water content of ~15, ~31, ~40 and ~48 wt %, respectively; panel (b): Line 1−4 represent the MS/water mixtures with a water content of ~16, ~24, ~36 and ~44 wt %, respectively; panel (c): Line 1−4 represent the MS/water mixtures with a water content of ~23, ~33, ~46 and ~57 wt %, respectively; panel (d): Line 1−4 represent the MS/water mixtures with a water content of ~16, ~30, ~38 and ~46 wt %, respectively. Point A-F in panel (a), panel (b), panel (c) and panel (d) correspond point A-F in Figure 3a, 3b, 3c and 3d respectively. Panel (e, f, g and h): line 1 represents the δ values of the MS/water mixtures at various water contents. [Legend: PL, pyrolytic lignin; MS, mixed solvent; MOPL, mallee oil pyrolytic lignin; AMOPL, aged mallee oil pyrolytic lignin; POPL, pine oil pyrolytic lignin; APOPL, aged pine oil pyrolytic lignin

6.4 Ternary phase diagrams of PL fractions/MS/water

To construct a comprehensive phase diagram that can be used to predict the phase stability of a given bio-oil sample, the solubilities of PL fractions in MS/water mixtures were studied and phase diagrams of PL fractions/MS/water were also constructed. Not surprisingly, phase conversion curves of HMWs are above those of corresponding LMWs. This is because the dissolution of polymers is affected by their average molecular weight; with similar polydispersity values, it is harder to dissolve larger polymers.[171, 172] For example, when the water contents are zero in the ternary systems (see point A in Figure 6-5a−6-5b), the solubility of AMOPL-HMW in MS (~80 g PL per 100 g of MS) is lower than that of AMOPL-LMW (~139 g PL per 100 g of MS) while the solubility of APOPL-HMW (~87 g PL per 100 g of MS) in MS is also lower than that of APOPL-LMW (~ 132 g PL per 100 g of MS).

With the addition of small amounts of water into the whole mixture also enhance the solubilities of PL fractions in the MS/water mixtures. At point B in Figure Figure 6-4a−6-4b AMOPL-HMW, AMOPL-LMW, APOPL-HMW and APOPL-LMW reach maximal concentrations of ~47, ~62, ~49 and ~61 wt % in PL fractions/MS/water ternary systems, which are equivalent to PL fractions solubilities of ~89, ~158, ~94 and ~156 g per 100 g of MS/water mixture. Similar as the phase diagrams of PL/MS/water mentioned in Section 3.3, further increasing in water contents of MS/water mixtures (starting from point B) will cause a reduction in the solubilities of PL fractions in MS/water mixtures. Point C represent The minimal MS contents required to form homogeneous mixtures are ~43, ~28, ~41, and ~29 wt % for AMOPL-HMW/MS/water, AMOPL-LMW/MS/water, APOPL-HMW/MS/water and APOPL-LMW/MS/water ternary systems, respectively. The solubilities of PL fractions in MS/water decrease to half of maximal solubilities (point D in Figure 6-5), and then to less than 10 g per 100 g of MS/water mixture (point E in Figure 6-5), with the increase in the water contents of MS/water mixtures (line 3−4 in Figure 6-4 and 6-Figure 6-5). In addition, point E represent that with MS contents > ~58, ~48, ~55 and ~49 wt %, the AMOPL-HMW/MS/water, AMOPL-LMW/MS/water, APOPL-HMW/MS/water and APOPL-LMW/MS/water ternary systems are always phase stable.

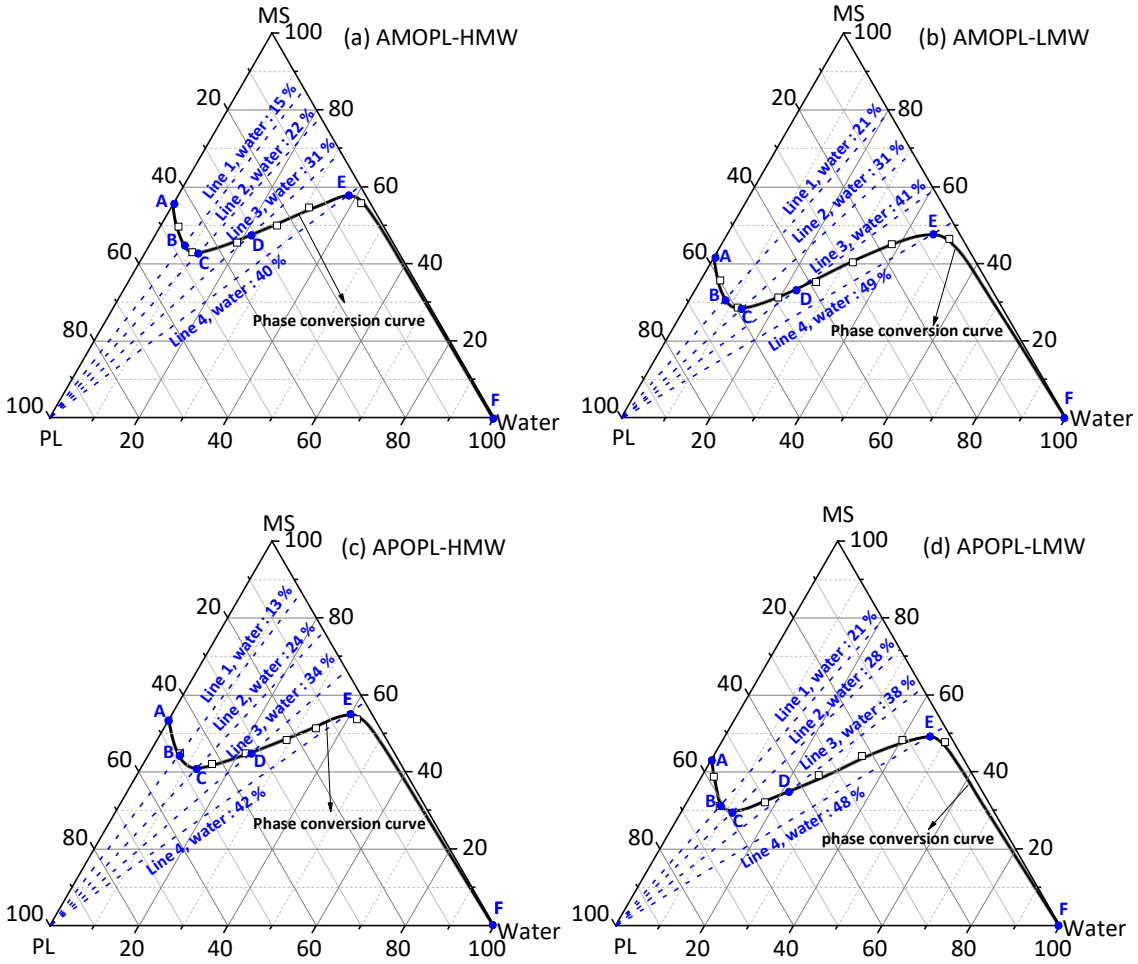

Figure 6-4 Ternary phase diagram of the PL/MS/water system for PL fractions: (a) AMOPL-HMW, Line 1−4 represent the MS/water mixtures with a water content of ~15, ~22, ~31 and ~40 wt %, respectively; (b) AMOPL-LMW, Line 1−4 represent the MS/water mixtures with a water content of ~21, ~31, ~41 and ~49 wt %, respectively; (c) APOPL-HMW, Line 1-4 represent the MS/water mixtures with a water content of ~13, ~24, ~34, and ~42 wt %, respectively; (d) APOPL-LMW, Line 1−4 represent the MS/water mixtures with a water content of ~21, ~28, ~38 and ~48 wt %, respectively. Point B in each figure represents the maximal solubility of PL in the MS/water mixture is achieved. Point C in each figure represents the minimal solvent needed to homogenize the PL/MS/water mixture. Point D in each figure represents that at which the solubility of PL in the MS/water mixture is half of the maximal solubility of PL in the MS/water mixture. Point E in each figure represents that the minimal solvent at which a homogeneous PL/MS/water mixture is also formed.

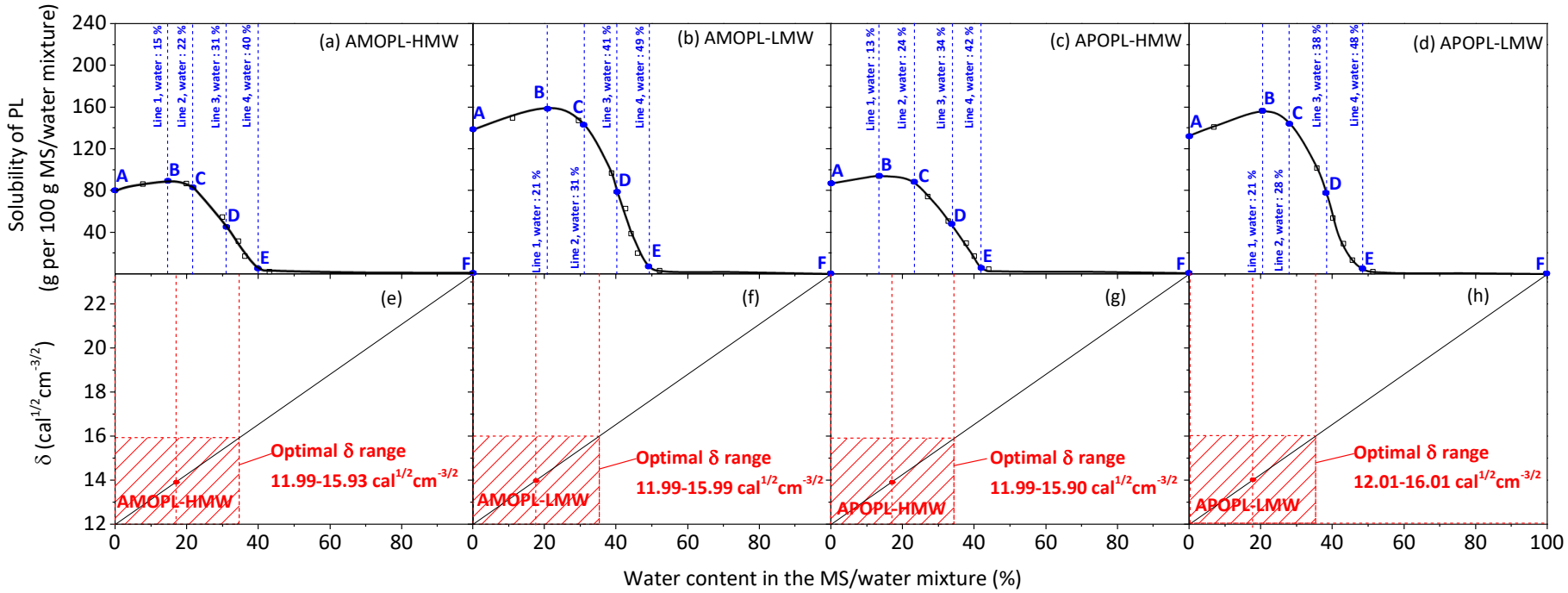

Figure 6-5 Solubilities of PL in various MS/water mixtures. Panel (a): Line 1−4 represent the MS/water mixtures with a water content of ~15, ~22, ~31 and ~40 wt %, respectively; panel (b): Line 1−4 represent the MS/water mixtures with a water content of ~21, ~31, ~41 and ~49 wt %, respectively; panel (c): Line 1−4 represent the MS/water mixtures with a water content of ~13, ~24, ~34 and ~42 wt %, respectively; panel (d): Line 1−4 represent the MS/water mixtures with a water content of ~21, ~28, ~38 and ~48 wt %, respectively. Point A-F in panel (a), panel (b), panel (c) and panel (d) correspond point A-F in Figure 3a, 3b, 3c and 3d respectively. Panel (e, f, g and h): line 1 represents the δ values of the MS/water mixtures at various water contents. [Legend: PL, pyrolytic lignin; MS, mixed solvent; AMOPL-HMW, aged mallee oil pyrolytic lignin CH_2Cl_2-insoluble; AMOPL-LMW, aged mallee oil pyrolytic lignin CH_2Cl_2-soluble; APOPL-HMW, aged pine oil pyrolytic lignin CH_2Cl_2-insoluble; APOPL-LMW, aged pine oil pyrolytic lignin CH_2Cl_2-soluble.

6.5 Predicting phase stability of bio-oil using the phase diagram

As mentioned above, both bio-oil samples were produced in a single-phase and phase separation of both bio-oil samples occurred after 24h accelerated ageing. To verify the correctness of the phase diagrams, the data on compositions of both fresh and aged bio-oils were processed and replotted in the corresponding phase diagrams.

Firstly, sugar contents of bio-oil samples (both fresh and aged) were determined by HPAEC-PAD. Figure 6-6 compares the contents of various anhydrosugar and sugar products in the bio-oils before and after accelerated ageing. Anhydrosugars, mainly levoglucosan and cellobiosan, are the major sugar products in both fresh and aged bio-oils, whereas the contents of sugar monomers are low. For example, fresh mallee oil has a levoglucosan and cellobiosan content of ~39.8 and 13.5 mg g^{-1} bio-oil respectively, which are much higher than those for other sugars, i.e., ~0.6, ~0.2, ~0.1, ~0.9, ~4.4 mg g^{-1} bio-oil for cellotriosan, arabinose, galactose, glucose, xylose respectively. Compared to mallee oil, fresh pine oil has a lower levoglucosan (~33.7 mg g^{-1} bio-oil) but higher cellobiosan content (~28.8 mg g^{-1} bio-oil), and lower xylose content (~2.1 mg g^{-1} bio-oil). Other sugars are not detected in fresh pine oil. After 24 hours accelerated ageing, some anhydrosugar are converted into sugar monomers, slightly increasing the contents of sugar monomers. For example, the content of arabinose increased to ~0.6 and ~1.75 mg g^{-1} bio-oil for mallee oil and pine oil respectively.

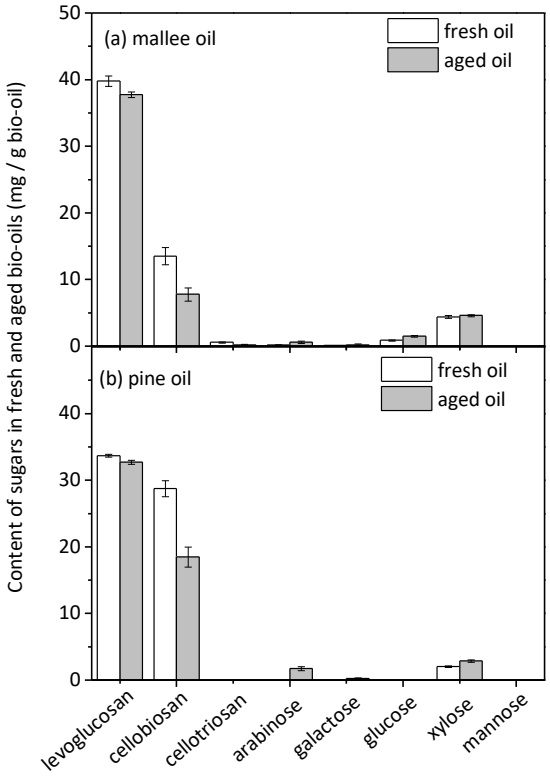

Figure 6-6 Contents of sugar products in fresh and aged bio-oil samples. (a) Mallee oil; (b) pine oil

Table 6-3 Composition of bio-oil

	Mallee oil	Aged mallee oil	Pine oil	Aged pine oil
water (wt %)	35.6	37.0	37.5	38.8
water-insoluble (wt %)	9.5	15.0	4.3	11.7
water-soluble (wt %)	49.0	42.6	51.7	43.8
total sugar content (wt %)	5.9	5.4	6.5	5.7

Therefore, the data on the compositions of both fresh and aged bio-oil samples are replotted in the phase diagrams. As shown in Figure 6-7, the fresh samples all locate above the corresponding phase conversion curve. It is recently reported that only when the water content in the ternary system is less than ~18 wt %, the existing of 7 wt % sugar will significantly affect the phase conversion curves.[121] In this study, the water

contents of both fresh and aged bio-oil samples are all > ~ 18 wt % and the sugar contents are all < 7 wt %, which means the effects of sugars on the phase diagrams should not be taken into consideration. It can be seen that both aged oil samples shift to below the corresponding phase conversion curves after 24 h ageing. The irreversible composition changes of bio-oil samples before and after ageing, i.e., significant increases in the PL content and decreases in the water-soluble content, resulted in the phase separation of bio-oil samples. Therefore, the correctness of the phase diagrams has been verified. Such a straightforward and precise tool can be extremely important in predicting the phase stability of bio-oil samples especially after long-term ageing.

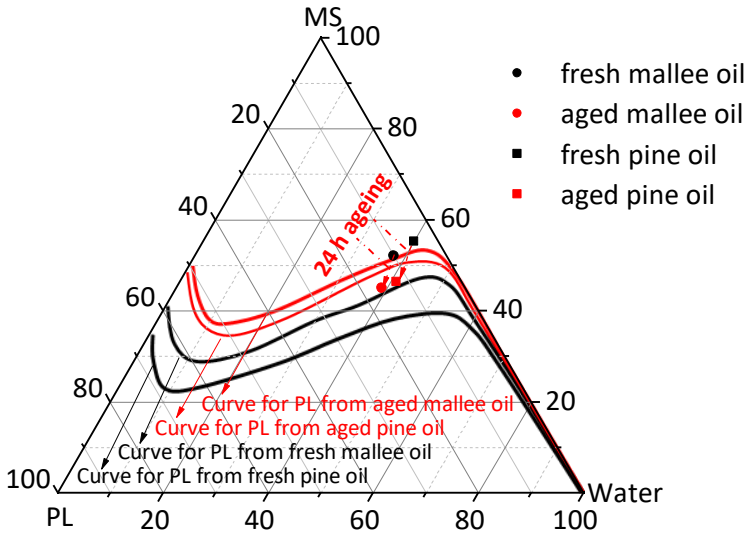

Figure 6-7 Application of the phase diagrams for predicting the phase stability of bio-oil samples. The ternary diagrams are plotted with the contents of PL, MS, and water normalized to 100% (excluding sugar in the system). The red dashed line in each figure represents 24h accelerated aging process at 80 °C.

6.6 Conclusion

In this study, bio-oils are produced from mallee and pine wood fast pyrolysis in a lab-scale auger reactor. Several phase diagrams of PL/MS/water are constructed for various PL samples. The maximal PL concentration in the PL/MS/water system is between ~47 wt % (equivalent to a PL solubility of ~89 g PL per 100 g of MS/water mixture) and ~69 wt % (equivalent to a PL solubility of ~221 g PL per 100 g of MS/water mixture) depending on its average molecular weight. This is because it is harder to dissolve large molecules than small ones. Besides, applications of predicting phase-separation of bio-oil samples using the phase diagrams are also studied. The results suggest the phase diagrams are useful tools to predict phase stability of bio-oil samples, especially after long-term ageing because of the irreversible changes in the compositions of bio-oils.

Chapter 7 Effect of Bio-Oil Minor Components on the Phase Diagrams of Pyrolytic Lignin, Mixed Solvent and Water

7.1 Introduction

Biomass fast pyrolysis is considered as a promising technology to convert biomass to liquid products (known as "bio-oil").[173] Bio-oil can be a renewable source for fuels and value-added chemicals.[5, 174] There are some samples in commercial bio-oil utilizations as fuel oils, such as BTG in The Netherlands,[175] Fortum in Finland.[176] Besides, the commercial utilization of the water-soluble fraction of bio-oil as value-added chemicals has been existing for more than a decade.[5] However, there are still some undesired features which hinder the commercial utilisation of bio-oil, including high oxygen content, high acidity, high viscosity and phase instability.[177] Consequently, it is necessary to upgrade bio-oils to obtain stable liquid products that can be widely used.

Bio-oil has very complex compositions including water, pyrolytic lignin, acids, aldehydes, phenols, sugars, etc.[5] The phase stability of bio-oil is highly influenced by the composition of the biomass feedstock.[9, 30, 99] Phase separation can take place immediately after the pyrolysis vapour is condensed when the biomass feedstock has a high ash content (> 2.0 wt %).[96, 178, 179] This is because high ash content will increase water and gas yields and decrease liquid yields by catalysing dehydration reactions in the pyrolysis.[179] Although > 95 wt % inorganic materials (mostly retained in the char) are separated in the pyrolysis process, a small part of inorganics will transfer to bio-oil during the process.[180] It is still not clear how the inorganic in the bio-oil affects the phase stability of bio-oil. Hilten et al. had proposed a in-line esterification of bio-oil, and in this process, esterification is coupled with biomass pyrolysis.[181] Carboxylic acids and aldehydes in bio-oil can be converted into esters (yield up to ~23 wt%) *in situ*, and two product phases (an oily and an aqueous phase) were obtained. The high content of esters may be related to the phase separation of bio-oil. It is, therefore,

important to investigate the effect of esters on the phase stability of bio-oil. Besides, bio-oil derived from biomass with high content of extractives tends to have phase separation immediately after pyrolysis, which is mainly attributed to polarity difference between those extractive-derived low-polar compounds and those high polar compounds derived from cellulose and hemi-cellulose.[30] However, how much the extractive compounds can be tolerated in bio-oil before phase separation remains unclear.

Previous chapters have considered a ternary phase diagram containing a mixed solvent (MS, representing water-soluble fraction), pyrolytic lignin (PL) and water.[121] This chapter aims to complete previous phase diagrams by considering the effect of minor components on ternary phase diagram of pyrolytic lignin, MS and water. The C, H, N and O (by difference) contents of the PL sample used in this chapter were determined to be 67.1, 6.2, 0.2 and 26.5 on a dry basis, respectively. The average molecular weight of the PL sample was determined to be 660 g/mol. Table 7-1 presents the model compound selected in this chapter.

7.2 Effect of extractive model compounds on the phase diagrams of PL/MS/water

The phase behaviours of PL/MS/water ternary systems in the presence of extractive model compounds are shown in Figure 7-1 with key points (A_1−C_1 and A_2−C_2) and lines (a1−c1 and a2−c2) and the solubilities of PL in the MS/water mixtures are also compared in Figure 7-2. Three important observations are made. Firstly, with the presence of extractive model compounds, the phase conversion curves no longer intersect with the MS/water side at apex "water". For example, when 0.1 wt % decane, 0.05 wt % pentadecane, 2.5 wt % BQ and 2.5 wt % CHCA are present, the minimum contents of MS in the MS/water mixtures required to obtain homogenous mixtures are ~38, ~43, ~27 and ~25 wt % respectively (see point C_1 in Figure 7-1). As shown in Figure 7-1, when the contents of extractive model compounds have doubled, the minimum MS contents in the MS/water mixtures required increase to> ~44, ~47, ~36

and ~33 wt % in presence of 0.2 wt % decane, 0.1 wt % pentadecane, 5.0 wt % BQ and 5.0 wt % CHCA, respectively. This is understandable considering the poor solubilities of the extractive model compounds in water.[182-184] Therefore, more MS contents in MS/water mixtures are required to dissolve the extractive model compounds.

Secondly, when the water content in the PL/MS/water ternary system is lower than a certain value, the extractive model compound has no effect on the phase behaviours of PL/MS/water ternary system. When decane, pentadecane, BQ and CHCA are added in the PL/MS/water mixture at 0.2, 0.1, 5.0 and 5.0 wt % respectively, no measurable influence is observed if water content in the ternary system of PL/MS/water is lower than ~24, ~21, ~27 and ~31 wt % (see point A_1 in Figure 7-1a−7-1b), corresponding to water contents in MS/water mixtures of ~43, ~41, ~44 and ~46 wt % respectively (see line a1 in Figure 7-1a−7-1d). When the contents of decane, pentadecane, BQ and CHCA reduce to 0.1, 0.05, 2.5 and 2.5 wt %, the critical water contents in PL/MS/water systems increase to ~27, ~25, ~35 and ~40 wt % respectively. It can be seen that the critical water content in the MS/water binary systems (or PL/MS/water ternary systems) reduces with increasing the concentrations of extractive model compounds. Moreover, when the water content in the PL/MS/water ternary system exceeds the critical values, the presence of extractive model compounds reduces the PL solubilities in the MS/water mixtures. Point A_1 in Figure 7-2 represent the PL solubilities at critical water contents are ~76, ~96, ~67 and ~51 g PL per 100 g of MS/water mixture in presence of 0.2 wt % decane, 0.1 wt % pentadecane, 5.0 wt % BQ and 5.0 wt % CHCA respectively. The solubilities of PL in the MS/water mixtures reduce to ~32, ~39, ~8 and ~10 g PL per 100 g of MS/water mixture in presence of 0.2 wt % decane, 0.1 wt % pentadecane, 5.0 wt % BQ and 5.0 wt % CHCA when the water contents in the MS/water mixtures increase to ~45, ~44, ~47 and ~48 wt % respectively, in contrast to the solubilities of PL in the same MS/water mixtures of ~63, ~72, ~35 and ~22 g PL per 100 g of MS/water mixture in presence of 0.1 wt % decane,

Table 7-1 Model compound selected to represent bio-oil minor components

Model compounds selected	Concentrations considered
extractives	
decane	0.1 %; 0.2 %
pentadecane	0.05 %; 0.1 %
1,4-benzoquinone (BQ)	2.5 %; 5.0 %
cyclohexanecarboxylic acid (CHCA)	2.5 %; 5.0 %
inorganic	
KCl	0.3 %; 0.6 %
esters	
methyl acetate (MA)	7.5 %; 15.0 %
furfuryl acetate (FA)	5.0 % ; 10.0 %
phenyl acetate (PA)	5.0 %; 10.0 %
methyl α-D-glucopyranoside (MDG)	5.0 %; 7.0 %

0.05 wt % pentadecane, 2.5 wt % BQ and 2.5 wt % CHCA respectively (see point A_2 in Figure 7-2a−7-2b). Point B_1 and B_2 in Figure 7-1 represent the minimal MS contents required to guarantee homogeneous PL/MS/water mixtures with a certain value of extractive model compounds being added. The whole mixtures are always stable when the MS contents of PL/MS/water systems are > ~50, ~52, ~51 and ~49 wt %, in presence of 0.2 wt % decane, 0.1 wt % pentadecane, 5.0 wt % BQ and 5.0 wt % CHCA, respectively (see point A_1 in Figure 7-1a−7-1d). When 0.1 wt % decane, 0.05 wt % pentadecane, 2.5 wt % BQ and 2.5 wt % CHCA are added into the ternary systems instead, the minimal MS contents in the ternary systems should be > ~47, ~48, ~49 and ~47 wt % to guarantee homogeneous mixtures, indicating that the minimal MS contents increase with increasing extractive model compound contents.

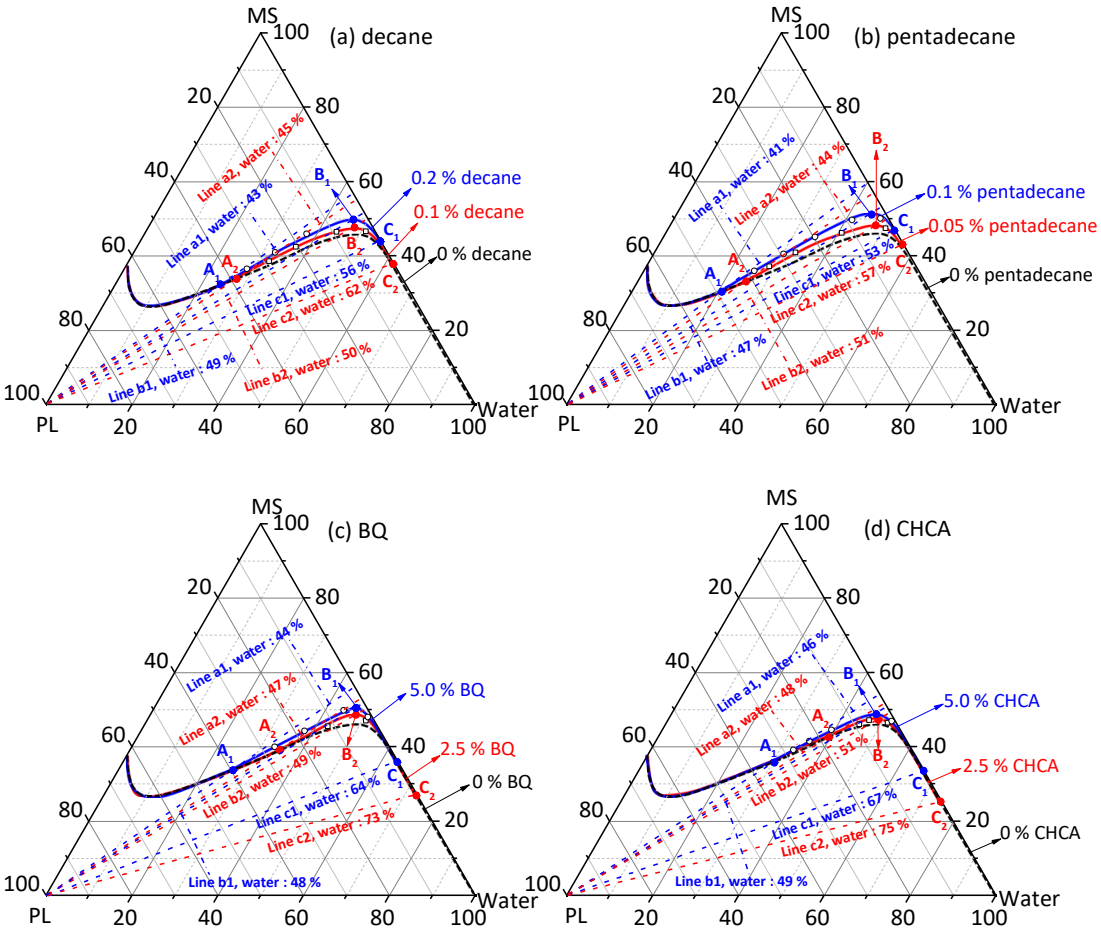

Figure 7-1 Ternary phase diagram of the PL/MS/water system in presence of extractive model compounds: (a) line a1, b1, c1, a2, b2, and c2 represent the MS/water mixtures with a water content of ~43, ~49, ~56, ~45, ~50 and ~62 wt %, respectively; (b) line a1, b1, c1, a2, b2, and c2 represent the MS/water mixtures with a water content of ~41, ~47, ~53, ~44, ~51 and ~57 wt %, respectively; (c) line a1, b1, c1, a2, b2, and c2 represent the MS/water mixtures with a water content of ~44, ~48, ~64, ~47, ~49 and ~73 wt %, respectively; (d) line a1, b1, c1, a2, b2, and c2 represent the MS/water mixtures with a water content of ~46, ~49, ~67, ~48, ~51 and ~75 wt %, respectively. Point A in each figure represents the critical water content in presence of extractive model compounds. Point B in each figure represents that the minimal solvent at which a homogeneous PL/MS/water mixture is also formed in presence of extractive model compounds. Point C in each figure represents the minimal MS content in the MS/water mixture to dissolve extractive model compounds.

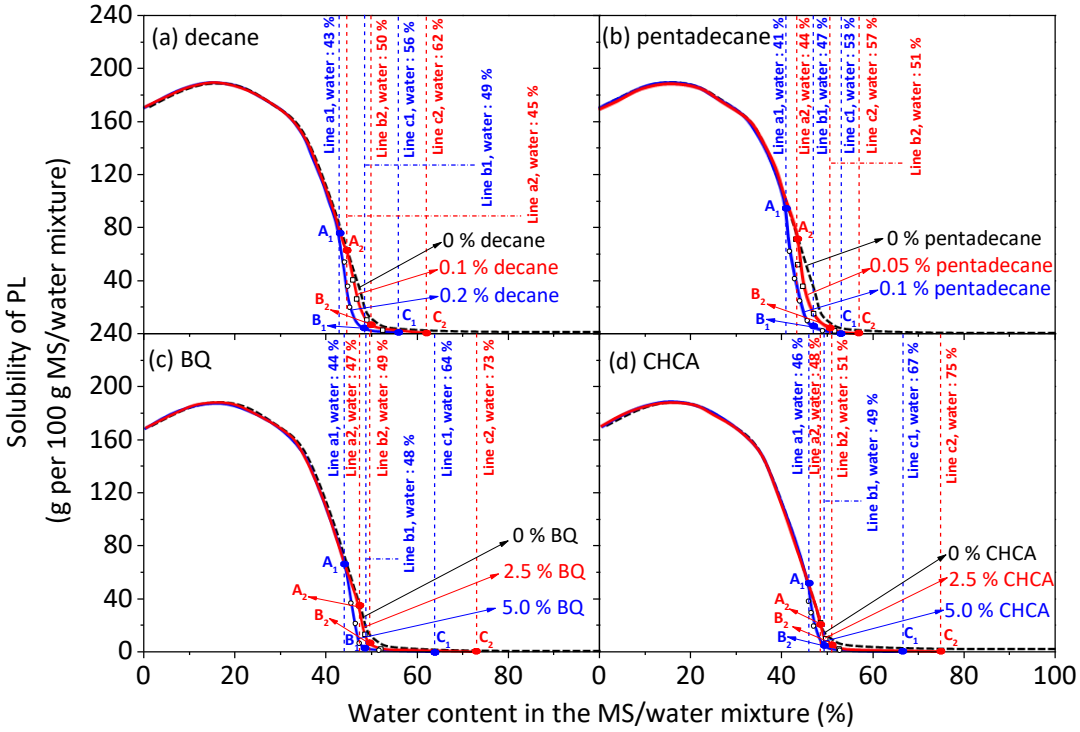

Figure 7-2 Solubilities of PL in various MS/water mixtures in presence of extractive model compounds. Panel (a): line a1, b1, c1, a2, b2, and c2 represent the MS/water mixtures with a water content of ~43, ~49, ~56, ~45, ~50 and ~62 wt %, respectively; panel (b): line a1, b1, c1, a2, b2, and c2 represent the MS/water mixtures with a water content of ~41, ~47, ~53, ~44, ~51 and ~57 wt %, respectively; panel (c): line a1, b1, c1, a2, b2, and c2 represent the MS/water mixtures with a water content of ~44, ~48, ~64, ~47, ~49 and ~73 wt %, respectively; panel (d): line a1, b1, c1, a2, b2, and c2 represent the MS/water mixtures with a water content of ~46, ~49, ~67, ~48, ~51 and ~75 wt %, respectively. Point A_1–C_1 and A_2–C_2 in panel (a), panel (b), panel (c) and panel (d) correspond point A_1–C_1 and A_2–C_2 in Figure 1a, 1b, 1c and 1d respectively. [Legend: PL, pyrolytic lignin; MS, mixed solvent; BQ, 1,4-benzoquinone; CHCA, cyclohexanecarboxylic acid]

7.3 Effect of the inorganic model compound on the phase diagrams of PL/MS/water

Firstly, the phase conversion curve of PL/MS/water ternary systems does not experience any change when 0.3 wt % KCl being added. Song et al. used salt addition method to separate bio-oil into a top phase and a bottom phase, and the major conclusion of this study is the addition of salt (3 wt % of bio-oil) into bio-oil will quickly result in bio-oil phase separations.[185] It is understandable that 0.3 wt % KCL does not affect the phase stability of PL/MS/water system. Therefore, a doubled 0.6 wt % KCl has been added into PL/MS/water mixtures to evaluate the effect of KCl on phase behaviours of PL/MS/water. As shown in Figure 7-3a, the 0.6 wt % KCl has slight effect on the phase diagrams of PL/MS/water when the water content is lower than ~3 wt % in ternary mixture (see point B in Figure 7-3a), corresponding to a water content of ~9 wt % in the MS/water mixture. This is because the inorganic model compound KCl, a salt, is more likely to dissolve in water rather in an organic MS. When there is no water in the whole system (see point A in Figure 3a), the minimal MS content required to maintain a homogenous mixture increases from ~36 wt % to ~39 wt % with the presence of 0.6 wt % KCl; while the PL solubility in MS dropped from ~170 to ~154 g per 100 g of MS.

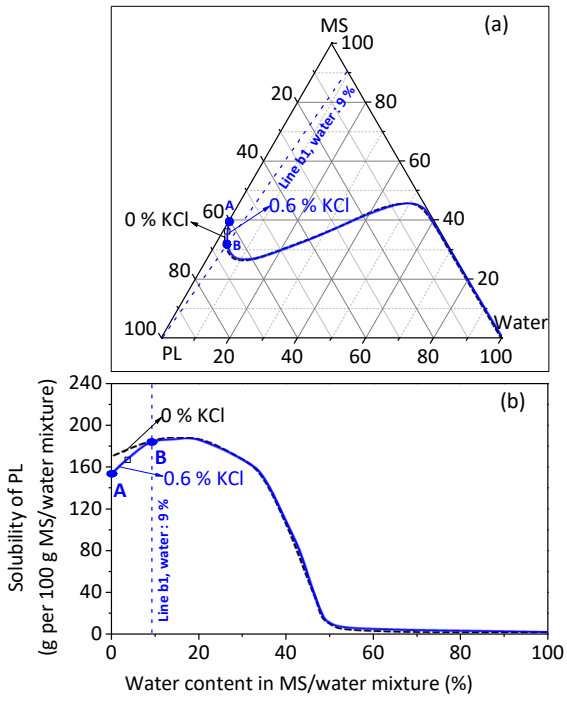

Figure 7-3 (a) Ternary phase diagram of the PL/MS/water system in presence of KCl; (b) solubilities of PL in various MS/water mixtures in presence of KCl. Line b1 in both figure (a) and (b) represent that the MS/water mixture with water contents of ~9 wt %.

7.4 Effect of ester model compounds on the phase diagrams of PL/MS/water.

The ternary phase diagrams of PL/MS/water systems in presence of ester model compounds were further developed to understand the effect of esters on the phase behaviours of PL/MS/water systems. Unlike the effects of extractive model compounds, additions of MA improve the PL solubilities in the MS/water mixtures. For example, in the PL/MS binary system as shown in Figure 7-4a, point A_2 and A_1 represent the maximal PL concentrations of ~64 and ~66 wt % in presence of 7.5 and 15.0 wt % MA, corresponding to a PL solubility of ~178 and ~193 g PL per 100 g of MS respectively. This is because the PL fraction in bio-oil or the PL/MS/water system can be dissolved by methyl acetate (MA) addition[186, 187], and therefore improving the phase stabilities of PL/MS/water systems. The maximal concentrations of PL in ternary systems of PL/MS/water increase to ~67 and ~69 wt % in presence of 7.5 and 15.0 wt % MA (see point B_2 and B_1 in Figure 7-4a), which correspond to the maximal

PL solubilities ~202 and ~225 g PL per 100 g of MS/water respectively. Point C_2 and C_1 represent that minimal MS contents (~24 and ~21 wt % in the PL/MS/water system, respectively) required to possibly form a homogeneous PL/MS/water system in presence of 7.5 and 15.0 wt % MA. In addition, the minimal MS contents required to guarantee homogeneous mixtures decrease to ~44 and ~41 wt % with the addition of 7.5 and 15.0 wt % MA (see point D_2 and D_1), in contrast to that of ~46 wt % without MA addition, indicating that MA can improve the phase stabilities of PL/MS/water mixtures. Figure 7-4b and 7-Figure 7-4c compare the effects of furfuryl acetate (FA) and phenyl acetate (PA) on the phase behaviours of PL/MS/water systems. It can be seen that the minimal MS contents in the MS/water mixtures to dissolve 5.0 wt % FA, 10.0 wt % FA, 5.0 wt % PA and 10.0 wt % PA are ~43, ~49, ~45 and ~51 wt % respectively, showing that PA has a poorer solubility in the same MS/water mixture than FA. At point B_1 and B_2 in Figure Figure 7-4b and Figure 7-4c, the PL/MS/water systems are always stable when the MS contents are >~47, ~50, ~48 and ~53 wt % in presence of 5.0 wt % FA, 10.0 wt % FA, 5.0 wt % PA and 10.0 wt % PA respectively. In addition, the phase conversion curves of the PL/MS/water systems will not be affected when the water contents in the ternary systems are < ~19 and ~18 wt % in presence of 5.0 wt % FA and PA respectively. The critical water contents in the ternary systems will decrease to ~16 and ~14 wt % with 10.0 wt % FA and PA being added into the ternary systems. Methyl-a-D-glucopyranoside (MDG) has significant effect on the phase conversion curve of PL/MS/water systems when the water content in the overall system is relatively low. For example, the maximal PL concentrations in the PL/MS binary systems reduce to ~58 and ~54 wt % in presence of 5 and 7 wt % MDG (see point A_2 and A_1 in Figure 4d), which are equivalent to PL solubilities of ~136 and ~120 g PL per 100 g of MS. A slightly increase in the water content increases the PL solubilities in the MS/water mixtures in presence of MDG.

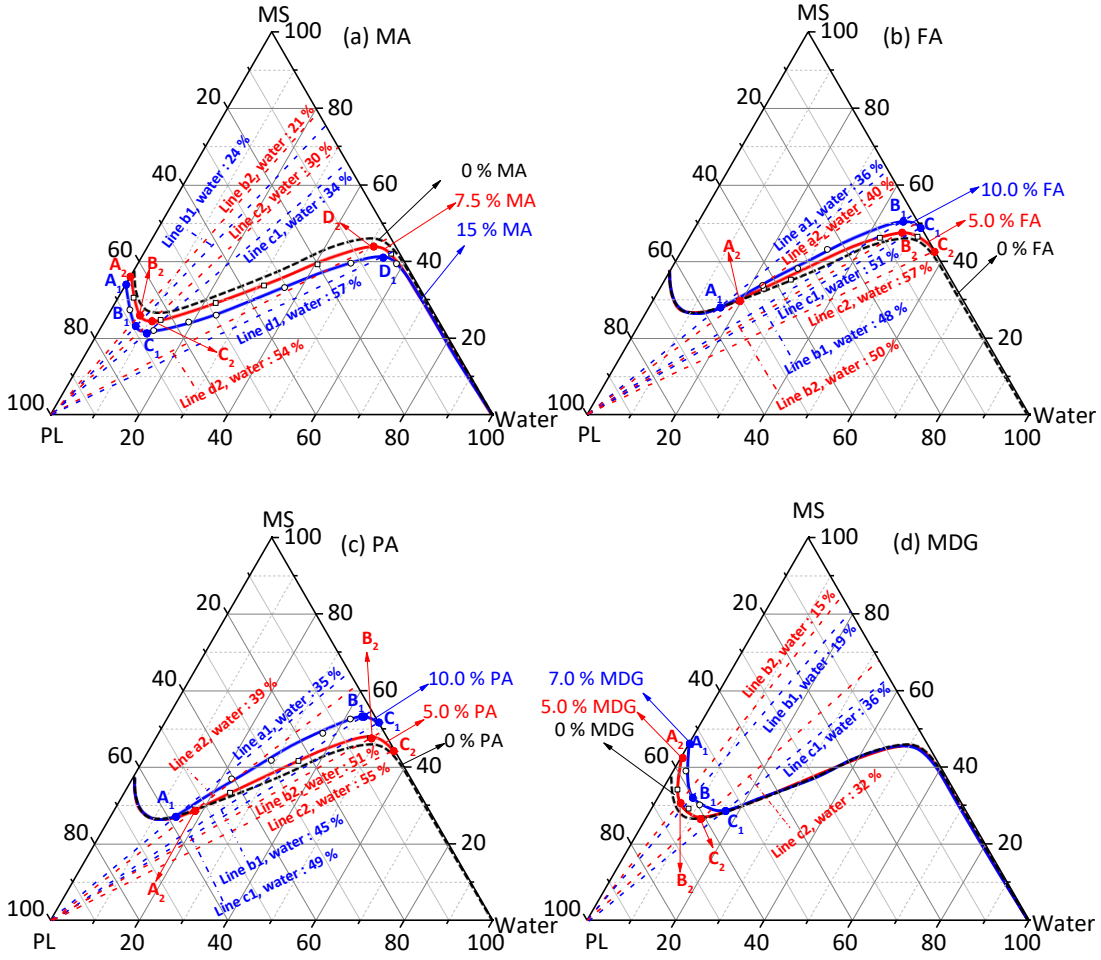

Figure 7-4 Ternary phase diagram of the PL/MS/water system in presence of ester model compounds: (a) line b1, c1, d1, b2, c2 and d2 represent the MS/water mixtures with a water content of ~24, ~34, ~57, ~21, ~30 and ~54 wt %, respectively; (b) line a1, b1, c1, a2, b2, and c2 represent the MS/water mixtures with a water content of ~36, ~48, ~51, ~40, ~50 and ~57 wt %, respectively; (c) line a1, b1, c1, a2, b2, and c2 represent the MS/water mixtures with a water content of ~35, ~45, ~49, ~39, ~51 and ~55 wt %, respectively; (d) line b1, c1, b2, and c2 represent the MS/water mixtures with a water content of ~19, ~36, ~15, and ~32 wt %, respectively. [Legend: PL, pyrolytic lignin; MS, mixed solvent; MA, methyl acetate; FA, furfuryl acetate; PA, phenyl acetate; MDG, methyl α-D-glucopyranoside.]

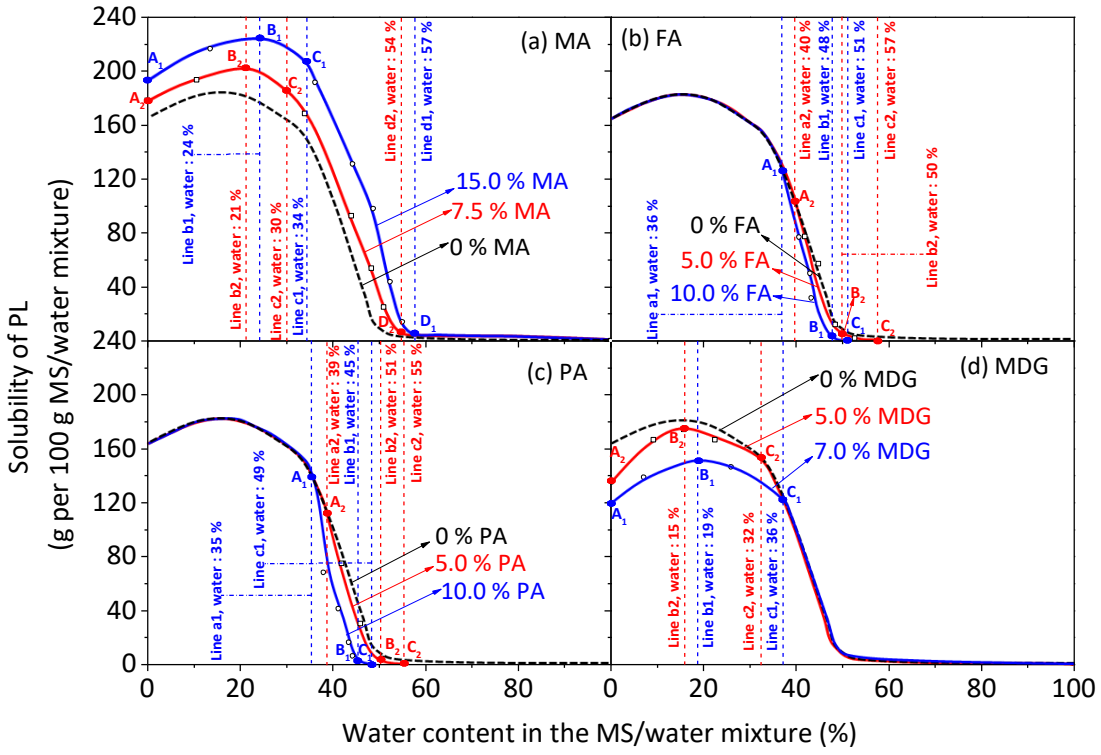

Figure 7-5 Solubilities of PL in various MS/water mixtures in presence of ester model compounds: (a) line b1, c1, d1, b2, c2 and d2 represent the MS/water mixtures with a water content of ~24, ~34, ~57, ~21, ~30 and ~54 wt %, respectively; (b) line a1, b1, c1, a2, b2, and c2 represent the MS/water mixtures with a water content of ~36, ~48, ~51, ~40, ~50 and ~57 wt %, respectively; (c) line a1, b1, c1, a2, b2, and c2 represent the MS/water mixtures with a water content of ~35, ~45, ~49, ~39, ~51 and ~55 wt %, respectively; (d) line b1, c1, b2, and c2 represent the MS/water mixtures with a water content of ~19, ~36, ~15, and ~32 wt %, respectively. [Legend: PL, pyrolytic lignin; MS, mixed solvent; MA, methyl acetate; FA, furfuryl acetate; PA, phenyl acetate; MDG, methyl α-D-glucopyranoside.]

It can be seen that at point B_2 and B_1 in Figure 7-4d whereas the PL concentrations increase to ~64 wt % (equivalent to a PL solubility of ~176 g PL per 100 g of MS/water mixture) and ~60 wt % (equivalent to a PL solubility of ~152 g PL per 100 g of MS/water mixture) in presence of 5 and 7 wt % MSG. Point C_2 and C_1 in Figure 7-4d represent the minimal MS content (~27 and ~29 wt % in the ternary system) required to possibly form a homogeneous PL/MS/water system in presence of 5 and 7 wt %

MSG. Increasing MSG contents leads to the decrease in the PL solubility in the same MS/water mixtures. For example, the PL solubility in the MS/water mixture is ~154 g PL per 100 g of MS/water mixture in presence of 5 wt % MDG (see point C_2 in Figure 5d), while that is ~134 g of MS/water mixture in the same MS/water mixture with 7 wt % MDG being added.

7.5 Conclusion

Several phase diagrams of PL/MS/water in presence of bio-oil minor components model compounds (extractives, inorganics and esters) were constructed to evaluate the effects of minor component model compounds on phase behaviours of PL/MS/water systems. The solubilities of PL in various MS/water mixtures with extractive/inorganic/ester model compounds being added were also examined. The results show that the minimal MS contents required to guarantee homogeneous PL/MS/water mixtures increase when extractive model compounds being added. For example, the PL/MS/water systems are always stable when MS contents are > ~50, ~52, ~51 and ~49 wt % in presence of 0.2 wt % decane, 0.1 wt % pentadecane, 5.0 wt % BQ and 5.0 wt % CHCA. The critical water content for the phase diagram of PL/MS/water in presence of 0.6 wt % inorganic model compound (KCl) is < ~3 wt %. Ester model compounds, furfural acetate and phenyl acetate have similar effects on the phase behaviours of PL/MS/water systems as extractive model compounds. The phase conversion curves of PL/MS/water systems in presence of 5.0 wt % furfural acetate and phenyl acetate will be not affected when water contents in the ternary systems are < ~20 and ~18 wt % respectively. The presence of 5 and 7 wt % methyl α-D-glucopyranoside also affects the phase stability of PL/MS/water systems, but only when water contents are <~12 and ~17 wt %. It is worth noting that methyl acetate can enhance the phase stabilities of PL/MS/water systems. For example, the maximal PL solubilities in PL/MS binary systems reduce to ~34 and ~36 wt % in presence of 7.5 and 15 wt % methyl acetate, in contrast to ~38 wt % without the addition of methyl acetate.

Chapter 8 Effect of Temperature on Ternary Phase Diagrams of Pyrolytic Lignin, Mixed Solvent and Water

8.1 Introduction

Phase stability of bio-oil must be taken into consideration in order to carefully handle bio-oil [10] and temperature is a key factor that is highly season-dependent. It is well known that the viscosity of bio-oil decreases as temperature increases from room temperature to 35~40 °C [188]. As temperature reduces, precipitates are likely formed in bio-oil due to the precipitation of high molecular compounds [48]. The resulting phase separation of bio-oil may cause severe consequences during storage and transport such as blockages and pumping difficulties [10]. Therefore, it is important to understand the phase behaviour of bio-oil at different temperatures, facilitating the development of guidelines on bio-oil storage and transport.

In our previous work, a mixed solvent (MS) was developed based on the composition of bio-oils from literature for understanding the phase behaviour of ternary systems among pyrolytic lignin (PL), MS and water, leading to the development of ternary phase diagrams of PL/MS/water systems at room temperature [121]. However, no study has been done on the effect of temperature on ternary phase diagram of PL/MS/water system before. Therefore, this is the key objective of this study that continues our work. The experimental program considers the effect of temperature on PL/MS/water ternary phase diagram with and without the presence of sugar (represented by levoglucosan), which may also affect the solubilities of PL in the MS/water mixtures. Table 8-1 presents the properties of the PL sample used in this chapter.

8.2 Effect of Temperature on Ternary Phase Diagrams of PL/MS/Water

The ternary phase diagrams of the PL/MS/water systems at different temperatures are presented in Figure 8-1. The phase conversion curves in Figure 8-1 are also replotted in the form of PL solubility in the MS/water mixture in Figure 8-2. The key points

(A−G) and their corresponding water contents in the MS/water mixture (lines 1-5) are highlighted in both Figure 8-1 and Figure 8-2. It can be seen from Figure 8-1 that the phase conversion curves at different temperatures follow a similar trend. However, an increase in temperature brings down the phase conversion curve in the ternary phase diagram, indicating that the PL solubility in the same MS/water mixture increases with temperature. This can be explained by the Le Chatelier's principle[189]. The PL dissolution equilibrium equation in MS/water mixtures can be illustrated as following:

$$PL\ (solid) \rightleftarrows PL\ (solution\ in\ MS/water) \quad (8\text{-}1)$$

To form a polymer solution, energy is needed to break bonds between the particles within the polymer molecule and the bonds in a solvent, which makes the polymer dissolution an endothermic process ($\Delta H_{solvation}>0$) [172]. Increasing temperature will prompt the PL dissolution equilibrium to shift towards the right side (PL solution in MS/water), thus increasing the PL solubility [189].

In the ternary phase diagram, point A represents the maximal PL concentration that can be achieved for a homogeneous PL/MS binary system. It can be seen in Figure 1 that the maximal PL concentration increases from ~59 wt % at 0 °C, to ~63 wt % at 25 °C, then to ~66 wt % at 40 °C. Correspondingly, the PL solubility increases from ~144 g PL per 100 g of MS at 0 °C, to ~170 g PL per 100 g of MS at 25 °C, then to ~194 g PL per 100 g of MS at 40 °C (see Figure 8-2a−8-2c). It can be found that the PL solubility in MS increases greatly (i.e., by ~35%) as temperature increases from 0 to 40° C. When a small amount of water is added in the PL/MS system, the PL concentration in the PL/MS/water system can be further increased. Point B represents the maximal PL concentration that can be achieved for a homogeneous PL/MS/water ternary system. It can be found that the maximal PL concentration increases from ~62 wt % at 0 °C (~13 wt % water in the MS/water mixture), to ~66 wt % at 25 °C (~18 wt % water in the MS/water mixture), then to 70 wt % at 40 °C (~19 wt % water in the MS/water mixture).

Table 8-1 Properties of the Pyrolytic Lignin Sample.

	Mw [a]	Moisture (wt %)	Ultimate (wt %)				Proximate (wt %. db [b])		
			C	H	N	O [c]	Ash	VM [d]	FC [e]
PL	660	0.6	67.14	6.21	0.23	26.42	0.8	83.5	15.7

[a] Average molecular weight determined by GPC. [b] Dry basis. [c] By difference. [d] volatile matter. [e] fixed carbon.

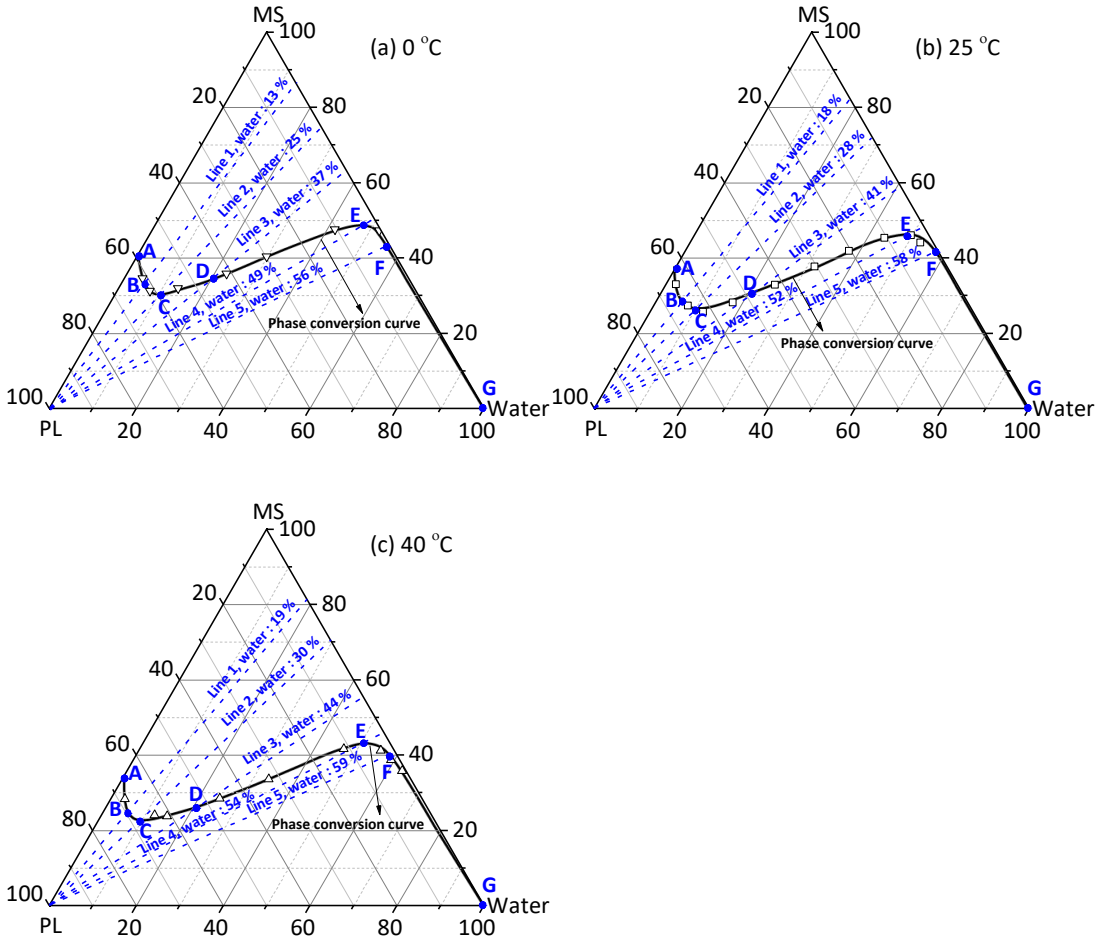

Figure 8-1 Ternary phase diagram of the PL/MS/water system at different temperatures: (a) Line 1-5 represent the MS/water mixtures with a water content of ~13, ~25, ~37, ~49 and ~56 wt %, respectively; (b) Line 1-5 represent the MS/water mixtures with a water content of ~18, ~28, ~41, ~52, and ~58 wt %, respectively; (c) Line 1-5 represent the MS/water mixtures with a water content of ~19, ~30, ~44, ~54 and ~59 wt %, respectively. Point B in each figure represents the maximal solubility of PL in the MS/water mixture is achieved. Point C in each figure represents the minimal solvent needed to homogenize the PL/MS/water mixture. Point D in each figure represents that at which the solubility of PL in the MS/water mixture is half of the maximal solubility of PL in the MS/water mixture. Point E in each figure represents that the minimal solvent at which a homogeneous PL/MS/water mixture is also formed. [Legend: PL, pyrolytic lignin; MS, mixed solvent.]

This leads to the PL solubility increasing from ~161 g PL per 100 g of MS/water mixture at 0 °C, to ~190 g PL per 100 g of MS/water mixture at 25 °C, then to ~229 g PL per 100 g of MS/water mixture at 40 °C (see Figure 8-2a−8-2c). The results clearly demonstrate that increasing temperature can lead to a substantial increase in the PL solubility in the PL/MS/water system. It is also interesting to see that increasing temperature also reduces the required content of MS and increases the required content of water in the ternary system to form a homogeneous PL/MS/water system.

As the water content in the MS/water mixture further increases, the PL solubility shows a continuous decrease. Point C represents the minimal MS required to possibly form a homogeneous PL/MS/water system. When the temperature increases from 0 to 40 °C, the minimal MS concentration at point C reduces from ~30 to ~23 wt %. In contrast, the PL concentration at point C increases from ~59 wt % (equivalent to a PL solubility of ~150 g PL per 100 g of MS/water mixture) at 0 °C to ~67 wt % (equivalent to a PL solubility of ~213 g PL per 100 g of MS/water mixture) at 40 °C. Further increasing the water content leads to a rapid decrease in the PL solubility in the MS/water mixture. Point D represents the composition of the PL/MS/water system at which the PL solubility reduces to half of the maximal value. For example, when the water content in the MS/water mixture increases to ~37, ~41, and ~44 wt % at 0, 25, and 40 °C, the PL solubility reduces to ~81, ~95 and ~114 g PL per 100 g of MS/water mixture at 0, 25 and 40 °C, respective. Point E represents the minimal MS concentration at which a homogeneous PL/MS/water system can be always formed. When the temperature increases from 0 to 40 °C, the MS concentration at point E reduces slightly from ~48 to ~43 wt %. Accordingly, the PL concentration at point E increases slightly from ~4 wt % (equivalent to a PL solubility of ~4 g PL per 100 g of MS/water mixture) at 0 °C to ~6 wt % (equivalent to a PL solubility of ~6 g PL per 100 g of MS/water mixture) at 40 °C. At point F, where the water content in the MS/water mixture is too high (i.e., 56, 58 and 59 wt % at 0, 25 and 40 °C, respectively), the PL solubility becomes very small (i.e., < 2 g PL per 100 g of MS/water mixture).

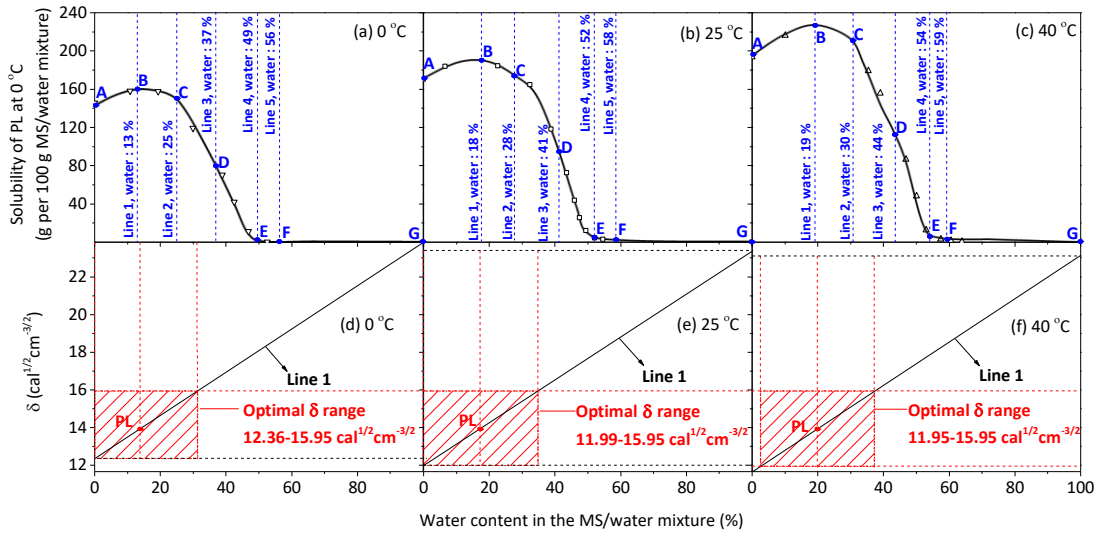

Figure 8-2 Solubilities of PL in various MS/water mixtures at different temperature. Panel (a): lines 1−5 represent the MS/water mixtures with water contents of ~13, ~25, ~37, ~49, and ~56 wt % respectively; panel (b): lines 1−5 represent the MS/water mixtures with water contents of ~18, ~28, ~41, ~52, and ~58 wt % respectively; panel (c): lines 1−5 represent the MS/water mixtures with water contents of ~19, ~30, ~44, ~54, and ~59 wt % respectively. Point A-G in panel (a), panel (b) and panel (c) correspond point A-G in Figure 1a, 1b and 1c respectively. Panel (d,e and f) : line 1 represents the δ values of the MS/water mixtures at various water contents. [Legend: PL, pyrolytic lignin; MS, mixed solvent.]

The effect of temperature on the PL solubility is mainly due to the changes in the solubility parameters of MS and water at different temperatures, as mentioned in Section 2.4. Figure 8-2 shows that the solubility parameter (δ) of the MS/water mixture (see line 1) slightly reduces as temperature increases. The optimal δ range (i.e., 11.95–15.95 $cal^{1/2}cm^{-3/2}$) for the dissolution of polymers (e.g. PL in this case) experiences little change with increasing temperature [149]. Thus, an increase in temperature leads to a change in the optimal water content range of the MS/water mixture for PL dissolution (see shaded areas in Figure 8-2a−8-2c), i.e., 0 − 31, 0 – 34, 2 − 37 wt % water in the MS/water mixture at 0, 25 and 40 °C, respectively. It is clear that the PL solubilities within the optimal δ ranges are high at all three temperatures, while those outside the

optimal δ ranges (i.e., line 3 in Figure 8-2a−8-2c) almost reduce to less than half of the maximal values. The water content in the MS/water mixture at the maximal PL solubility also increases with temperature, from 15 wt % at 0 °C, to 18 wt % at 25 °C, then to 19 wt % at 40 °C. It should be pointed out that the δ values of the MS/water at the maximal PL solubilities for different temperatures (i.e., 13.9, 14.0 and 13.8 $cal^{1/2}cm^{-3/2}$ at 0, 25 and 40 °C, respectively) are all close to that (i.e., 13.95 $cal^{1/2}cm^{-3/2}$) of the PL sample. This indicates that the effect of temperature on the ternary diagram of PL/MS/water system is due to the change in solvent solubility parameter of MS/water at different temperatures.

8.3 Effect of Temperature on the Phase Diagrams of PL/MS/Water in the Presence of Sugar

It is known that sugar is the 6th largest chemical family in bio-oil [121] with a concentration of approximately 5−7 wt % (mainly in form of levoglucosan) [120]. Our previous work has demonstrated that at room temperature, the presence of sugar (i.e., levoglucosan) influences the ternary phase diagram of the PL/MS/water system, but only at a low water content (i.e., < 20 wt %) [121]. In this study, the presence of levoglucosan at two different concentrations (i.e. 5 and 7 wt %) were considered for studying the effect of temperature on the phase behaviours of the PL/MS/water ternary systems in the presence of sugar. The ternary phase diagrams of the PL/MS/water systems in presence of 5 and 7 wt % sugar at different temperatures (i.e., 0, 25 and 40 °C) are presented in Figure 8-3. It can be seen that the PL solubility at the same temperature reduces with increasing the sugar concentration, but only up to a certain water content which increases with the sugar concentration. The PL solubilities in the MS/water mixtures in presence of 5 and 7 wt % sugar were also calculated and the results are presented in Figure 8-4. Some key points (A_1−C_1, A_2-C_2) are highlighted in both Figure 8-3a−8-3c and Figure 8-4a−8-4c.

Points A_1 and A_2 in Figure 8-3 represent the maximal PL concentrations in a homogeneous PL/MS binary system in the presence of 5 and 7 wt % sugar, respectively. The PL solubility at the same sugar concentration also increases with temperature. For example, at a sugar concentration of 5 wt %, the maximal PL concentration at point A_1 increases with temperature, i.e., from ~45 wt % at 0 °C, to ~49 wt % at 25 °C, and then to ~51 wt % at 40 °C. As a result, the PL solubility in MS increases from ~81 g PL per 100 g of MS at 0 °C, to ~97 g PL per 100 g of MS at 25 °C, then to ~108 g PL per 100 g of MS at 40 °C (see Figure 8-4a−8-4c). When the sugar concentration increases to 7 wt %, the maximal PL concentrations in the PL/MS binary system also increases with temperature, i.e., from ~33 to ~41 wt % when temperature increases from 0 to 40 °C (see point A_2 in Figure 8-3a−8-3c). It is obvious to see that the maximal PL concentrations at 7 wt % sugar concentration are much lower than those at 5 wt % sugar concentration, when compared at the same temperature.

Similarly, an increase in the water content increases the PL solubility in the MS/water mixture in the presence of sugar. As shown in Figure 8-3 and Figure 8-4, points B_1 and B_2 represent the maximal PL concentrations that can be achieved for a homogeneous PL/MS/water ternary system in presence of 5 and 7 wt % sugar, respectively. As expected, the maximal PL concentration in the PL/MS/water ternary mixture at 5 wt % sugar concentration increases from ~57 wt % (equivalent to a PL solubility of ~132 g PL per 100 g of MS/water mixture) at 0 °C, to ~63 wt % (equivalent to a PL solubility of ~171 g PL per 100 g of MS/water mixture) at 25 °C, then to ~67 wt % (equivalent to a PL solubility of ~204 g PL per 100 g of MS/water mixture) at 40 °C. When the sugar concentration increases to 7 wt %, the maximal PL concentration in the PL/MS/water ternary system increases from ~52 wt % (equivalent to a PL solubility of ~110 g PL per 100 g of MS/water mixture) at 0 °C to ~64 % (equivalent to a PL solubility of ~181 g PL per 100 g of MS/water mixture) at 40 °C. Similarly, an increase in temperature also increases the water content in the MS/water mixture at the maximal

PL concentration, i.e., from 19 to 26 wt % for 5 wt % sugar and from 23 to 30 wt % for 7 wt % sugar, when temperature increases from 0 to 40 °C.

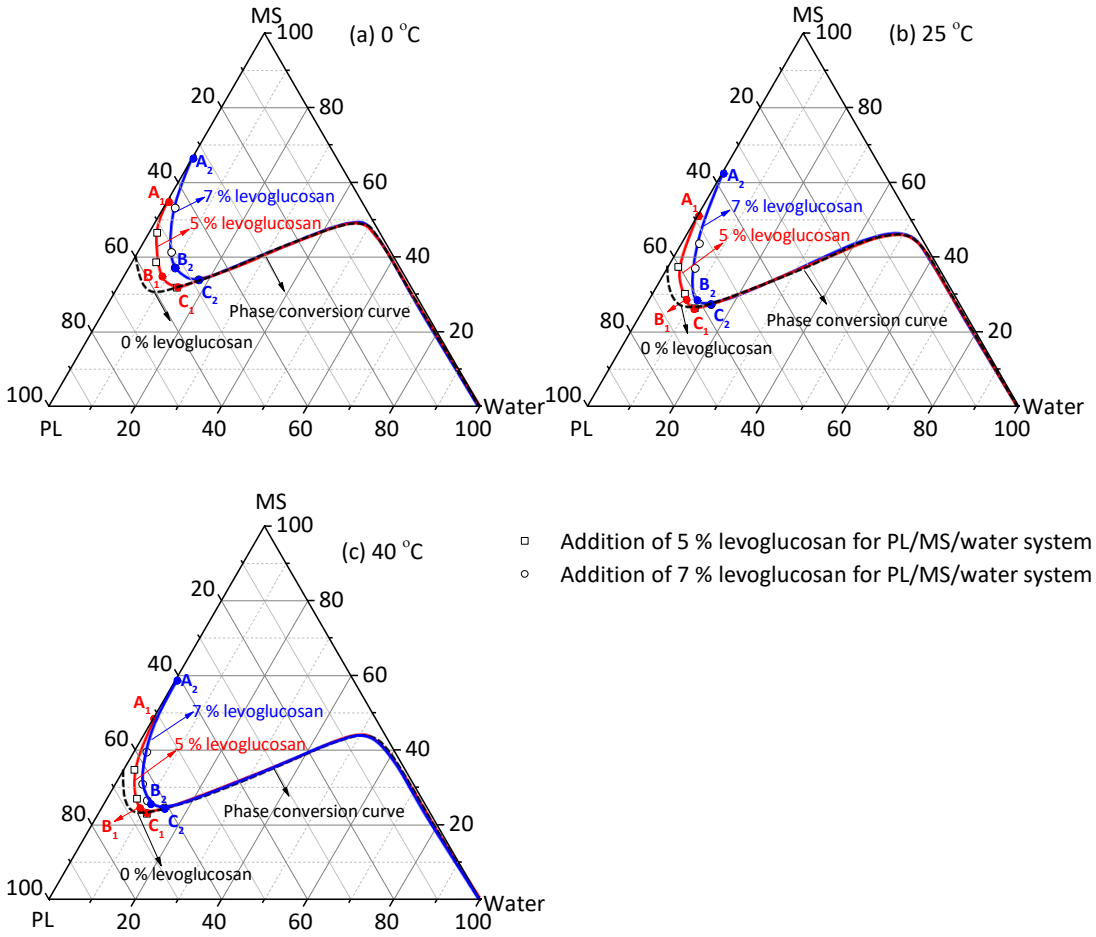

Figure 8-3 Ternary phase diagrams of PL/MS/water system with the contents of levoglucosan being 5 and 7 wt % in the overall systems at different temperature. The ternary diagrams are plotted with the contents of PL, MS, and water normalized to 100% (excluding levoglucosan in the system). Point A_1 and A_2 in figure (a), (b), (c) represent the minimal MS required to homogenize the PL/MS binary mixture with the presence of 5 and 7 wt % sugar, respectively. Point B_1 and B_2 in figure (a), (b) and (c) represents the maximal solubility of PL is achieved in the MS/water mixture with the presence of 5 and 7 wt % sugar, respectively. Point C_1 and C_2 in figure (a), (b), and (c) represent that the minimal water content at which the sugar being added has no effect on the phase conversion curves with the presence of 5 and 7 wt % sugar, respectively. [Legend: PL, pyrolytic lignin; MS, mixed solvent.]

Points C_1 and C_2 in Figure 8-3 and Figure 8-4 represent the minimal MS content required to possibly form a homogeneous PL/MS/water system in presence of 5 and 7 wt % sugar, respectively. It can be found out that the minimal MS content reduces with increasing the temperature. For example, when the temperature increases from 0 to 40 °C, the minimal MS concentration at point C_1 reduces from ~32 to ~23 wt % in presence of 5 wt % sugar, while that at point C_2 reduces from ~34 to ~24 wt % in presence of 7 wt % sugar. As a result, the PL solubility in the MS/water mixture increases from ~120 to ~193 g PL per 100 g of MS/water mixture and from ~93 to ~156 g PL per 100 g of MS/water mixture in the presence of 5 and 7 wt % sugar, respectively, when the temperature increases from 0 to 40 °C. It is noteworthy that points C_1 and C_2 also represent the critical water content below which the sugar shows significant effect on the phase conversion curve in the presence of 5 and 7 wt % sugar, respectively. It can be seen that the critical water content in the PL/MS/water system for point C_1 decreases from ~14 wt % at 0 °C (equivalent to ~30 wt % water content in the MS/water mixture), to ~12 wt % at 25 °C (equivalent to ~31 wt % water content in the MS/water mixture), and further to 11 wt % at 40 °C (equivalent to ~33 wt % water content in the MS/water mixture) in the presence of 5 wt % sugar. At a sugar concentration of 7 wt %, the critical water content in the PL/MS/water system for point C_2 decreases from ~18 wt % (equivalent to ~35 wt % water content in the MS/water mixture) to ~14 wt % (equivalent to ~38 wt % water content in the MS/water mixture), when the temperature increases from 0 to 40 °C (see point C_2 in Figure 8-3 and Figure 8-4). This is because the dissolution of sugars in water is also an endothermic process, since the enthalpies of sugar dissolution in water are > 0 kJ/mol.[190, 191] Therefore, increasing temperature leads to the increase in the sugar solubility in MS/water mixtures. It should be pointed out that, although the critical water content in the MS/water mixture increases with temperature, the water content in the PL/MS/water

ternary system reduces with temperature, mainly due to an increase in the PL solubility as temperature increases.

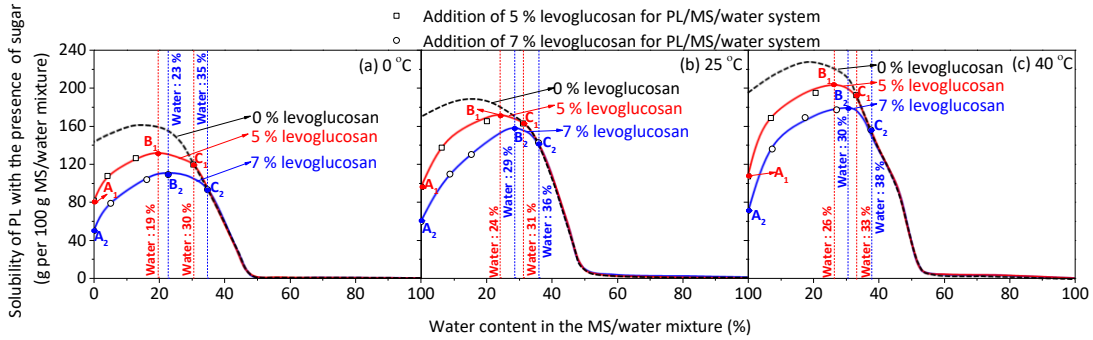

Figure 8-4 Solubilities of PL in various MS/water mixtures with the presence of sugar at different temperature. Point A_1-C_1 and A_2-C_2 in panel (a), (b) and (c) correspond to point A_1-C_1 and A_2-C_2 in Figure 3a, 3b and 3c respectively. Panel (a): at 0 °C the maximal solubilities of PL with 5 % and 7 % levoglucosan being added are achieved at point B_1 or B_2, corresponding to water contents of ~19 and ~23 % respectively; the 5 % and 7 % levoglucosan has no effect beyond point C_1 and C_2, corresponding to water contents of ~30 or ~35 % respectively. Panel (b): at 25 °C the maximal solubilities of PL with 5 % and 7 % levoglucosan being added are achieved at point B_1 and B_2, corresponding to water contents of ~24 or ~29 % respectively; the 5 % or 7 % levoglucosan has no effect beyond point C_1 and C_2, corresponding to water contents of ~31 or ~36 % respectively. Panel (c): at 40 °C the maximal solubilities of PL with 5 % and 7 % levoglucosan being added are achieved at point B_1 and B_2, corresponding to water contents of ~26 and ~30 % respectively; the 5 % or 7 % levoglucosan has no effect beyond point C_1 and C_2, corresponding to water contents of ~33 or ~38 % respectively. [Legend: PL, pyrolytic lignin; MS, mixed solvent.]

8.4 Discussion on Phase Stability Prediction Using the Phase Diagram

The ternary phase diagrams of the PL/MS/water systems at different temperatures are of critical importance for predicting the phase stability of bio-oil due to a temperature

change. Based on the results presented in this study, there are some useful guidelines to choose the appropriate ternary phase diagram for predicting bio-oil phase stability.

First, in order to maintain a homogeneous bio-oil during storage and transport, it is important to make sure the phase separation of bio-oil does not occur at the lowest temperature conditions. Since the PL solubility reduces with temperature, the ternary phase diagram of the PL/MS/water system at the lowest temperature should be always used for predicting the phase stability of bio-oil. If the bio-oil is predicted to be phase separated based on the phase diagram at the lowest temperature, the addition of the MS solvent into the bio-oil can be an effective strategy to enhance the bio-oil stability at low temperatures. The required amount of solvent to avoid phase separation at a specific temperature can be also obtained based on the phase diagram at that temperature.

Second, the effect of sugar needs to be considered for predicting the phase stability of bio-oil at different temperatures using the ternary phase diagrams of the PL/MS/water systems. The sugar concentration determines the critical water content below which the phase diagram is strongly affected. The critical water content increases with increasing sugar concentration in the system, and reduces with increasing temperature. Therefore, it is essential to know the critical water content under specific sugar concentration and temperature conditions, i.e., ~11–14 and ~14–18 wt % at 5 and 7 wt % sugar concentration, respectively. If the water content in the bio-oil is less than the critical water content, the effect of sugar on the PL solubility is large so the ternary phase diagram of PL/MS/water system in the presence of sugar must be used for predicting the bio-oil stability. If the water content in the bio-oil is higher than the critical water content, the ternary phase diagram of PL/MS/water system without sugar can be used, since the effect of sugar on PL solubility is negligible.

8.5 Conclusions

This work investigates the effect of temperature on the phase behaviour of the PL sample in various MS/water systems, and the ternary phase diagrams of the PL/MS/water systems at different temperatures are developed. The results clearly show that an increase in temperature largely increases the solubility of PL in the MS/water system. The maximal PL concentration in the PL/MS/water system increases from ~62 wt % at 0 °C (equivalent to a PL solubility of ~161 g PL per 100 g of MS/water mixture) to ~70 wt % (equivalent to a PL solubility of ~229 g PL per 100 g of MS/water mixture) at 40 °C. This is because the dissolution of PL in the MS/water mixture is an endothermic process, and therefore increasing the temperature will shift the dissolution equilibrium towards the PL solution side. The presence of sugar also influences the PL solubility in the MS/water system, but only up to a critical water content (i.e., ~11–18 wt % at 5–7 wt % sugar concentration and 0–40 °C) depending on the temperature and sugar concentration. The results suggest that a set of ternary phase diagrams of PL/MS/water systems at different temperatures and sugar concentrations are essential to predicting the phase stability of bio-oil during storage and transport.

Chapter 9 Conclusions and Recommendations

9.1 Introduction

This chapter presents the significant findings of this PhD research. Overall, this thesis has summarised the series of systematic study on phase diagrams of various PL/MS/water systems. Firstly, this study has examined the solubilities of PL in various water-soluble fraction model compounds, and corresponding phase diagrams were constructed. Secondly, this thesis also reported the development of an MS for the construction of phase diagrams of PL/MS/water systems. Thirdly, fresh bio-oils were produced in the lab, and phase diagrams were constructed for the systems of PL separated from fresh bio-oil, MS and water. Finally, efforts were made to understand the effects of extractive/ash/ester and temperature on the phase diagrams of PL/MS/water systems. The following sections list the detailed findings from this PhD study and some recommendations for future work.

9.2 Conclusions

Conclusions are outlined based on the four targets of this thesis study, which are detailed below.

9.2.1 Effect of Single/Mixed Model Solvents on the Phase Diagrams of Pyrolytic Lignin, Model Solvent and Water

- Phase diagrams of PL/model solvents/water were constructed in this study, and the PL solubilities in model solvent/water mixtures were also examined. Various single-component, two-component, three-component and four-component model solvents are prepared for the dissolution of PL.
- The PL solubilities in acetic acid, hydroxyacetone and methanol are ~214, ~239 and ~615 g per 100 g of solvent, respectively. When furfural or phenol is

being added to form two-component model solvents, the PL solubilities in corresponding solvents experienced reductions.

- Furfural and phenol can be widely found in fast pyrolysis bio-oil; therefore, it is still necessary to include furfural and phenol in the mixed model solvents when developing a universal tool for the prediction of bio-oil phase stability.

9.2.2 Ternary System of Pyrolytic Lignin, Mixed-Solvent and Water: Phase Diagram and Implications

- An MS is developed based on the composition of bio-oils in existing literature, and the dissolution of PL and its fractions in various MS/water mixtures are studied. Several ternary phase diagrams are constructed for PL and its fractions, and the solubility of PL and its fractions are also estimated.
- The stability of the PL/MS/water system is found to strongly depend on the composition of each fraction. For example, the PL/MS/water system is always phased separated, if the PL content is >54 wt %, or the water content is >60 wt %, or the MS content is <35 wt %, while the PL/MS/water system is always stable if the MS content is >50 wt %.
- The solubility of different PL fractions is strongly affected by the average molecular weight, and the PL with lower average molecular weight has a higher solubility in the same MS/water mixture.

9.2.3 Effect of Ageing on the Phase Diagrams of Pyrolytic Lignin, Mixed Solvent and Water

- Bio-oils are produced from mallee and pine wood fast pyrolysis in a lab-scale auger reactor. Several phase diagrams of PL/MS/water are constructed for various PL samples.
- The maximal PL concentration in the PL/MS/water system is between ~47 wt % (equivalent to a PL solubility of ~89 g PL per 100 g of MS/water mixture) and

~69 wt % (equivalent to a PL solubility of ~221 g PL per 100 g of MS/water mixture) depending on its average molecular weight.

- Applications of predicting phase-separation of bio-oil samples using the phase diagrams are also studied. The results suggest the phase diagrams are useful tools to predict phase stability of bio-oil samples, especially after long-term ageing because of the irreversible changes in the compositions of bio-oils.

9.2.4 Effect of Bio-Oil Minor Components on the Phase Diagrams of Pyrolytic Lignin, Mixed Solvent and Water

- The minimal MS contents required to guarantee homogeneous PL/MS/water mixtures increase when extractive model compounds being added. For example, the PL/MS/water systems are always stable when MS contents are > ~50, ~52, ~51 and ~49 wt % in presence of 0.2 wt % decane, 0.1 wt % pentadecane, 5.0 wt % BQ and 5.0 wt % CHCA. The critical water content for the phase diagram of PL/MS/water in the presence of 0.6 wt % ash model compound (KCl) is < ~3 wt %.
- Ester model compounds, furfural acetate and phenylacetate have similar effects on the phase behaviours of PL/MS/water systems as extractive model compounds. The phase conversion curves of PL/MS/water systems in the presence of 5.0 wt % furfural acetate and phenylacetate will be not affected when water contents in the ternary systems are < ~20 and ~18 wt % respectively. The presence of 5 and 7 wt % methyl α-D-glucopyranoside also affects the phase stability of PL/MS/water systems, but only when water contents are <~12 and ~17 wt %.
- It is worth noting that methyl acetate can enhance the phase stabilities of PL/MS/water systems. For example, the maximal PL solubilities in PL/MS binary systems reduce to ~34 and ~36 wt % in the presence of 7.5 and 15 wt % methyl acetate, in contrast to ~38 wt % without the addition of methyl acetate.

9.2.5 Effect of Temperature on Ternary Phase Diagrams of Pyrolytic Lignin, Mixed Solvent and Water

- This work investigates the effect of temperature on the phase behaviour of the PL sample in various MS/water systems, and the ternary phase diagrams of the PL/MS/water systems at different temperatures are developed.
- An increase in temperature largely increases the solubility of PL in the MS/water system. The maximal PL concentration in the PL/MS/water system increases from ~62 wt % at 0 °C (equivalent to a PL solubility of ~161 g PL per 100 g of MS/water mixture) to ~70 wt % (equivalent to a PL solubility of ~229 g PL per 100 g of MS/water mixture) at 40 °C.
- The presence of sugar also influences the PL solubility in the MS/water system, but only up to a critical water content (i.e., ~11–18 wt % at 5–7 wt % sugar concentration and 0–40 °C) depending on the temperature and sugar concentration.

9.3 Recommendations

Potential recommendations for future work are listed below:

1. Limited by present experiment rigs, this study has produced fresh bio-oil from fast pyrolysis of one biomass under one single reaction condition. Future works should be extended to various biomass feedstocks under a wide range of pyrolysis conditions. This will enable preparations of PLs of various properties.
2. This study only considers the effect of three temperatures (0, 25, 40 °C) on phase diagrams. In real life, bio-oil may be handled at sub-zero so that future work should be extended to temperatures below 0 °C.
3. The development of quantitative models to describe the experimental observations, thereby allowing for prediction of behaviours of various bio-oil-water solvent mixtures.

References

1. BP *BP Statistical Review of World Energy*; London, UK., 2017.

2. Akhtar, A.; Krepl, V.; Ivanova, T., A Combined Overview of Combustion, Pyrolysis, and Gasification of Biomass. *Energy & Fuels* **2018,** *32* (7), 7294-7318.

3. Tsai, W. T.; Lee, M. K.; Chang, Y. M., Fast pyrolysis of rice straw, sugarcane bagasse and coconut shell in an induction-heating reactor. *Journal of Analytical and Applied Pyrolysis* **2006,** *76* (1–2), 230-237.

4. Bridgwater, A. V.; Czernik, S.; Diebold, J.; Meier, D.; Oasmaa, A.; Peacocke, C.; Piskorz, J.; Radlein, D., *Fast pyrolysis of biomass: a handbook*. CPL press Berkshire: 1999; Vol. 1.

5. Czernik, S.; Bridgwater, A. V., Overview of Applications of Biomass Fast Pyrolysis Oil. *Energy & Fuels* **2004,** *18* (2), 590-598.

6. Guo, X.; Wang, S.; Wang, Q.; Guo, Z.; Luo, Z., Properties of Bio-oil from Fast Pyrolysis of Rice Husk. *Chinese Journal of Chemical Engineering* **2011,** *19* (1), 116-121.

7. Oasmaa, A.; Fonts, I.; Pelaez-Samaniego, M. R.; Garcia-Perez, M. E.; Garcia-Perez, M., Pyrolysis Oil Multiphase Behavior and Phase Stability: A Review. *Energy & Fuels* **2016,** *30* (8), 6179-6200.

8. Chheda, J. N.; Huber, G. W.; Dumesic, J. A., Liquid‐phase catalytic processing of biomass‐derived oxygenated hydrocarbons to fuels and chemicals. *Angewandte Chemie International Edition* **2007,** *46* (38), 7164-7183.

9. Oasmaa, A.; Kuoppala, E., Fast Pyrolysis of Forestry Residue. 3. Storage Stability of Liquid Fuel. *Energy & Fuels* **2003,** *17* (4), 1075-1084.

10. Oasmaa, A.; Sundqvist, T.; Kuoppala, E.; Garcia-Perez, M.; Solantausta, Y.; Lindfors, C.; Paasikallio, V., Controlling the phase stability of biomass fast pyrolysis bio-oils. *Energy & Fuels* **2015,** *29* (7), 4373-4381.

11. PLC, B., BP Statistical Review of WorldEnergy 2016. London, UK: BP plc https://www. bp. com/content/dam/bp/pdf/energyeconomics …: 2017.

12. Bridgwater, A. V., Review of fast pyrolysis of biomass and product upgrading. *Biomass and Bioenergy* **2012,** *38*, 68-94.

13. Zhang, Q.; Chang, J.; Wang, T.; Xu, Y., Review of biomass pyrolysis oil properties and upgrading research. *Energy Conversion and Management* **2007,** *48* (1), 87-92.

14. Organization, W. H., Quantitative risk assessment of the effects of climate change on selected causes of death, 2030s and 2050s. **2014**.

15. Rockström, J.; Gaffney, O.; Rogelj, J.; Meinshausen, M.; Nakicenovic, N.; Schellnhuber, H. J., A roadmap for rapid decarbonization. *Science* **2017,** *355* (6331), 1269-1271.

16. Markandya, A.; Wilkinson, P., Electricity generation and health. *The lancet* **2007,** *370* (9591), 979-990.

17. Olejarnik, P., World energy outlook 2013. *International Energy Agency: France* **2013**.

18. Vassilev, S. V.; Baxter, D.; Andersen, L. K.; Vassileva, C. G., An overview of the chemical composition of biomass. *Fuel* **2010,** *89* (5), 913-933.

19. McKendry, P., Energy production from biomass (part 1): overview of biomass. *Bioresource Technology* **2002,** *83* (1), 37-46.

20. Khan, A. A.; de Jong, W.; Jansens, P. J.; Spliethoff, H., Biomass combustion in fluidized bed boilers: Potential problems and remedies. *Fuel Processing Technology* **2009,** *90* (1), 21-50.

21. Ni, M.; Leung, D. Y. C.; Leung, M. K. H.; Sumathy, K., An overview of hydrogen production from biomass. *Fuel Processing Technology* **2006,** *87* (5), 461-472.

22. Panwar, N.; Kothari, R.; Tyagi, V., Thermo chemical conversion of biomass–Eco friendly energy routes. *Renewable and Sustainable Energy Reviews* **2012,** *16* (4), 1801-1816.

23. Bridgwater, A. V.; Peacocke, G. V. C., Fast pyrolysis processes for biomass. *Renewable and Sustainable Energy Reviews* **2000,** *4* (1), 1-73.

24. Speight, J. G., *Handbook of industrial hydrocarbon processes*. Gulf Professional Publishing: 2010.

25. Jahirul, I. M.; Rasul, G. M.; Chowdhury, A. A.; Ashwath, N., Biofuels Production through Biomass Pyrolysis —A Technological Review. *Energies* **2012,** *5* (12).

26. Mohan, D.; Pittman, C. U.; Steele, P. H., Pyrolysis of Wood/Biomass for Bio-oil: A Critical Review. *Energy & Fuels* **2006,** *20* (3), 848-889.

27. Lee, S. Y.; Sankaran, R.; Chew, K. W.; Tan, C. H.; Krishnamoorthy, R.; Chu, D.-T.; Show, P.-L., Waste to bioenergy: a review on the recent conversion technologies. *BMC Energy* **2019,** *1* (1), 4.

28. Wang, X.; Kersten, S. R.; Prins, W.; van Swaaij, W. P., Biomass pyrolysis in a fluidized bed reactor. Part 2: Experimental validation of model results. *Industrial & engineering chemistry research* **2005,** *44* (23), 8786-8795.

29. Liaw, S.-S.; Wang, Z.; Ndegwa, P.; Frear, C.; Ha, S.; Li, C.-Z.; Garcia-Perez, M., Effect of pyrolysis temperature on the yield and properties of bio-oils obtained from the auger pyrolysis of Douglas Fir wood. *Journal of Analytical and Applied Pyrolysis* **2012,** *93*, 52-62.

30. Oasmaa, A.; Kuoppala, E.; Gust, S.; Solantausta, Y., Fast Pyrolysis of Forestry Residue. 1. Effect of Extractives on Phase Separation of Pyrolysis Liquids. *Energy & Fuels* **2003,** *17* (1), 1-12.

31. Garcia-Perez, M.; Chaala, A.; Pakdel, H.; Kretschmer, D.; Roy, C., Characterization of bio-oils in chemical families. *Biomass and Bioenergy* **2007,** *31* (4), 222-242.

32. Shen, J.; Wang, X.-S.; Garcia-Perez, M.; Mourant, D.; Rhodes, M. J.; Li, C.-Z., Effects of particle size on the fast pyrolysis of oil mallee woody biomass. *Fuel* **2009,** *88* (10), 1810-1817.

33. Westerhof, R. J. M.; Nygard, H.; van Swaaij, W. P. M.; Kersten, S. R.; Brilman, D. W. F., Effect of particle geometry and microstructure on fast pyrolysis of beech wood. *Energy & fuels* **2012,** *26* (4), 2274-2280.

34. Ciesielski, P. N.; Crowley, M. F.; Nimlos, M. R.; Sanders, A. W.; Wiggins, G. M.; Robichaud, D.; Donohoe, B. S.; Foust, T. D., Biomass particle models with realistic morphology and resolved microstructure for simulations of intraparticle transport phenomena. *Energy & Fuels* **2014,** *29* (1), 242-254.

35. Oasmaa, A.; Sipilä, K.; Solantausta, Y.; Kuoppala, E., Quality improvement of pyrolysis liquid: effect of light volatiles on the stability of pyrolysis liquids. *Energy & fuels* **2005,** *19* (6), 2556-2561.

36. Westerhof, R. J.; Kuipers, N. J.; Kersten, S. R.; van Swaaij, W. P., Controlling the water content of biomass fast pyrolysis oil. *Industrial & Engineering Chemistry Research* **2007,** *46* (26), 9238-9247.

37. Mullen, C. A.; Boateng, A. A.; Goldberg, N. M.; Lima, I. M.; Laird, D. A.; Hicks, K. B., Bio-oil and bio-char production from corn cobs and stover by fast pyrolysis. *Biomass and bioenergy* **2010,** *34* (1), 67-74.

38. Sipilä, K.; Kuoppala, E.; Fagernäs, L.; Oasmaa, A., Characterization of biomass-based flash pyrolysis oils. *Biomass and Bioenergy* **1998,** *14* (2), 103-113.

39. Lu, Q.; Li, W.-Z.; Zhu, X.-F., Overview of fuel properties of biomass fast pyrolysis oils. *Energy Conversion and Management* **2009,** *50* (5), 1376-1383.

40. Elliott, D. C.; Hart, T. R.; Neuenschwander, G. G.; Rotness, L. J.; Zacher, A. H., Catalytic hydroprocessing of biomass fast pyrolysis bio‐oil to produce hydrocarbon products. *Environmental progress & sustainable energy* **2009,** *28* (3), 441-449.

41. Christensen, E.; Ferrell, J.; Olarte, M. V.; Padmaperuma, A. B. *Quantification of Semi-Volatile Oxygenated Components of Pyrolysis Bio-Oil by Gas Chromatography/Mass Spectrometry (GC/MS). Laboratory Analytical Procedure (LAP)*; National Renewable Energy Lab.(NREL), Golden, CO (United States): 2016.

42. Ferrell III, J. R.; Olarte, M. V.; Christensen, E. D.; Padmaperuma, A. B.; Connatser, R. M.; Stankovikj, F.; Meier, D.; Paasikallio, V., Standardization of chemical analytical techniques for pyrolysis bio‐oil: history, challenges, and current status of methods. *Biofuels, Bioproducts and Biorefining* **2016,** *10* (5), 496-507.

43. Scholze, B.; Hanser, C.; Meier, D., Characterization of the water-insoluble fraction from fast pyrolysis liquids (pyrolytic lignin): Part II. GPC, carbonyl goups, and 13C-NMR. *Journal of Analytical and Applied Pyrolysis* **2001,** *58*, 387-400.

44. Wyman, C. E., *Aqueous pretreatment of plant biomass for biological and chemical conversion to fuels and chemicals*. John Wiley & Sons: 2013.

45. Joseph, J.; Baker, C.; Mukkamala, S.; Beis, S. H.; Wheeler, M. C.; DeSisto, W. J.; Jensen, B. L.; Frederick, B. G., Chemical shifts and lifetimes for nuclear magnetic resonance (NMR) analysis of biofuels. *Energy & Fuels* **2010,** *24* (9), 5153-5162.

46. Lehto, J.; Solantausta, A.; Kytö, Y.; Matti, K.; David, C., Fuel oil quality and combustion of fast pyrolysis bio-oils. VTT. VTT Technical research centre of Finland: 2013.

47. Garcia-Perez, M.; Chaala, A.; Pakdel, H.; Kretschmer, D.; Rodrigue, D.; Roy, C., Multiphase structure of bio-oils. *Energy & Fuels* **2006,** *20* (1), 364-375.

48. Oasmaa, A.; Leppämäki, E.; Koponen, P.; Levander, J.; Tapola, E., Physical characterisation of biomass-based pyrolysis liquids: application of standard fuel oil analyses. *VTT PUBLICATIONS* **1997**.

49. Diebold, J. P. *A review of the chemical and physical mechanisms of the storage stability of fast pyrolysis bio-oils*; National Renewable Energy Lab., Golden, CO (US): 1999.

50. Alsbou, E.; Helleur, B., Accelerated Aging of Bio-oil from Fast Pyrolysis of Hardwood. *Energy & Fuels* **2014,** *28* (5), 3224-3235.

51. Scholze, B.; Meier, D., Characterization of the water-insoluble fraction from pyrolysis oil (pyrolytic lignin). Part I. PY–GC/MS, FTIR, and functional groups. *Journal of Analytical and Applied Pyrolysis* **2001,** *60* (1), 41-54.

52. Oasmaa, A.; Kuoppala, E.; Solantausta, Y., Fast Pyrolysis of Forestry Residue. 2. Physicochemical Composition of Product Liquid. *Energy & Fuels* **2003,** *17* (2), 433-443.

53. Vispute, T., Pyrolysis oils: characterization, stability analysis, and catalytic upgrading to fuels and chemicals. **2011**.

54. Meier, D.; Faix, O., State of the art of applied fast pyrolysis of lignocellulosic materials—a review. *Bioresource technology* **1999,** *68* (1), 71-77.

55. Mortensen, P. M.; Grunwaldt, J. D.; Jensen, P. A.; Knudsen, K. G.; Jensen, A. D., A review of catalytic upgrading of bio-oil to engine fuels. *Applied Catalysis A: General* **2011,** *407* (1), 1-19.

56. Shaddix, C.; Huey, S., Combustion characteristics of fast pyrolysis oils derived from hybrid poplar. In *Developments in thermochemical biomass conversion*, Springer: 1997; pp 465-480.

57. Khosravanipour Mostafazadeh, A.; Solomatnikova, O.; Drogui, P.; Tyagi, R. D., A review of recent research and developments in fast pyrolysis and bio-oil upgrading. *Biomass Conversion and Biorefinery* **2018,** *8* (3), 739-773.

58. Bridgwater, A., Production of high grade fuels and chemicals from catalytic pyrolysis of biomass. *Catalysis today* **1996,** *29* (1-4), 285-295.

59. Elliott, D.; Baker, E. *Hydrotreating biomass liquids to produce hydrocarbon fuels*; Pacific Northwest Lab., Richland, WA (USA): 1986.

60. Bridgwater, A., Fast pyrolysis of biomass for the production of liquids. In *Biomass combustion science, technology and engineering*, Elsevier: 2013; pp 130-171.

61. Bridgwater, A., Catalysis in thermal biomass conversion. *Applied Catalysis A: General* **1994,** *116* (1-2), 5-47.

62. Huber, G. W.; Iborra, S.; Corma, A., Synthesis of transportation fuels from biomass: chemistry, catalysts, and engineering. *Chemical reviews* **2006,** *106* (9), 4044-4098.

63. Bridgwater, A. V., Upgrading biomass fast pyrolysis liquids. *Environmental Progress & Sustainable Energy* **2012,** *31* (2), 261-268.

64. Williams, P. T.; Horne, P. A., Characterisation of oils from the fluidised bed pyrolysis of biomass with zeolite catalyst upgrading. *Biomass and Bioenergy* **1994,** *7* (1-6), 223-236.

65. Jahromi, H.; Agblevor, F. A., Upgrading of pinyon-juniper catalytic pyrolysis oil via hydrodeoxygenation. *Energy* **2017,** *141*, 2186-2195.

66. Peters, J. F.; Petrakopoulou, F.; Dufour, J., Exergy analysis of synthetic biofuel production via fast pyrolysis and hydroupgrading. *Energy* **2015,** *79*, 325-336.

67. Saber, M.; Nakhshiniev, B.; Yoshikawa, K., A review of production and upgrading of algal bio-oil. *Renewable and Sustainable Energy Reviews* **2016,** *58*, 918-930.

68. Li, X.; Chen, G.; Liu, C.; Ma, W.; Yan, B.; Zhang, J., Hydrodeoxygenation of lignin-derived bio-oil using molecular sieves supported metal catalysts: A critical review. *Renewable and Sustainable Energy Reviews* **2017,** *71*, 296-308.

69. Arregi, A.; Amutio, M.; Lopez, G.; Bilbao, J.; Olazar, M., Evaluation of thermochemical routes for hydrogen production from biomass: A review. *Energy conversion and management* **2018,** *165*, 696-719.

70. Xiao, X.; Meng, X.; Le, D. D.; Takarada, T., Two-stage steam gasification of waste biomass in fluidized bed at low temperature: Parametric investigations and performance optimization. *Bioresource technology* **2011,** *102* (2), 1975-1981.

71. Ba, T.; Chaala, A.; Garcia-Perez, M.; Rodrigue, D.; Roy, C., Colloidal properties of bio-oils obtained by vacuum pyrolysis of softwood bark. Characterization of water-soluble and water-insoluble fractions. *Energy & Fuels* **2004,** *18* (3), 704-712.

72. Ren, S.; Ye, X. P.; Borole, A. P., Separation of chemical groups from bio-oil water-extract via sequential organic solvent extraction. *Journal of Analytical and Applied Pyrolysis* **2017,** *123*, 30-39.

73. Underwood, G., Commercialisation of fast pyrolysis products. CPL Press: Newbury, UK: 1992; pp 226-228.

74. Underwood, G.; Graham, R. G., Method of using fast pyrolysis liquids as liquid smoke. Google Patents: 1989.

75. Oehr, K. H.; Scott, D. S.; Czernik, S., Method of producing calcium salts from biomass. Google Patents: 1993.

76. Gancy, A. B., Process of making calcium acetate deicing agents and product. Google Patents: 1984.

77. Radlein, D. S.; Piskorz, J.; Scott, D. S., Lignin derived oils from the fast pyrolysis of poplar wood. *Journal of Analytical and Applied Pyrolysis* **1987,** *12* (1), 51-59.

78. Roy, C.; Lu, X.; Pakdel, H., Process for the production of phenolic-rich pyrolysis oils for use in making phenol-formaldehyde resole resins. Google Patents: 2000.

79. Nakos, P.; Tsiantzi, S.; Athanassiadou, E. In *Wood adhesives made with pyrolysis oils*, Proceedings of the 3rd European wood-based panel symposium, European Panel Federation and Wilhelm Klauditz Institute Brussels: 2001; pp 12-14.

80. Athanassiadou, E.; Tsiantzi, S.; Nakos, P., Wood adhesives made with pyrolysis oils. *ACM Wood Chemicals plc* **2002**.

81. Mullen, C. A.; Boateng, A. A., Chemical composition of bio-oils produced by fast pyrolysis of two energy crops. *Energy & fuels* **2008,** *22* (3), 2104-2109.

82. Peacocke, G.; Russell, P.; Jenkins, J.; Bridgwater, A., Physical properties of flash pyrolysis liquids. *Biomass and Bioenergy* **1994,** *7* (1-6), 169-177.

83. Ba, T.; Chaala, A.; Garcia-Perez, M.; Roy, C., Colloidal properties of bio-oils obtained by vacuum pyrolysis of softwood bark. Storage stability. *Energy & fuels* **2004,** *18* (1), 188-201.

84. Demirbas, A., Combustion characteristics of different biomass fuels. *Progress in Energy and Combustion Science* **2004,** *30* (2), 219-230.

85. Fahmi, R.; Bridgwater, A.; Donnison, I.; Yates, N.; Jones, J., The effect of lignin and inorganic species in biomass on pyrolysis oil yields, quality and stability. *Fuel* **2008,** *87* (7), 1230-1240.

86. Fahmi, R.; Bridgwater, A.; Darvell, L.; Jones, J.; Yates, N.; Thain, S.; Donnison, I., The effect of alkali metals on combustion and pyrolysis of Lolium and Festuca grasses, switchgrass and willow. *Fuel* **2007,** *86* (10-11), 1560-1569.

87. Garcia-Perez, M.; Wang, S.; Shen, J.; Rhodes, M.; Lee, W. J.; Li, C.-Z., Effects of Temperature on the Formation of Lignin-Derived Oligomers during the Fast Pyrolysis of Mallee Woody Biomass. *Energy & Fuels* **2008,** *22* (3), 2022-2032.

88. Jones, S. B.; Valkenburt, C.; Walton, C. W.; Elliott, D. C.; Holladay, J. E.; Stevens, D. J.; Kinchin, C.; Czernik, S. *Production of gasoline and diesel from biomass via fast pyrolysis, hydrotreating and hydrocracking: a design case*; Pacific Northwest National Lab.(PNNL), Richland, WA (United States): 2009.

89. Garcìa-Pèrez, M.; Chaala, A.; Roy, C., Vacuum pyrolysis of sugarcane bagasse. *Journal of Analytical and Applied Pyrolysis* **2002,** *65* (2), 111-136.

90. Oasmaa, A.; Elliott, D. C.; Korhonen, J., Acidity of Biomass Fast Pyrolysis Bio-oils. *Energy & Fuels* **2010,** *24* (12), 6548-6554.

91. Westerhof, R. J. M.; Brilman, D. W. F.; van Swaaij, W. P. M.; Kersten, S. R. A., Effect of Temperature in Fluidized Bed Fast Pyrolysis of Biomass: Oil Quality Assessment in Test Units. *Industrial & Engineering Chemistry Research* **2010,** *49* (3), 1160-1168.

92. Oasmaa, A.; Peacocke, C., *A guide to physical property characterisation of biomass-derived fast pyrolysis liquids*. Technical Research Centre of Finland Espoo: 2001.

93. Garcia-Perez, M.; Chaala, A.; Pakdel, H.; Kretschmer, D.; Rodrigue, D.; Roy, C., Evaluation of the influence of stainless steel and copper on the aging process of bio-oil. *Energy & fuels* **2006,** *20* (2), 786-795.

94. Czernik, S.; Johnson, D. K.; Black, S., Stability of wood fast pyrolysis oil. *Biomass and Bioenergy* **1994,** *7* (1), 187-192.

95. Oasmaa, A.; Korhonen, J.; Kuoppala, E., An approach for stability measurement of wood-based fast pyrolysis bio-oils. *Energy & Fuels* **2011,** *25* (7), 3307-3313.

96. Hoekstra, E.; Westerhof, R. J.; Brilman, W.; Van Swaaij, W. P.; Kersten, S. R.; Hogendoorn, K. J.; Windt, M., Heterogeneous and homogeneous reactions of pyrolysis vapors from pine wood. *AIChE journal* **2012,** *58* (9), 2830-2842.

97. Rosendahl, L., *Biomass combustion science, technology and engineering*. Elsevier: 2013.

98. Luque, R.; Clark, J., *Handbook of biofuels production: Processes and technologies*. Elsevier: 2010.

99. Oasmaa, A.; Kuoppala, E.; Selin, J.-F.; Gust, S.; Solantausta, Y., Fast Pyrolysis of Forestry Residue and Pine. 4. Improvement of the Product Quality by Solvent Addition. *Energy & Fuels* **2004,** *18* (5), 1578-1583.

100. Xiu, S.; Shahbazi, A., Bio-oil production and upgrading research: A review. *Renewable and Sustainable Energy Reviews* **2012,** *16* (7), 4406-4414.

101. Oasmaa, A.; Czernik, S., Fuel oil quality of biomass pyrolysis oils state of the art for the end users. *Energy & Fuels* **1999,** *13* (4), 914-921.

102. Radlein, D. In *Method of upgrading biomass pyrolysis liquids for use as fuels and as a source of chemicals by reaction with alcohols*, Fuel and Energy Abstracts, 1997; p 79.

103. Diebold, J. P.; Czernik, S., Additives to lower and stabilize the viscosity of pyrolysis oils during storage. *Energy & Fuels* **1997,** *11* (5), 1081-1091.

104. Boucher, M.; Chaala, A.; Roy, C., Bio-oils obtained by vacuum pyrolysis of softwood bark as a liquid fuel for gas turbines. Part I: Properties of bio-oil and its

blends with methanol and a pyrolytic aqueous phase. *Biomass and Bioenergy* **2000,** *19* (5), 337-350.

105. Bertoli, C.; D'Alessio, J.; Giacomo, N. D.; Lazzaro, M.; Massoli, P.; Moccia, V., Running light-duty DI diesel engines with wood pyrolysis oil. *SAE transactions* **2000**, 3090-3096.

106. Juste, G. L.; Monfort, J. S., Preliminary test on combustion of wood derived fast pyrolysis oils in a gas turbine combustor. *Biomass and Bioenergy* **2000,** *19* (2), 119-128.

107. Doshi, V. A.; Vuthaluru, H. B.; Bastow, T., Investigations into the control of odour and viscosity of biomass oil derived from pyrolysis of sewage sludge. *Fuel Processing Technology* **2005,** *86* (8), 885-897.

108. Mahfud, F. H.; Melián-Cabrera, I.; Manurung, R.; Heeres, H. J., Biomass to Fuels: Upgrading of Flash Pyrolysis Oil by Reactive Distillation Using a High Boiling Alcohol and Acid Catalysts. *Process Safety and Environmental Protection* **2007,** *85* (5), 466-472.

109. Zhang, M.; Wu, H., Phase Behavior and Fuel Properties of Bio-Oil/Glycerol/Methanol Blends. *Energy & Fuels* **2014,** *28* (7), 4650-4656.

110. Li, X.; Gunawan, R.; Lievens, C.; Wang, Y.; Mourant, D.; Wang, S.; Wu, H.; Garcia-Perez, M.; Li, C.-Z., Simultaneous catalytic esterification of carboxylic acids and acetalisation of aldehydes in a fast pyrolysis bio-oil from mallee biomass. *Fuel* **2011,** *90* (7), 2530-2537.

111. Gunawan, R.; Li, X.; Larcher, A.; Hu, X.; Mourant, D.; Chaiwat, W.; Wu, H.; Li, C.-Z., Hydrolysis and glycosidation of sugars during the esterification of fast pyrolysis bio-oil. *Fuel* **2012,** *95*, 146-151.

112. Wang, J.-J.; Chang, J.; Fan, J., Upgrading of Bio-oil by Catalytic Esterification and Determination of Acid Number for Evaluating Esterification Degree. *Energy & Fuels* **2010,** *24* (5), 3251-3255.

113. Adjaye, J.; Bakhshi, N., Characterization and stabilization study of the ENSYN fast pyrolysis bio-oil. *DSS Contract* **1995,** (23440-3), 9472.

114. Weerachanchai, P.; Tangsathitkulchai, C.; Tangsathitkulchai, M., Phase behaviors and fuel properties of bio-oil-diesel-alcohol blends. *World Academy of Science, Engineering and Technology* **2009,** *56*, 387-393.

115. Meier, D.; Schoell, S.; Klaubert, H., New ablative pyrolyser in operation in Germany. *PyNe newsletter* **2004,** *17* (1).

116. Chiaramonti, D.; Bonini, M.; Fratini, E.; Tondi, G.; Gartner, K.; Bridgwater, A.; Grimm, H.; Soldaini, I.; Webster, A.; Baglioni, P., Development of emulsions from biomass pyrolysis liquid and diesel and their use in engines—Part 1: emulsion production. *Biomass and bioenergy* **2003,** *25* (1), 85-99.

117. Chiaramonti, D.; Bonini, M.; Fratini, E.; Tondi, G.; Gartner, K.; Bridgwater, A.; Grimm, H.; Soldaini, I.; Webster, A.; Baglioni, P., Development of emulsions from biomass pyrolysis liquid and diesel and their use in engines—Part 2: tests in diesel engines. *Biomass and Bioenergy* **2003,** *25* (1), 101-111.

118. Ikura, M.; Stanciulescu, M.; Hogan, E., Emulsification of pyrolysis derived bio-oil in diesel fuel. *Biomass and bioenergy* **2003,** *24* (3), 221-232.

119. Chua, Y. W.; Yu, Y.; Wu, H., Thermal decomposition of pyrolytic lignin under inert conditions at low temperatures. *Fuel* **2017,** *200*, 70-75.

120. Yu, Y.; Chua, Y. W.; Wu, H., Characterization of Pyrolytic Sugars in Bio-Oil Produced from Biomass Fast Pyrolysis. *Energy & Fuels* **2016,** *30* (5), 4145-4149.

121. Li, M.; Zhang, M.; Yu, Y.; Wu, H., Ternary System of Pyrolytic Lignin, Mixed Solvent, and Water: Phase Diagram and Implications. *Energy & Fuels* **2018,** *32* (1), 465-474.

122. Yanik, J.; Kornmayer, C.; Saglam, M.; Yüksel, M., Fast pyrolysis of agricultural wastes: Characterization of pyrolysis products. *Fuel Processing Technology* **2007,** *88* (10), 942-947.

123. Zheng, J.-l., Bio-oil from fast pyrolysis of rice husk: Yields and related properties and improvement of the pyrolysis system. *Journal of Analytical and Applied Pyrolysis* **2007,** *80* (1), 30-35.

124. Ingram, L.; Mohan, D.; Bricka, M.; Steele, P.; Strobel, D.; Crocker, D.; Mitchell, B.; Mohammad, J.; Cantrell, K.; Pittman, C. U., Pyrolysis of Wood and Bark in an Auger Reactor: Physical Properties and Chemical Analysis of the Produced Bio-oils. *Energy & Fuels* **2008,** *22* (1), 614-625.

125. Jung, S.-H.; Kang, B.-S.; Kim, J.-S., Production of bio-oil from rice straw and bamboo sawdust under various reaction conditions in a fast pyrolysis plant equipped with a fluidized bed and a char separation system. *Journal of Analytical and Applied Pyrolysis* **2008,** *82* (2), 240-247.

126. Das, D. D.; Schnitzer, M. I.; Monreal, C. M.; Mayer, P., Chemical composition of acid–base fractions separated from biooil derived by fast pyrolysis of chicken manure. *Bioresource Technology* **2009,** *100* (24), 6524-6532.

127. Heo, H. S.; Park, H. J.; Dong, J.-I.; Park, S. H.; Kim, S.; Suh, D. J.; Suh, Y.-W.; Kim, S.-S.; Park, Y.-K., Fast pyrolysis of rice husk under different

reaction conditions. *Journal of Industrial and Engineering Chemistry* **2010,** *16* (1), 27-31.

128. Oasmaa, A.; Peacocke, C., Properties and fuel use of biomass-derived fast pyrolysis liquids. *VTT Publications: Finland* **2010,** *731*, 79.

129. Chen, T.; Wu, C.; Liu, R.; Fei, W.; Liu, S., Effect of hot vapor filtration on the characterization of bio-oil from rice husks with fast pyrolysis in a fluidized-bed reactor. *Bioresource Technology* **2011,** *102* (10), 6178-6185.

130. Bertero, M.; de la Puente, G.; Sedran, U., Fuels from bio-oils: Bio-oil production from different residual sources, characterization and thermal conditioning. *Fuel* **2012,** *95*, 263-271.

131. Oasmaa, A.; Källi, A.; Lindfors, C.; Elliott, D. C.; Springer, D.; Peacocke, C.; Chiaramonti, D., Guidelines for Transportation, Handling, and Use of Fast Pyrolysis Bio-Oil. 1. Flammability and Toxicity. *Energy & Fuels* **2012,** *26* (6), 3864-3873.

132. Hu, Z.; Zheng, Y.; Yan, F.; Xiao, B.; Liu, S., Bio-oil production through pyrolysis of blue-green algae blooms (BGAB): Product distribution and bio-oil characterization. *Energy* **2013,** *52*, 119-125.

133. Alvarez, J.; Lopez, G.; Amutio, M.; Bilbao, J.; Olazar, M., Bio-oil production from rice husk fast pyrolysis in a conical spouted bed reactor. *Fuel* **2014,** *128*, 162-169.

134. Artigues, A.; Puy, N.; Bartrolí, J.; Fábregas, E., Comparative Assessment of Internal Standards for Quantitative Analysis of Bio-oil Compounds by Gas Chromatography/Mass Spectrometry Using Statistical Criteria. *Energy & Fuels* **2014,** *28* (6), 3908-3915.

135. Stankovikj, F.; McDonald, A. G.; Helms, G. L.; Olarte, M. V.; Garcia-Perez, M., Characterization of the Water-Soluble Fraction of Woody Biomass Pyrolysis Oils. *Energy & Fuels* **2017,** *31* (2), 1650-1664.

136. Hansen, C. M., *Hansen solubility parameters: a user's handbook*. CRC press: 2007.

137. Song, B.; Yu, Y.; Wu, H., Insights into Hydrothermal Decomposition of Cellobiose in Gamma-Valerolactone/Water Mixtures. *Industrial & Engineering Chemistry Research* **2017,** *56* (28), 7957-7963.

138. Barton, A. F., *CRC handbook of solubility parameters and other cohesion parameters*. Routledge: 2017.

139. Stephenson, R. M., *Handbook of the thermodynamics of organic compounds*. Springer Science & Business Media: 2012.

140. Emel'yanenko, V. N.; Dabrowska, A.; Hertel, M. O.; Scheuren, H.; Sommer, K., Vapor Pressures, Enthalpies of Vaporization, and Limiting Activity Coefficients in Water at 100 °C of 2-Furanaldehyde, Benzaldehyde, Phenylethanal, and 2-Phenylethanol. *Journal of Chemical & Engineering Data* **2007,** *52* (2), 468-471.

141. Majer, V.; Svoboda, V.; Kehiaian, H. V., Enthalpies of vaporization of organic compounds: a critical review and data compilation. **1985**.

142. Osborne, N. S., Measurements of Heat Capacity and Heat of Vaporization of Water in the Range 0℃ to 100℃. *J. Res. Nat. Bur. Stand.* **1939,** *23*, 197-260.

143. Bendiaf, L.; Bahadur, I.; Negadi, A.; Naidoo, P.; Ramjugernath, D.; Negadi, L., Effects of alkyl group and temperature on the interactions between furfural and alcohol: Insight from density and sound velocity studies. *Thermochimica Acta* **2015,** *599*, 13-22.

144. Wilhoit, R. C.; Zwolinski, B. J. *Physical and thermodynamic properties of aliphatic alcohols*; NATIONAL STANDARD REFERENCE DATA SYSTEM: 1973.

145. Badachhape, R.; Gharpurey, M.; Biswas, A., Density and Surface Tension of Phenol,(Mono-, Di-, and Tri-)-chlorophenols, Salol, and (o-and m-) Chloronitrobenzenes. *Journal of Chemical and Engineering Data* **1965,** *10* (2), 143-145.

146. Kell, G. S., Density, thermal expansivity, and compressibility of liquid water from 0.deg. to 150.deg.. Correlations and tables for atmospheric pressure and saturation reviewed and expressed on 1968 temperature scale. *Journal of Chemical & Engineering Data* **1975,** *20* (1), 97-105.

147. Joback, K. G.; Reid, R. C., Estimation of pure-component properties from group-contributions. *Chemical Engineering Communications* **1987,** *57* (1-6), 233-243.

148. Liaw, S. B.; Yu, Y.; Wu, H., Association of inorganic species release with sugar recovery during wood hydrothermal processing. *Fuel* **2016,** *166*, 581-584.

149. Hansen, C. M., *Hansen solubility parameters: a user's handbook*. CRC press: 2002.

150. Schuerch, C., The Solvent Properties of Liquids and Their Relation to the Solubility, Swelling, Isolation and Fractionation of Lignin. *Journal of the American Chemical Society* **1952,** *74* (20), 5061-5067.

151. Xu, A.; Guo, X.; Zhang, Y.; Li, Z.; Wang, J., Efficient and sustainable solvents for lignin dissolution: Aqueous choline carboxylate solutions. *Green Chemistry* **2017,** *19* (17), 4067-4073.

152. Yu, O.; Yoo, C. G.; Kim, C. S.; Kim, K. H., Understanding the Effects of Ethylene Glycol-Assisted Biomass Fractionation Parameters on Lignin Characteristics Using a Full Factorial Design and Computational Modeling. *ACS Omega* **2019,** *4* (14), 16103-16110.

153. Li, M.; Zhang, M.; Yu, Y.; Wu, H., Effect of temperature on ternary phase diagrams of pyrolytic lignin, mixed solvent and water. *Fuel* **2019**, 116458.

154. Azadi, P.; Inderwildi, O. R.; Farnood, R.; King, D. A., Liquid fuels, hydrogen and chemicals from lignin: A critical review. *Renew. Sustainable Energy Rev.* **2013,** *21*, 506-523.

155. Scholze, B.; Hanser, C.; Meier, D., Characterization of the water-insoluble fraction from fast pyrolysis liquids (pyrolytic lignin): Part II. GPC, carbonyl goups, and 13C-NMR. *Journal of Analytical and Applied Pyrolysis* **2001,** *58–59*, 387-400.

156. Li, H.; Qu, R.; Li, C.; Guo, W.; Han, X.; He, F.; Ma, Y.; Xing, B., Selective removal of polycyclic aromatic hydrocarbons (PAHs) from soil washing effluents using biochars produced at different pyrolytic temperatures. *Bioresource Technology* **2014,** *163*, 193-198.

157. Ray, P. Z.; Chen, H.; Podgorski, D. C.; McKenna, A. M.; Tarr, M. A., Sunlight creates oxygenated species in water-soluble fractions of Deepwater horizon oil. *Journal of Hazardous Materials* **2014,** *280*, 636-643.

158. Ahmad, M.; Lee, S. S.; Dou, X.; Mohan, D.; Sung, J.-K.; Yang, J. E.; Ok, Y. S., Effects of pyrolysis temperature on soybean stover- and peanut shell-derived biochar properties and TCE adsorption in water. *Bioresource Technology* **2012,** *118*, 536-544.

159. Wang, Y.; Li, X.; Mourant, D.; Gunawan, R.; Zhang, S.; Li, C.-Z., Formation of Aromatic Structures during the Pyrolysis of Bio-oil. *Energy & Fuels* **2012,** *26* (1), 241-247.

160. Wang, Q.; Chen, K.; Li, J.; Yang, G.; Liu, S.; Xu, J., The solubility of lignin from bagasse in a 1, 4-butanediol/water system. *BioResources* **2011,** *6* (3), 3034-3043.

161. Zhou, S.; Mourant, D.; Lievens, C.; Wang, Y.; Li, C.-Z.; Garcia-Perez, M., Effect of sulfuric acid concentration on the yield and properties of the bio-oils obtained from the auger and fast pyrolysis of Douglas Fir. *Fuel* **2013,** *104*, 536-546.

162. Mourant, D.; Wang, Z.; He, M.; Wang, X. S.; Garcia-Perez, M.; Ling, K.; Li, C.-Z., Mallee wood fast pyrolysis: Effects of alkali and alkaline earth metallic species on the yield and composition of bio-oil. *Fuel* **2011,** *90* (9), 2915-2922.

163. Oasmaa, A.; Koponen, P., *Physical characterisation of biomass-based pyrolysis liquids*. Espoo: 1997.

164. Liaw, S.-S.; Zhou, S.; Wu, H.; Garcia-Perez, M., Effect of pretreatment temperature on the yield and properties of bio-oils obtained from the auger pyrolysis of Douglas fir wood. *Fuel* **2013,** *103*, 672-682.

165. Bahng, M.-K.; Mukarakate, C.; Robichaud, D. J.; Nimlos, M. R., Current technologies for analysis of biomass thermochemical processing: A review. *Analytica Chimica Acta* **2009,** *651* (2), 117-138.

166. Van de Velden, M.; Baeyens, J.; Brems, A.; Janssens, B.; Dewil, R., Fundamentals, kinetics and endothermicity of the biomass pyrolysis reaction. *Renewable Energy* **2010,** *35* (1), 232-242.

167. ABRI-Tech, https://abritechinc.com/en/products/.

168. Biogreen®, http://www.biogreen-energy.com/.

169. Industries, G., https://www.egenindustries.com/.

170. Campuzano, F.; Brown, R. C.; Martínez, J. D., Auger reactors for pyrolysis of biomass and wastes. *Renewable and Sustainable Energy Reviews* **2019,** *102*, 372-409.

171. Manjkow, J.; Papanu, J.; Hess, D.; Soane, D.; Bell, A., Influence of processing and molecular parameters on the dissolution rate of poly ‐ (methyl methacrylate) thin films. *Journal of The Electrochemical Society* **1987,** *134* (8), 2003-2007.

172. Miller-Chou, B. A.; Koenig, J. L., A review of polymer dissolution. *Progress in Polymer Science* **2003,** *28* (8), 1223-1270.

173. Zhang, C.; Zhang, R.; Li, X.; Li, Y.; Shi, W.; Ren, X.; Xu, X., Bench ‐ scale fluidized ‐ bed fast pyrolysis of peanut shell for bio ‐ oil production. *Environmental Progress & Sustainable Energy* **2011,** *30* (1), 11-18.

174. Solantausta, Y.; Oasmaa, A.; Sipila, K.; Lindfors, C.; Lehto, J.; Autio, J.; Jokela, P.; Alin, J.; Heiskanen, J., Bio-oil production from biomass: steps toward demonstration. *Energy & Fuels* **2011,** *26* (1), 233-240.

175. http://www.btgworld.com/en/rtd/technologies/fast-pyrolysis.

176. https://www.fortum.com/products-and-services/bio-oil.

177. Zacher, A. H.; Olarte, M. V.; Santosa, D. M.; Elliott, D. C.; Jones, S. B., A review and perspective of recent bio-oil hydrotreating research. *Green Chemistry* **2014,** *16* (2), 491-515.

178. Fahmi, R.; Bridgwater, A. V.; Darvell, L. I.; Jones, J. M.; Yates, N.; Thain, S.; Donnison, I. S., The effect of alkali metals on combustion and pyrolysis of Lolium and Festuca grasses, switchgrass and willow. *Fuel* **2007,** *86* (10), 1560-1569.

179. Oasmaa, A.; Solantausta, Y.; Arpiainen, V.; Kuoppala, E.; Sipilä, K., Fast Pyrolysis Bio-Oils from Wood and Agricultural Residues. *Energy & Fuels* **2010,** *24* (2), 1380-1388.

180. Leijenhorst, E. J.; Wolters, W.; van de Beld, L.; Prins, W., Inorganic element transfer from biomass to fast pyrolysis oil: Review and experiments. *Fuel Processing Technology* **2016,** *149*, 96-111.

181. Hilten, R. N.; Bibens, B. P.; Kastner, J. R.; Das, K. C., In-Line Esterification of Pyrolysis Vapor with Ethanol Improves Bio-oil Quality. *Energy & Fuels* **2010,** *24* (1), 673-682.

182. Ferguson, A. L.; Debenedetti, P. G.; Panagiotopoulos, A. Z., Solubility and Molecular Conformations of n-Alkane Chains in Water. *The Journal of Physical Chemistry B* **2009,** *113* (18), 6405-6414.

183. Polak, J.; Lu, B. C.-Y., Mutual solubilities of hydrocarbons and water at 0 and 25 C. *Canadian Journal of Chemistry* **1973,** *51* (24), 4018-4023.

184. Yalkowsky, S. H.; Dannenfelser, R. M., Aquasol database of aqueous solubility. *College of Pharmacy, University of Arizona, Tucson, AZ* **1992,** *189*.

185. Song, Q.-H.; Nie, J.-Q.; Ren, M.-G.; Guo, Q.-X., Effective Phase Separation of Biomass Pyrolysis Oils by Adding Aqueous Salt Solutions. *Energy & Fuels* **2009,** *23* (6), 3307-3312.

186. Mei, Y.; Liu, R.; Zhang, L., Influence of industrial alcohol and additive combination on the physicochemical characteristics of bio-oil from fast pyrolysis of pine sawdust in a fluidized bed reactor with hot vapor filter. *Journal of the Energy Institute* **2017,** *90* (6), 923-932.

187. Samec, J.; Löfstedt, J.; Dahlstrand, C.; Orebom, A.; Sawadjoon, S., Composition Comprising Esters Of Lignin And Organic Solvent. Google Patents: 2016.

188. Bridgwater, A. V., Principles and practice of biomass fast pyrolysis processes for liquids. *Journal of Analytical and Applied Pyrolysis* **1999,** *51* (1), 3-22.

189. Miller, F. P.; Vandome, A. F.; McBrewster, J., *Le Chatelier´s Principle: Chemistry, Chemical Equilibrium, Henry Louis Le Chatelier, Karl Ferdinand Braun, Concentration, Temperature, Volume, Pressure, Lenz´s Law, Homeostasis, Status Quo*. Alphascript Publishing: 2009.

190. Higbie, H.; Stegeman, G., The Heat of Solution of Sucrose in Water at 25°1. *Journal of the American Chemical Society* **1950,** *72* (8), 3799-3799.

191. Taylor, J.; Rowlinson, J., The thermodynamic properties of aqueous solutions of glucose. *Transactions of the Faraday Society* **1955,** *51*, 1183-1192.

APPENDIX I: ATTRIBUTION TABLES

A. Ternary System of Pyrolytic Lignin, Mixed Solvent, and Water: Phase Diagram and Implications, Mingyang Li; Mingming Zhang; Yun Yu; Hongwei Wu*, Energy & Fuels, 2018, 32, 465.

Authors and full affiliations:

	Conception and design	**Experiments conduction & data acquisition**	**Data processing & analysis**	**Interpretation & discussion**	**Manuscript writing, revision and finalisation**	**Final Approval**
Mingming Zhang				×	×	×
I acknowledge that these represent my contribution to the above research output. Sign:						
Yun Yu				×	×	×
I acknowledge that these represent my contribution to the above research output. Sign:						
Hongwei Wu	×			×	×	×
I acknowledge that these represent my contribution to the above research output. Sign:						

B. Effect of temperature on ternary phase diagrams of pyrolytic lignin, mixed solvent and water, Mingyang Li; Mingming Zhang; Yun Yu; Hongwei Wu*, Fuel. 2020, 265, 116458.

Authors and full affiliations:

	Conception and design	**Experiments conduction & data acquisition**	**Data processing & analysis**	**Interpretation & discussion**	**Manuscript writing, revision and finalisation**	**Final Approval**
Mingming Zhang				×	×	×
I acknowledge that these represent my contribution to the above research output. Sign:						
Yun Yu	×			×	×	×
I acknowledge that these represent my contribution to the above research output. Sign:						
Hongwei Wu	×			×	×	×
I acknowledge that these represent my contribution to the above research output. Sign:						

APPENDIX II: COPYRIGHT PERMISSION STATEMENTS

A. Chapter 4, reprinted with permission from "Mingyang Li, Mingming Zhang, Yun Yu, Hongwei Wu. Ternary System of Pyrolytic Lignin, Mixed Solvent, and Water: Phase Diagram and Implications. Energy Fuels 2018, 32, 1, 465-474".

Open access, permission not required

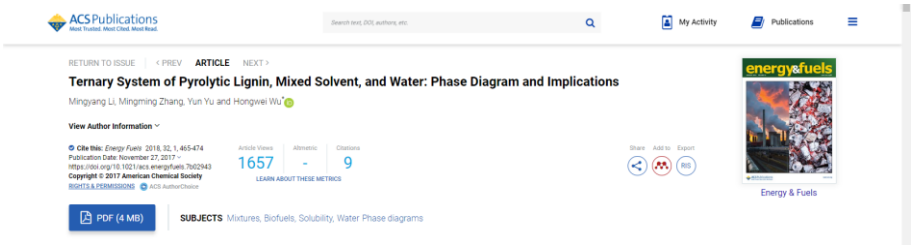

B. Chapter 5, reprinted with permission from “Mingyang Li, Mingming Zhang, Yun Yu, Hongwei Wu. Effect of temperature on ternary phase diagrams of pyrolytic lignin, mixed solvent and water. Fuel. 2020, 265, 116458”.

Permission not required